Center for Adhesion Science

Virginia Polytechnic Institute and State University

Blacksburg, Virginia 24061

College of Engineering
Virginia Polytechnic Institute and State University
Blacksburg, VA 24061

VPI-E-84-15 April 1984

FINITE ELEMENT ANALYSIS OF BONDED JOINTS

by

Barthelemy, B. M.* Research Assistant
Kamat, M. P. Professor
Brinson, H. F. Professor

Center for Adhesion Science
and
Department of Engineering Science and Mechanics
Virginia Polytechnic Institute and State University
Blacksburg, Virginia 24061

Prepared for:

Office of Naval Research (ONR)
Grant No: N00014-82-K-0185
Arlington, VA 22217

*This report is essentially the Master thesis of B. M. Barthelemy.

BIBLIOGRAPHIC DATA	1. Report No. VPI-E-84-15	2.	3. Recipient's Accession No. AD-A140 559
4. Title and Subtitle: Finite Element Analysis of Bonded Joints			5. Report Date: April 1984
			6.
7. Author(s): Barthelemy, B. M.; Kamat, M. P.; and Brinson, H. F.			8. Performing Organization Rept. No.
9. Performing Organization Name and Address: Department of Engineering Science and Mechanics, Virginia Polytechnic Institute and State University, Blacksburg, VA 24061			10. Project/Task/Work Unit No.
			11. Contract/Grant No. (ONR) N00014-82-K-0185
12. Sponsoring Organization Name and Address: Office of Naval Research (ONR), Arlington, VA 22217			13. Type of Report & Period Covered
			14.

15. Supplementary Notes

16. Abstracts

See page ii

17. Key Words and Document Analysis. 17a. Descriptors

Bonded joints, finite element analysis, single-lap, thick-adherend, crack-lap.

17b. Identifiers/Open-Ended Terms

A-1

17c. COSATI Field Group

18. Availability Statement: Distribution unlimited	19. Security Class (This Report) UNCLASSIFIED	21. No. of Pages
	20. Security Class (This Page) UNCLASSIFIED	22. Price

FINITE ELEMENT ANALYSIS OF

BONDED JOINTS

(ABSTRACT)

A finite element program called STAP was modified for use. Specifically, an eight noded isoparametric element and a non-linear material law was integrated with the STAP program. Details of the element formulation and material law are included.

The finite element program was used to analyze a single-lap joint. The results are compared with the closed-form solution due to Goland and Reissner. The finite element analysis of this type of adhesive joint is also compared with experimental data.

Another single-lap geometry was analyzed using the finite element program, and the results are compared with two preceding analyses due to Nagaraja and Alwar, and Botha. The thick-adherend and crack-lap adhesive joints are also studied using both linear and non-linear material laws. Some of the results for the thick-adherend specimen also compared with the Botha analysis.

Acknowledgement

The authors acknowledge with gratitude the source of funding for this work. The financial support was provided by the Office of Naval Research (ONR) N00014-82-K-0185, Arlington, VA, 22217; the project monitor being Dr. L. H. Peebles.

Thanks are given to Dr. R. T. Haftka and Dr. J. P. Wightman, for their suggestions and encouragment. The numerous and helpful discussions with Dr. M. E. Tuttle are also gratefully acknowledged.

TABLE OF CONTENTS

LIST OF FIGURES

LIST OF TABLES

List of Symbol

u_i : Displacement of node i in x direction.

v_i : Displacement of node i in y direction.

X_i : x coordinate of node i.

Y_i : y coordinate of node i.

J : Jacobian.

q : Displacement.

S : Surface of the element.

Γ : Boundary of the element.

$\partial_{,x}$: $\frac{\partial}{\partial x}$.

δF : Variation of function F.

ν : Poisson ratio.

CHAPTER 1 INTRODUCTION

1. 1. Motivation

Structures are often made from an assembly of many components. In the past, the usual methods of joining components were rivets, welds, bolts, adhesives, etc. But adhesive bonding was essentially only used for non-strutural parts. However, in recent years, bonding has become of more interest for structural applications due to improvements in the types of adhesives available, and improved knowledge of bonding procedures. The major advantages of adhesive bonding include an increase in fatigue resistance, improved damping characteristics, and a smooth surface finish. Because of these facts, this joining technique has been used more and more in aerospace structures. Boeing, Fokker, McDonald-Douglas, and other air frame manufactures are currently using adhesives in many applications. Nevertheless, the adhesive bonding method has limitations and disadvantages which must be understood before their potential can be fully utilized. Essentially, due to the little knowledge that we have of these materials, we still do not know how to characterize adhesive failure or

viscoelastic properties, for example. Also for many structural adhesives, curing processes are longer than convenient or acceptable in practice. For example, the curing time for a popular modified epoxy adhesive, FM-300, is 4 hours at 350F. In certain industries this curing time is prohibitive in terms of speed and cost.

Considerable work is needed in a variety of areas in order to fully characterize and understand the performance of an adhesive and use it at 100% of its capability. One such need is a good stress analysis of test specimens such as the single-lap, thick-adherend, and crack-lap geometries. Towards this end, the development of a finite element program which provides a frame work of a viable analysis procedure was undertaken. In such an endeaver, one must realize that material and geometric non-linearities, viscoelastic properties, plasticity , failure mechanisms, and enviromental effects must be considered in order to accurately predict joint performance. However, this report is directed primarily towards only the consideration of material non-linearities and the singular nature of the elasticity solution for several typical bonded joints which are widely used to measure or quantify adhesive performance.

1. 2. Literature Review

In order to fully understand adhesives from a mechanical viewpoint, it is a necessity that researchers in experimental, analytical, and numerical techniques collaborate to investigate bonded joints. This literature review will not be an exhaustive one, but will briefly report on research findings in these three fields.

Many new materials such as graphite-epoxy or adhesives possess viscoelastic properties in general. In order to characterize these properties, methods such as the time temperature superposition principle, time stress superposition principle, the Findley viscoelastic model, or the Schapery non-linear viscoelastic model have been used [1-9]. The basic concept of such theories is to use short-term tests (on the order of hours) to predict long-term response (on the order of years). These methods have been applied at VPI&SU primarily for the characterization of the composite materials [4-8]. The reader is referred to the bibliographies given in the cited references for a more complete review of viscoelasticity. Rochefort [9] used the Findley power law creep model to study FM-300 and FM-73 adhesives in bulk or neat resin form . Note, however, that it may be neccessary to determine adhesive properties as

they exist inside a joint such as the single-lap joint, thick-adherend, or crack-lap specimen geometries. It is not yet clear whether the properties of the bulk adhesive and the adhesive inside a joint are the same.

The study of the adhesive deformation inside a bonded joint is difficult. Surface measurements using optical methods such as Moire have been used [10]. The "Krieger-gage" is a specific gage designed to measure shear deformation of the adhesive layer in a thick-adherend specimen [11]. Recently a strain gage has been placed inside a bonded joint to measure the axial strain [18].

In 1944 Goland and Reissner [12] presented a solution for the stresses inside the single lap joint shown in Fig. 1.1. The initial assumption made in their theory was to assume that $l>>c>>t>>n$. The first part of their work was to determine T_0, M_0, and V_0; the tension, bending moment, and shear in section AA' shown in Fig. 1.2. A second set of assumptions was to neglect the axial normal stress, σ_x parallel to the bond line, inside the adhesive layer, and to assume the peel and shear stresses to be constant across the thickness of the adhesive layer. Then, based on strain energy considerations, they developed two theories; one neglecting the flexibility of the adhesive layer under the condition $10 \frac{n}{t} \frac{E}{E_c} < 1$, and the other neglecting the flexibility of the adherends under the condition $10 \frac{t}{n} \frac{E_c}{E} < 1$.

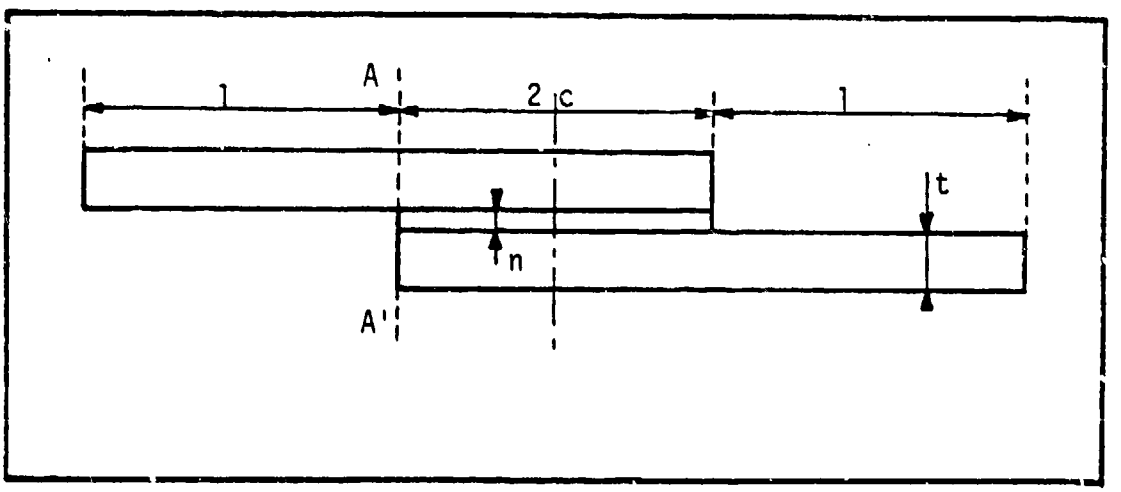

Figure 1.1: Single-Lap Joint Geometry.

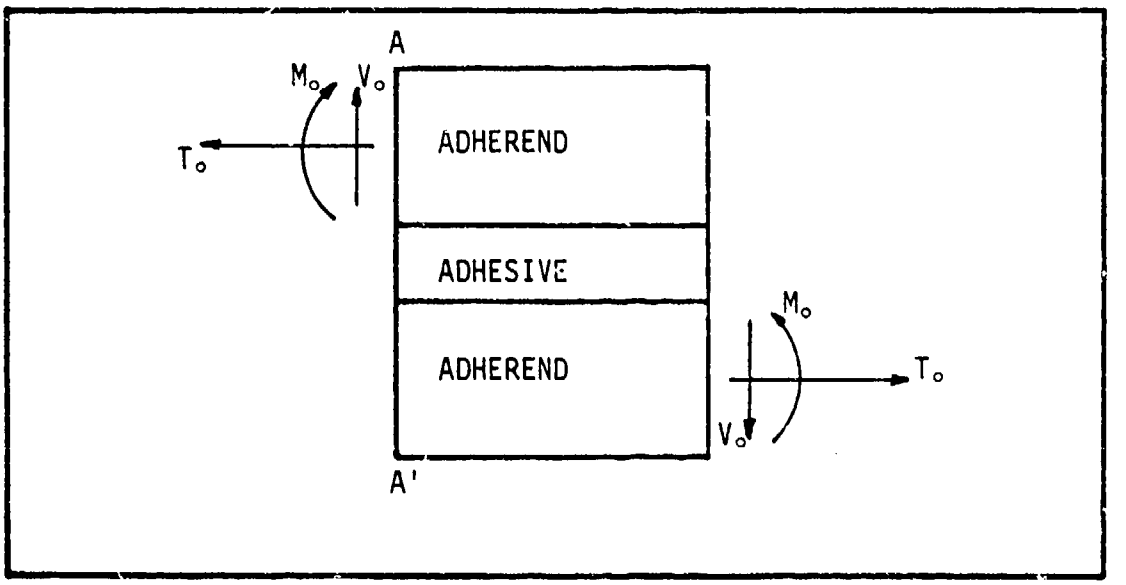

Figure 1.2: Free Body Diagram of the Central Part of the Single-Lap Joint. Applied Load at Section AA' Fig. 1.1 .

They refered to the cement satisfying the first or second condition as flexible or inflexible, respectively.

In 1973 Hart-Smith [13] modified the solution of Goland and Reissner. His major contribution was to provide a better estimate of M_0 which he felt the Goland and Reissner's solution overestimated, with this approach, however, the theory could be applied only for short overlap lengths or light loads.

In the theories of Goland and Reissner or even Hart-Smith, all single lap joint configurations cannot be treated. Indeed, if in the inequalities that must be satisfied to apply the first or second theories we assume $\frac{E}{E_c} = 50$, then the inequalities become

$$\frac{n}{t} < \frac{1}{500}$$

$$\frac{n}{t} > \frac{1}{5}.$$

Therefore the above theories cannot be applied if $\frac{1}{500} < \frac{n}{t} < \frac{1}{5}$. Another problem in these theories is that the shear stress inside the adhesive layer has a non-zero value at the free edge.

Du Chen, et al. [14] in 1983 overcame some of these problems with their analysis. They began their analysis in a manner similar to Goland and Reissner's but instead of treating separately the cases of flexible or inflexible adhesive layers, they used a variational method based on the

principle of complementary energy without making any assumption on the flexibility of the adhesive. Figure 1.3 [14] shows a comparison of their results with those of Goland and Reissner for a flexible adhesive layer. The main differences with the preceding studies are that the theory of Du Chen, et al. is applicable for any single-lap joint that satisfies l>>c>>t>>n, and that their peel and shear stresses are equal to zero at the free boundaries. As with the preceding theories, however no axial stresses exist and no stress gradients occur through the thickness of the adhesive layer.

Finite element analyses have been used to find the stress distributions inside bonded joints, and they have demonstrated the existance of a normal axial stress and stress gradients across the thickness of the adhesive layer. Sen, et al.[15] analyzed an aluminum-epoxy double-lap joint and compared their results with experiments. They used Shapery's direct and quasi-elastic methods for the solution of linear viscoelastic problems. Their finite element code used a composi e element made of four constant stress and strain triangles.

Botha, et al. [16] used the same technique to analyze the single-lap joint and the thick-adherend specimen. They pointed out that constant strain elements used might not

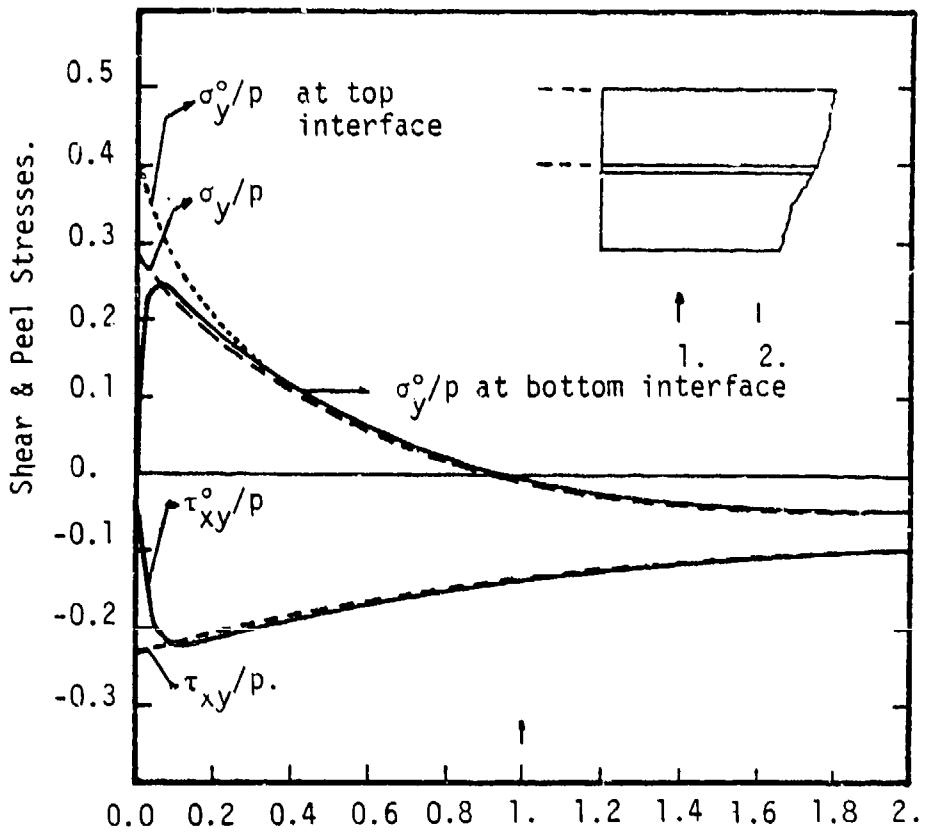

Figure 1.3: Peel& Shear Distribution Inside the Adhesive Layer of a Single-Lap Joint. Comparison Between the Results of Goland and Reissner (σ_y/p, τ_{xy}/p) and Du Chen et al. [14] (σ_y°/p, τ_{xy}°).

provide a good representation of the stress singularities near the edge, and they suggested that a higher order element could better take into account the high stress and strain gradients at this location.

Anderson, et al.[17] show that the tensile and shear stress singularities are of the order of $\frac{1}{r^n}$, where n is not function of the adherends thickness.

More references on finite element analyses of bonded joints can be found in Botha's work [16].

1. 3. Objectives

The purpose of this reseach was to analyze three different bonded joints, i.e., the single-lap, the thick-adherend, and crack-lap test specimens using a finite element program. From the suggestions of Botha et al. it was decided to use an higher order element than the element uses in their analysis. This difference allowed us to look at stress and strain distributions near the free edges of the adhesive layer. The eight noded isoparametric element was choosen for this study, and it was added to the library of an existing finite element program (STAP [21]).

Chapter 2 presents the finite element background needed to develop the linear and non-linear eight noded

isoparametric element, the non-linear law used in the program, and the input of data for the program. Chapter 3 shows correlation between stress distributions found by the new finite element analysis, and Goland and Reissner's analytical solution, as well as providing some experimental results. Stress and strain distributions for the single-lap, thi -adherend, and crack-lap joints are presented in Chapter 4. Some of the results are compared with previous finite element analyses. Chapter 5 presents the conclusions and a few recommendations.

CHAPTER 2 FINITE ELEMENT BACKGROUND

2. 1. Introduction

The main objective of this research is to develop a theoretical tool capable of predicting stress and strain distribution in a bonded joint. Both closed form analytical methods or numerical methods can be used for that purpose. Usually closed form methods lead to solutions in the form of equations which are functions of all the parameters of the problem (temperature, moisture ..), and are easy to use. However, closed form solutions can be obtained only for a small number of classical problems and thus this approach is severly restricted. Numerical methods, on the other hand, solve a problem for a set of given parameters. Any change in the parameters requires a new computation, but the solution method can be used for a wide range of problems for which no closed form solution exists.

Finite difference and finite element are the two most commoly used numerical methods for predicting stresses in solids. The finite difference method is used mainly for applications that have simple geometrical boundaries. This method has been used extensively in plate bending and

torsion problems, for example. The finite element method is not restricted to such simple geometries and is applicable to a wide range of structures. The latter is the method used in the present study.

The finite element program used herein is a modified version of the STAP program (Structural Analysis Program) developed by Bathe and Wilson [27]. The modifications to the program so as to render it useful for our purposes were to enlarge the element library by including an eight noded isoparametric element and to generalize the program to non-linear material behavior.

This chapter will be devoted to outlining the theoretical basis of the modified STAP program, including the development of the eight noded isoparametric element, the algorithms of the initial and the modified program, and tests that have been made for testing the program.

2. 2. THEORY

2. 2. 1. The Eight Noded Isoparametric Element

The first step in modifying the program was to develop a new element. We decided to base the element upon a two-dimensional analysis of plane strain and plane stress

because it was felt that the single-lap, thick-adherend, and crack-lap joints could be considered two-dimensional strutures. Indeed, full three dimensional effects are likely present only near the edges of the specimen. Another reason for not using a more general three dimensional analysis of these bonded joints w s the potentially high computational expense. The time required by a finite element program to solve a problem is a power function of the number of degrees of freedom: for N nodes in each direction, a two-dimensional analysis will have $2*N^2$ degrees of freedom while a three dimensional analysis will have $3*N^3$ degree of freedom. Obviously, the cost of the latter would be far greater than the former.

In a two-dimensional analysis there are many different elements that can be used. The eight noded isoparametric element was chosen for three main reasons. These were,

1) Previous finite element studies [16] of bonded joints used a quadrilateral element made of four constant strain triangles. The displacement field inside a constant strain element can only model a linear displacement variation. As a result, the response using this type of element is very sensitive to the discretization near high stress and strain gradients. In other words, discretizations using such elements may not give

accurate results. On the other hand, the eight noded isoparametric element is better able to model high strain gradients because its displacement field is of the second order.

2) As shown in reference [18] the eight noded element is also able to model on its boundaries singularities that occur near a crack in a body which suggest its usefulness for the singular stress fields near the boundary of our geometries.

3) A third advantage is that the element can model curved boundaries with the field distribution at the boundaries being of the second order, as shown in Fig. 2.1.

2. 2. 1. 1. Element Description [21]

Figure 2.1 shows an eight noded isoparametric element with two degrees of freedom at each node. The element defined in a global coordinate system (x,y), can be transformed to a square in a local or natural coordinate system (r,s) where $-1 < (r,s) < +1$, as shown in Fig. 2.2. The transformation from one system to the other is given by

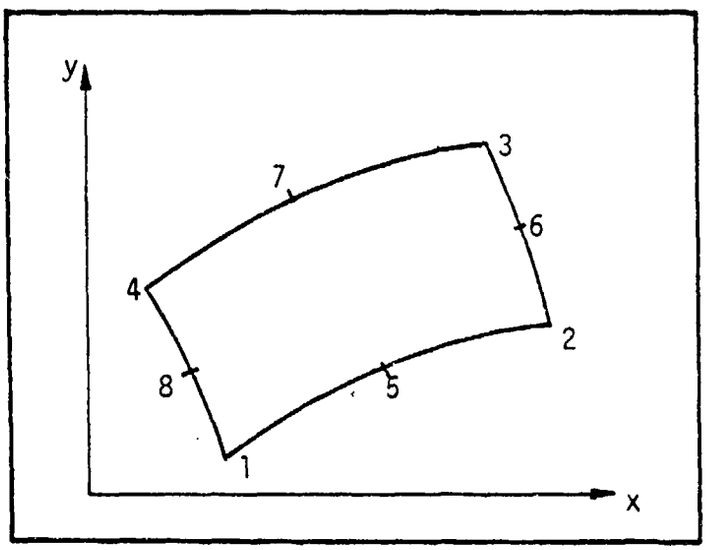

Figure 2.1: Eight-Noded Isoparametric Element.

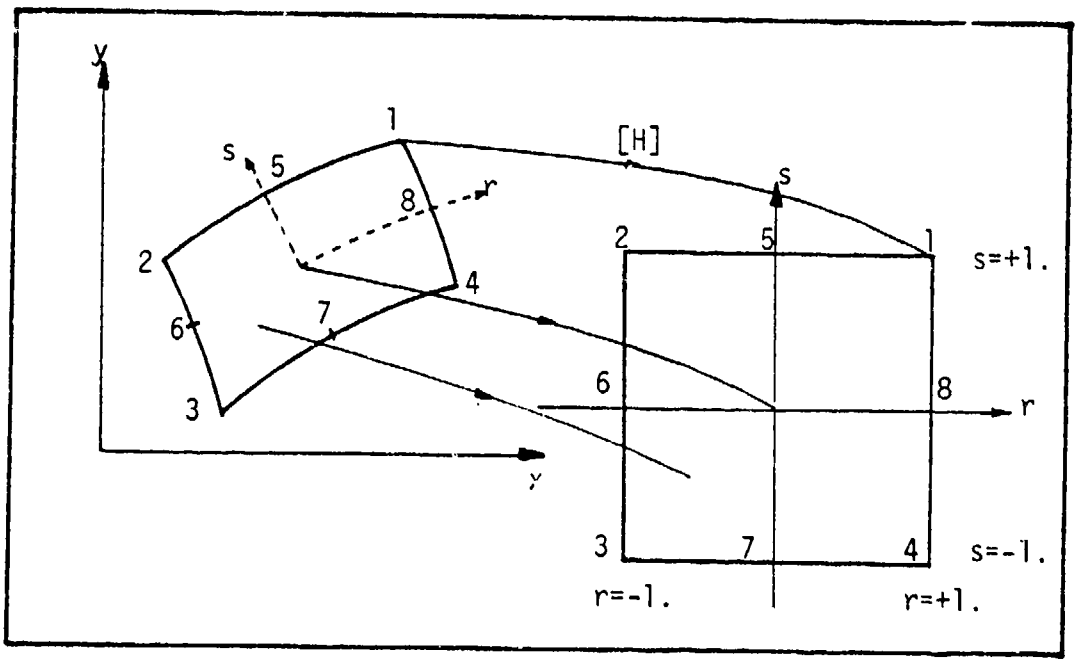

Figure 2.2: Transformation of the Global Coordinate System (x,y) into a Natural (Local) Coordinate System (r,s) of the Element.

$$\begin{Bmatrix} x \\ y \end{Bmatrix} = \sum_{i=1}^{8} h_i(r,s) \begin{Bmatrix} X_i \\ Y_i \end{Bmatrix} \tag{2.1}$$

where (x,y) are the coordinates of a generic point inside the element, (X_i,Y_i) are the coordinates of the nodal points of the element, and h_i $i = 1,2,\ldots,8$ are functions of r and s, called shape functions or interpolation functions, and define the transformation from the natural coordinate system to the global coordinate system. Equation (2.1) can be rewritten as

$$\begin{Bmatrix} x \\ y \end{Bmatrix} = [H] \begin{Bmatrix} X_1 \\ \vdots \\ Y_8 \end{Bmatrix} \tag{2.2}$$

where [H] is defined as

$$[H] = \begin{bmatrix} h_1 & 0 & h_2 & 0 & h_3 & 0 & h_4 & 0 & h_5 & 0 & h_6 & 0 & h_7 & 0 & h_8 & 0 \\ 0 & h_1 & 0 & h_2 & 0 & h_3 & 0 & h_4 & 0 & h_5 & 0 & h_6 & 0 & h_7 & 0 & h_8 \end{bmatrix} \tag{2.3}$$

The element defined in the natural coordinate system is called the parent element. This transformation is essential in developing and integrating the stiffness matrix.

2. 2. 1. 2. Geometry Interpolation

Equations (2.1) and (2.2) express the interpolation of any point (x,y) inside the element as a function of (X_i, Y_i). The interpolation functions h_i can be determined in a systematic way or by an inspection method.

The procedure for the systematic method is quite long and we will only briefly outline it here. Assuming that the transformation is unique, each point of the parent element corresponds to a unique point in the original element itself and vice versa. The correspondances for the nodes, shown in Fig. 2.2, can then be written as

$$X_1 , Y_1 \rightarrow r_1 = -1 , s_1 = -1 \qquad (2.4a)$$

$$X_2 , Y_2 \rightarrow r_2 = +1 , s_2 = -1 \qquad (2.4b)$$

$$X_3 , Y_3 \rightarrow r_3 = +1 , s_3 = +1 \qquad (2.4c)$$

$$X_4 , Y_4 \rightarrow r_4 = -1 , s_4 = +1 \qquad (2.4d)$$

$$X_5 , Y_5 \rightarrow r_5 = 0 , s_5 = -1 \qquad (2.4e)$$

$$X_6 , Y_6 \rightarrow r_6 = +1 , s_6 = 0 \qquad (2.4f)$$

$$X_7 , Y_7 \rightarrow r_7 = 0 , s_7 = +1 \qquad (2.4g)$$

$$X_8 , Y_8 \rightarrow r_8 = -1 , s_8 = 0 \qquad (2.4h)$$

In general

$$X_i , Y_j \rightarrow r_i , s_j \qquad (2.5)$$

If we suppose that interpolation functions h_i have a polynomial form in r and s, then the first of the relations

in eqs. (2.4a-h) can be written as

$$x = a_1 + a_2 r + a_3 s + a_4 rs + a_5 r^2 + a_6 s^2 + a_7 r^2 s + a_8 r s^2 + a_9 r^2 s^2 + \ldots \quad (2.6)$$

where a_i, $i=1,2,\ldots,n$ are the unknown functions of X_i. Having only eight X_i, in the interest of uniqueness, it is natural to assume $a_j = 0$ for $j = 9,10,\ldots,n$.
Hence it follows that

$$x = a_1 + a_2 r + a_3 s + a_4 rs + a_5 r^2 + a_6 s^2 + a_7 r^2 s + a_8 r s^2 \quad (2.7a)$$

$$y = b_1 + b_2 r + b_3 s + b_4 rs + b_5 r^2 + b_6 s^2 + b_7 r^2 s + b_8 r s^2 \quad (2.7b)$$

In order to find the a_i and b_i we have to introduce eq. (2.4) into eqs. (2.7a) and (2.7b). Solving the two systems of 8 equations with 8 unknowns, we can express the a_i and b_i as functions of X_i and Y_i.

The approach for the inspection method is slightly different. Since eq. (2.1) applies for any point in the element, it also applies for every node (X_j, Y_j) of the element. Hence

$$\begin{Bmatrix} X_j \\ Y_j \end{Bmatrix} = [H] \begin{Bmatrix} X_1 \\ \vdots \\ Y_8 \end{Bmatrix} = \sum_{i=1}^{8} h_i(r_j, s_j) \begin{Bmatrix} X_i \\ Y_i \end{Bmatrix} = \delta_{ij} \begin{Bmatrix} X_i \\ Y_i \end{Bmatrix} \qquad (2.8)$$

where $h_i(r_j, s_i) = \delta_{ij}$. The h_i can be constructed by inspection. In this case we know from eq. (2.7) that each h_i is a quadratic form in r and s with the term r^2s^2 missing.

Either by the first or the second method h_i can be expressed as follows

$$h_1 = (1+r)(1+s)/4 - h_5/2 - h_8/2 \qquad (2.9a)$$

$$h_2 = (1-r)(1+s)/4 - h_5/2 - h_6/2 \qquad (2.9b)$$

$$h_3 = (1-r)(1-s)/4 - h_6/2 - h_7/2 \qquad (2.9c)$$

$$h_4 = (1+r)(1-s)/4 - h_7/2 - h_8/2 \qquad (2.9d)$$

$$h_5 = (1-r^2)(1+s)/2 \qquad (2.9e)$$

$$h_6 = (1-r)(1-s^2)/2 \qquad (2.9f)$$

$$h_7 = (1-r^2)(1-s)/2 \qquad (2.9g)$$

$$h_8 = (1+r)(1-s^2)/2 \qquad (2.9h)$$

2. 2. 1. 3. Displacement Interpolation

Displacement field in isoparametric formulation uses the same interpolation functions as the geometry and hence can be expressed as

$$\begin{Bmatrix} u \\ v \end{Bmatrix} = [H] \begin{Bmatrix} u_1 \\ \vdots \\ v_8 \end{Bmatrix} \tag{2.10}$$

where $(u,v)^t$ is the displacement vector of a point $(x,y)^t$ inside the element, [H] is the interpolation matrix defined in eq. (2.3) , and $(u_i,v_i)^t$ is the vector of the nodal displacements of the element defined as

$$(u_i,v_i)^t = (u_1,v_1,u_2,v_2,.,...,u_8,v_8)^t \tag{2.11}$$

2. 2. 1. 4. Strain Displacement Relations [21]

The general expression for the strain is given in the following equation

$$L_{ij} = \frac{1}{2}(\partial_{,j}u_i + \partial_{,i}u_j + \partial_{,i}u_m\partial_{,j}u_m) \tag{2.12}$$

where L_{ij} is known as the Lagrangian non-linear strain tensor, the commas denote differentiation, and

$$u_i = (u,v,w) = (u_1,u_2,u_3) \tag{2.13}$$

$$x_i = (x,y,z) = (x_1,x_2,x_3)$$

If $\partial_{,i}u_m \ll 1$, then the term in eq. (2.12) involving the product of these derivatives is negligible. For the two dimensional elasticity the linear strain tensor ε_{ij} in term of the displacements u_i, is given by

$$\varepsilon_{ij} = \frac{1}{2}(\partial_{,j} u_i + \partial_{,i} u_j) \qquad i=1,2 \tag{2.14}$$

where $u_1 = u$, $u_2 = v$, $x_1 = x$, $x_2 = y$. Thus

$$\begin{aligned} \varepsilon_{11} = \varepsilon_{xx} &= \frac{1}{2}(\partial_{,1} u_1 + \partial_{,1} u_1) = \partial_{,1}\, u \\ \varepsilon_{22} = \varepsilon_{yy} &= \frac{1}{2}(\partial_{,2} u_2 + \partial_{,2} u_2) = \partial_{,2}\, v \\ \varepsilon_{12} = \varepsilon_{xy} &= \frac{1}{2}(\partial_{,1} u_2 + \partial_{,1} u_2) = \frac{1}{2}\gamma_{xy} \end{aligned} \tag{2.15}$$

Using matrix notation, eq. (2.15) may be written as

$$\{\varepsilon\} = [B] \begin{Bmatrix} u \\ v \end{Bmatrix} \tag{2.16}$$

where $\{\varepsilon\}^t = \{\varepsilon_{xx} , \varepsilon_{yy} , \gamma_{xy}\}$

$$[B] = \begin{bmatrix} \partial_{,x} & 0 \\ 0 & \partial_{,y} \\ \partial_{,y} & \partial_{,x} \end{bmatrix} \tag{2.17}$$

For the isoparametric element under consideration, use of eq. (2.10) yields

$$\{\varepsilon\} = [B][H] \begin{Bmatrix} U_i \\ V_i \end{Bmatrix} \tag{2.18}$$

Recall that in eq. (2.18) [H] was defined as a function of (r,s), whereas [B] is a matrix of derivatives with respect to x and y. The next step is therefore to transform $[B(\partial_{,x}, \partial_{,y})]$ to $[B'(\partial_{,r}, \partial_{,s})]$. The transformation of derivatives from one set of coordinates to another set is

accomplished by using the following relations

$$\begin{Bmatrix} \partial_{,r} \\ \\ \partial_{,s} \end{Bmatrix} = [J] \begin{Bmatrix} \partial_{,x} \\ \\ \partial_{,y} \end{Bmatrix} \tag{2.19}$$

or,

$$\begin{Bmatrix} \partial_{,x} \\ \\ \partial_{,y} \end{Bmatrix} = [J]^{-1} \begin{Bmatrix} \partial_{,r} \\ \\ \partial_{,s} \end{Bmatrix} \tag{2.20}$$

where [J] is the Jacobian or the transformation and is defined to be

$$[J] = \begin{bmatrix} \partial_{,r}\, x & \partial_{,r}\, y \\ \\ \partial_{,s}\, x & \partial_{,s}\, y \end{bmatrix} \tag{2.21}$$

Thus using eqs. (2.17) and (2.21), $[B']=[B'(\partial_{,r},\partial_{,s})]$ can be expressed as

$$[B'] = \begin{bmatrix} J^*_{11}\partial_{,r} + J^*_{12}\partial_{,s} & 0 \\ \\ 0 & J^*_{21}\partial_{,r} + J^*_{22}\partial_{,s} \\ \\ J^*_{21}\partial_{,r} + J^*_{22}\partial_{,s} & J^*_{11}\partial_{,r} + J^*_{12}\partial_{,s} \end{bmatrix} \tag{2.22}$$

where J^{*}_{ij} is $[J]^{-1}_{ij}$ (2.23)

Thus

$$\{\varepsilon(r,s)\} = [B'][H]\begin{Bmatrix} U_i \\ V_i \end{Bmatrix} \tag{2.24}$$

2. 2. 2. Formulation of the Stiffness Matrix [20,21]

2. 2. 2. 1. Minimum Potential Energy Principle

There are different variational principles used in Solids Mechanics, the one used in this program is called the "Minimum Potential Energy Principle". This principle can been stated as: The displacement (u,v,w) which satisfies the differential equations of equilibrium, and all the field boundary conditions, yields a smaller value for the potential energy than any other kinematically admissible displacement field. Mathematically we can state the principle as follows

$$\delta \Pi = \delta(U + V) = 0 \tag{2.25}$$

where Π is the potential energy, U is the strain energy, and δV is the negative work of the external loads.

The expressions for U and V in the linear case are

$$U = \frac{1}{2}\int_S \{\varepsilon\}^t\{\sigma\}dS \tag{2.26}$$

$$V = -\int_\Gamma \{t\}^t\{u\}d\Gamma \tag{2.27}$$

where $\{t\}^t = \{t_x, t_y\}$ is the surface traction vector with the body force considered equal to zero. The principle, eq. (2.25), can be rewritten now as

$$\delta(\frac{1}{2}\int_S \{\varepsilon\}^t[C]\{\varepsilon\}dS) = \delta(\int_\Gamma \{t\}^t\{u\}d\Gamma) \tag{2.28}$$

where [C] is the Hookean matrix of elastic constants.

2. 2. 2. 2. Integration of the Stiffness Matrix

Expression of the strain vector in eq. (2.28) in terms of the displacements in eq. (2.23) yields

$$\delta(\frac{1}{2}\int_{-1}^{+1}\int_{-1}^{+1}\{U_i\}^t[H]^t[B']^t[C][B'][H]\{U_i\}|J|drds) = \delta(\int_\Gamma \{t\}^t\{U_i\}d\Gamma) \tag{2.29}$$

where

$$|J|drds = dxdy = dS \tag{2.30}$$

The above equation is a quadratic form of the displacements, and its first variation with respect to the displacements yields

$$[S]\{U_i\}_s = \{P\} \quad \text{for } i = 1,2, \ldots ,n \tag{2.31}$$

where n is the total number of degrees of freedom of the structure, [S] is the stiffness matrix, and {P} the generalized load vector.

In order to integrate the stiffness matrix, the STAP program use a Gaussian integration scheme [21], with 2 points in each direction. Integration using a 3x3 quadrature scheme was found to result in a high stiffness for the structure tested in this study.

2. 2. 2. 3. Linear Constitutive Law

The program has the option of analysing a structure for either plane stress or plane strain. The generalized stress-strain matrix for the plane stress case is

$$[C] = \frac{E}{1-\nu^2} \begin{bmatrix} 1 & \nu & 0 \\ \nu & 1 & 0 \\ 0 & 0 & \frac{1-\nu}{2} \end{bmatrix} \tag{2.32}$$

and for the plane strain case is

$$[C] = \frac{E(1-\nu)}{(1-2\nu)(1+\nu)} \begin{bmatrix} 1 & \frac{\nu}{1-\nu} & 0 \\ \frac{\nu}{1-\nu} & 1 & 0 \\ 0 & 0 & \frac{1-2\nu}{2(1-\nu)} \end{bmatrix} \tag{2.33}$$

where E is the Young's modulus of elasticity and ν is the Poisson's ratio.

2. 2. 2. 4. Non-Linear Constitutive Law

With a view to assessing the effect of material non-linearity on the stress distribution, it is necessary to have a non-linear constitutive material law. There are different ways of describing non-linear material behavior. The Ramberg-Osgood is a three-parameter law that expresses the uniaxial strain as a non-linear function of the uniaxial stress, and may be written as

$$\varepsilon = \frac{\sigma}{E'} + K'\left(\frac{\sigma}{E'}\right)^{n'} \qquad (2.34)$$

where E', K', and n' are the three parameters of the law. Figure 2.3 shows an example of this law.

In this program a modification of the Ramberg-Osgood law was used. Inverting eq. (2.34), the stress can be expressed as a non-linear function of the strain such that

$$\sigma = E\varepsilon - K(E\varepsilon)^{n} \qquad (2.35)$$

or

$$\sigma = \left(E - KE(E\varepsilon)^{n-1}\right)\varepsilon \qquad (2.36)$$

Figure 2.4 shows experimental data points [9] for the FM-73

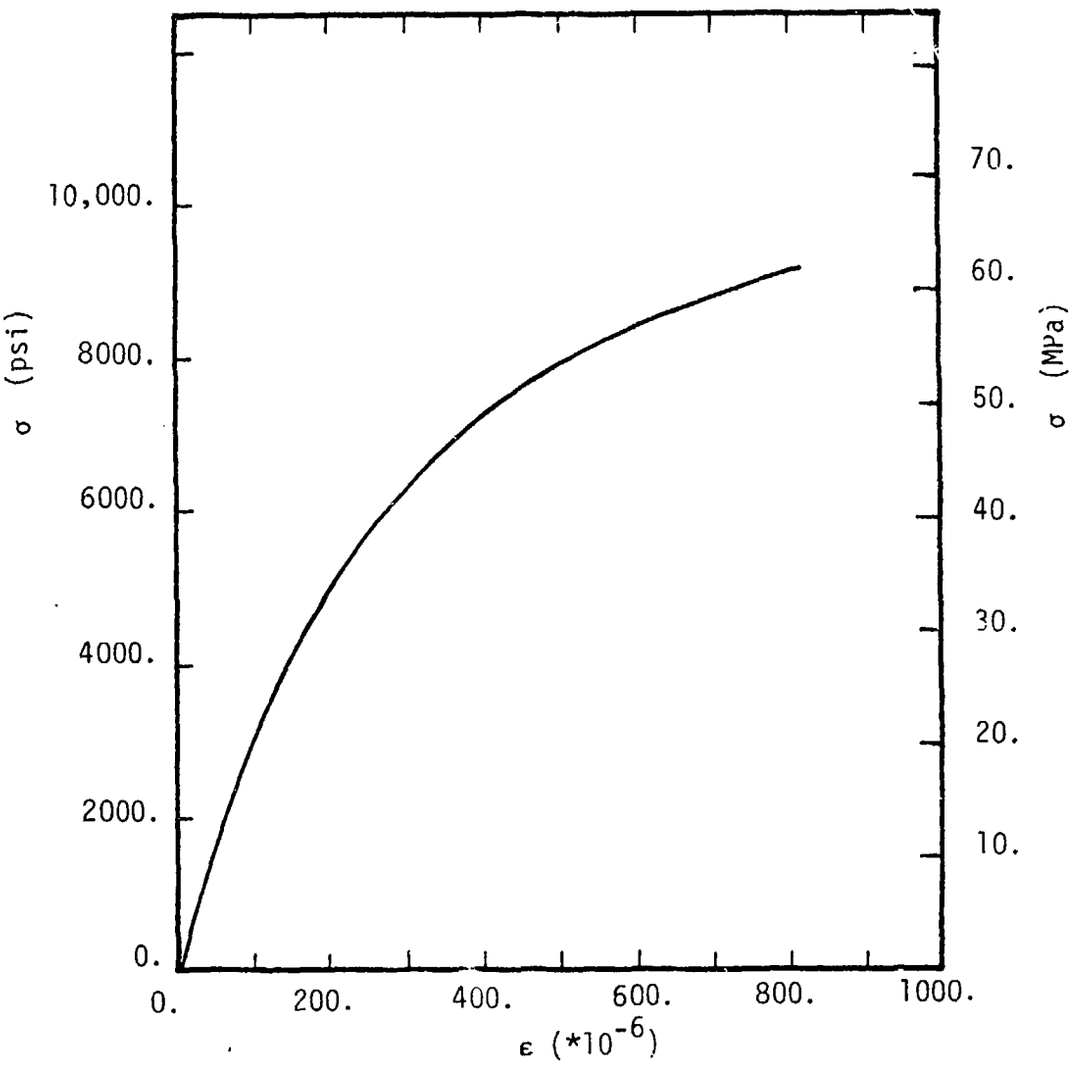

Figure 2.3: Hypothetical Uniaxial Stress-Strain Curve Fitted with the Ramberg-Osgood Law, $E' = 29.5\ 10^6$ psi (203,402 MPa), $n' = 5.049$, and $K' = 26{,}200$.

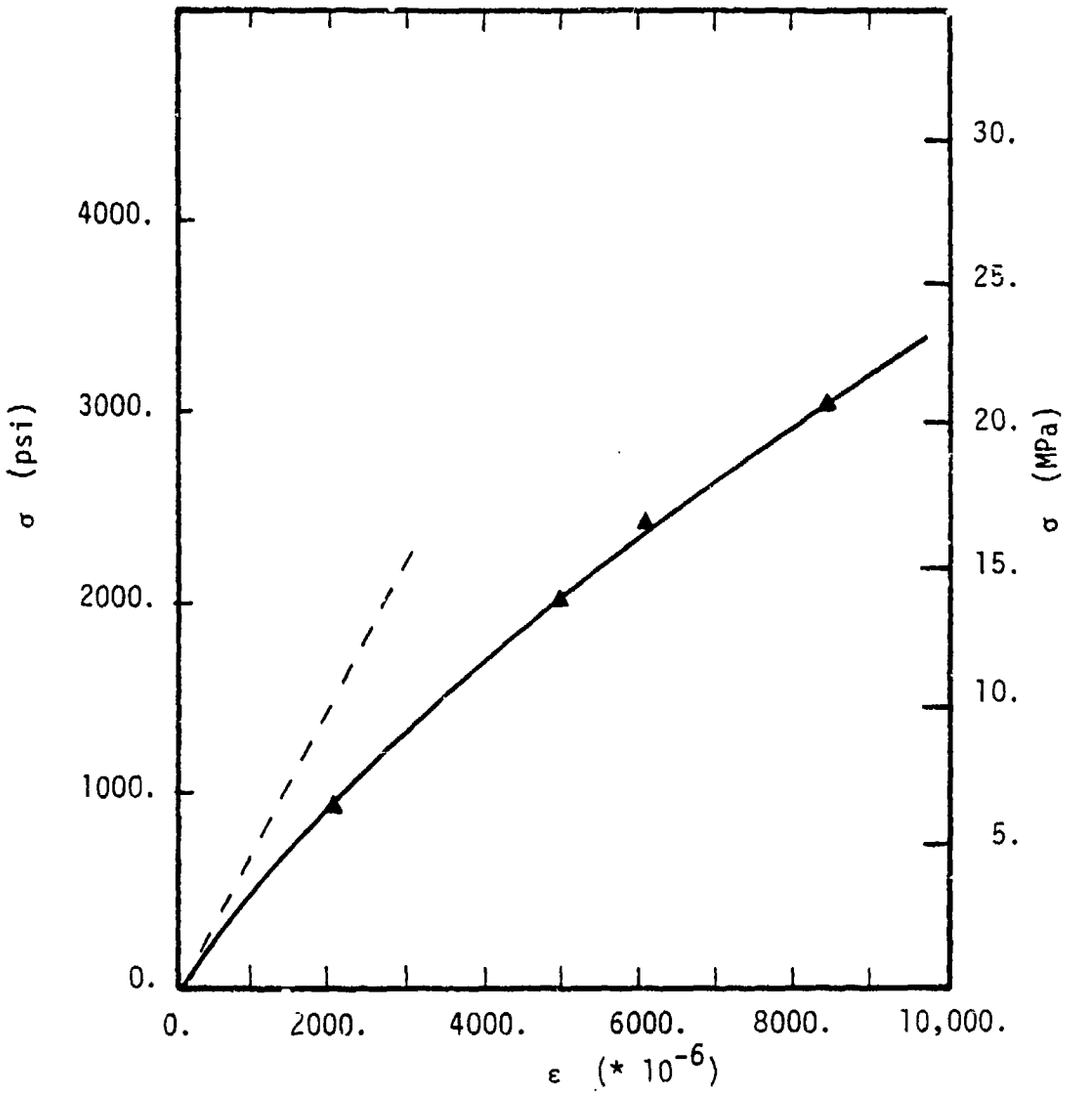

Figure 2.4: Uniaxial Stress-Strain Curve,
▲: Creep Data T = 30°C, Time = 1 minute [9]
Parameters of the Ramberg-Osgood Law: E = 725,000 psi (4999 MPa), K = 64.01, n = 1.75.
Parameters of eq. (2.35): E = 725,000 psi (4999 MPa), K = 0.04063, n = 1.287 .

fitted by the Ramberg-Osgood law and the law given by eq. (2.35).

In the Ramberg-Osgood equation, K' and n' are unitless. In eqs. (2.35) and (2.36) n is also unitless. However, K has the unit $(psi)^{-(n-1)}$, $(6895\ Pa)^{-(n-1)}$.

Generalization to Two Dimensions

The generalization of the law to two dimensions is based on the following hypotheses

1) The Poisson ratio stays constant under any loading.
2) The principal axes of the material corresponds to the principal strain axes.

From these hypotheses we can derive the stress-strain relationship. Eq. 2.32 can be generalized as

$$\{\sigma_{1x}\} = [C_{Tot}]\{\varepsilon_1\} \tag{2.37}$$

where $\{\varepsilon_1\}$ is the principal strain vector, $\{\sigma_{1x}\}$ is the corresponding stress vector, and $[C_{Tot}]$ is defined as

$$[C_{Tot}] = [C] + [C_{nl}] \tag{2.38}$$

$[C_{Tot}]$ is the generalized non-linear Hooke's matrix, and is defined in the principal strain axes. [C] is defined by eqs. (2.32) or (2.33), and $[C_{nl}]$ is the non-linear portion of the total stiffness matrix.

Using the transformation defined in Fig. 2.5, eq. (2.37) can be expressed in the x,y system of axes as

$$[T]\{\sigma_x\} = [C_{Tot}][R][T][R]^{-1}\{\varepsilon_x\} \tag{2.39}$$

where

$$[T] = \begin{bmatrix} c^2 & s^2 & 2sc \\ s^2 & c^2 & -2sc \\ -sc & sc & c^2-s^2 \end{bmatrix} \tag{2.40}$$

$c = \cos\theta$

$s = \sin\theta$

$$[R] = \begin{bmatrix} 1 & 0 & 0 \\ 0 & 1 & 0 \\ 0 & 0 & 2 \end{bmatrix} \tag{2.41}$$

Eq. 2.39 can also be put in the following form

$$\{\sigma_x\} = [T]^{-1}[C_{Tot}][R][T][R]^{-1}\{\varepsilon_x\} \tag{2.42}$$

In the plane stress case $[C_{nl}]$ is defined as

$$[C_{nl}] = K \frac{E^n}{1-\nu^2} \begin{bmatrix} A & B & 0 \\ B & C & 0 \\ 0 & 0 & 0 \end{bmatrix} \tag{2.43}$$

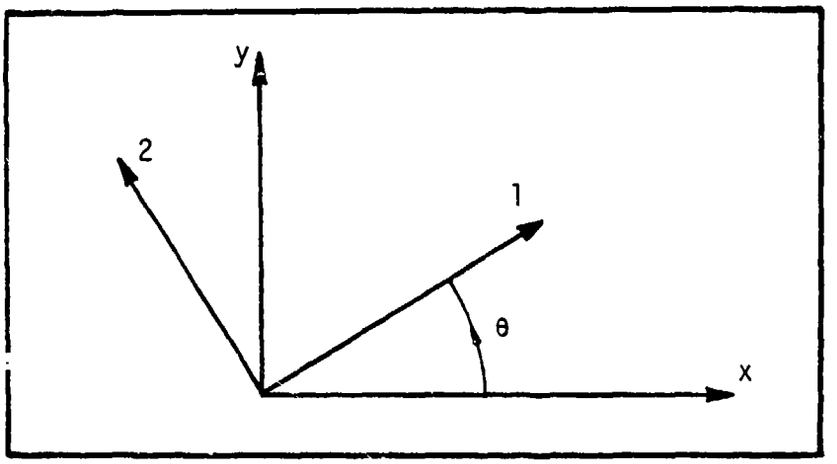

Figure 2.5: Positive Transformation from the (x,y) Axes to the (1,2) Axes.

where

$$A = \varepsilon_1^{n-1}$$

$$B = \nu(\sqrt{\nu|\varepsilon_1\varepsilon_2|})^{n-1}$$

$$C = \varepsilon_2^{n-1}$$

and in the plane strain case

$$[C_{nl}] = H \begin{bmatrix} A' & B' & 0 \\ B' & C' & 0 \\ 0 & 0 & 0 \end{bmatrix} \qquad (2.44)$$

where

$$A' = \varepsilon_1^{n-1}$$

$$B' = \frac{\nu}{1-\nu}(\sqrt{\frac{\nu}{1-\nu}|\varepsilon_1\varepsilon_2|})^{n-1}$$

$$C' = \varepsilon_2^{n-1}$$

$$H = K\frac{E^n(1-\nu)}{(1-\nu)(1-2\nu)}$$

Generalization of terms $[C_{nl}]_{11}$ and $[C_{nl}]_{22}$ from eq. (2.36) is straightforward. The terms $[C_{nl}]_{12}$ and $[C_{nl}]_{21}$ are subject to two requirements

1) Energy considerations require a symmetry in the $[C_{Tot}]$ matrix. This requirement forces symmetry in ε_1 and ε_2 in the $[C_{nl}]_{12}$ and $[C_{nl}]_{21}$ terms.

2) In the low loading case, our assumption of isotropy implies that the strain vector for plane stress

$$\{\varepsilon\}^t = \{\varepsilon, -\nu\varepsilon, 0\}$$

and the strain vector for plane strain

$$\{\varepsilon\}^t = \{\varepsilon, -\frac{\nu}{1-\nu}\varepsilon, 0\}$$

must result in a stress σ_y equal to zero.

Note that eqs (2.43) and (2.44) satisfy these requirements.

2. 2. 2. 5. Application of the Non-Linear Law

The non-linear law discussed in the preceding section was evaluated for a polyvinyl chloride copolymer using data given in [24] for uniaxial and biaxial states of stress. The object was to reproduce their biaxial results based only on the material behavior in the uniaxial testing. Figure 2.6 shows the uniaxial stress strain relationship. The triangles are data points coming from reference [24], and the experimental value can be fitted with the eq. (2.35) where E, n, and K take the following values

E = 500000. psi, (3447. MPa)

n = 1.56

K = 0.00147 $\text{psi}^{-0.56}$ ($1.04\ 10^{-5}\ \text{Pa}^{-0.56}$).

Table 2.1 shows the comparison between experimental and theoretical results. The formulation of the non-linear law is given in eqs (2,38) and(2,44). The Young's modulus

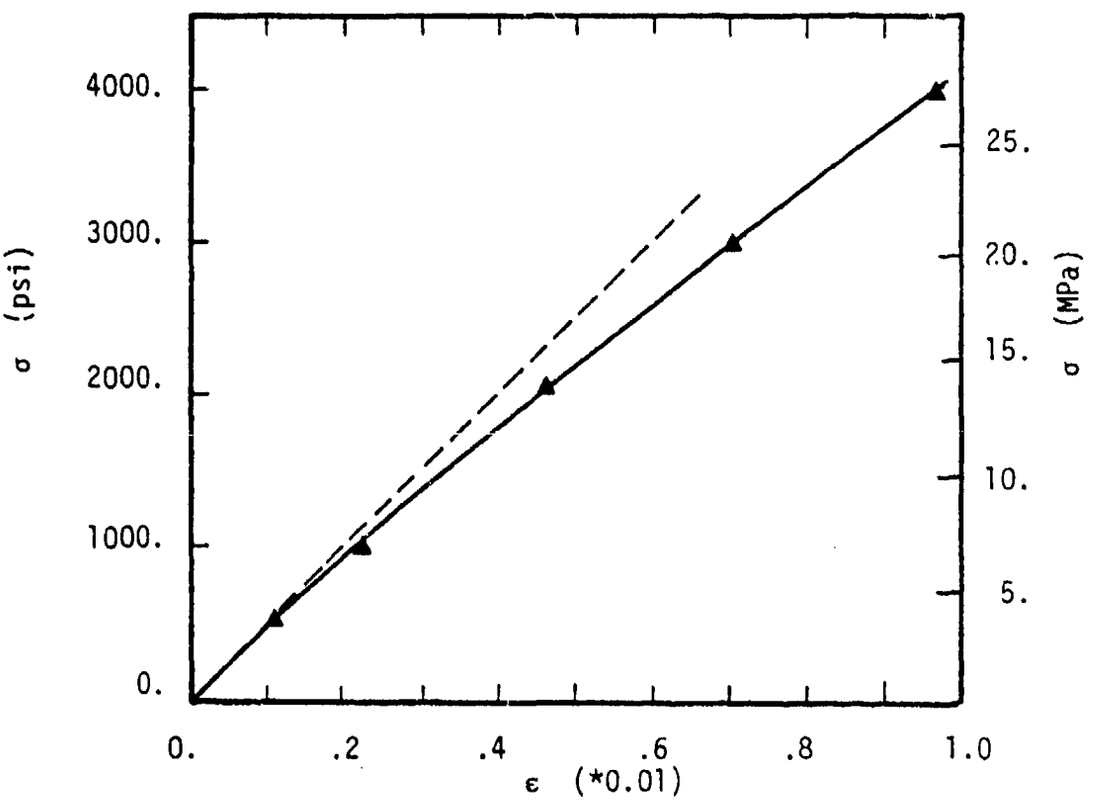

Figure 2.6: Uniaxial Stress-Strain Curve for Polyvinyl Chloride [24].

Table 2.1: Comparison Between Experimental and Predicted Stresses for Different Constitutive Laws.

EXPERIMENTAL [24]				ERRORS IN PREDICTED STRESSES COMPARED TO THE APPLIED STRESSES					
APPLIED STRESSES		MEASURED STRAINS		NON-LINEAR MODEL		FIRST LINEAR MODEL		SECOND LINEAR MODEL	
σ_x psi	τ_{xy} psi	ϵ_x %	γ_{xy} %	$\Delta\sigma_x$ %	$\Delta\tau_{xy}$ %	$\Delta\sigma_x$ %	$\Delta\tau_{xy}$ %	$\Delta\sigma_x$ %	$\Delta\tau_{xy}$ %
875.	1508.	0.21	0.95	0.10	0.60	17.0	15.0	3.50	5.30
960.	880.	0.22	0.56	1.40	3.60	15.0	16.0	5.60	4.30
1075.	2543.	0.36	1.60	2.30	2.90	22.0	19.0	0.60	1.90
1500.	1405.	0.35	0.88	1.20	1.60	16.0	14.0	4.40	5.80
2190.	1150.	0.51	0.73	2.10	0.90	15.0	16.0	5.00	4.60
2800.	2625.	0.73	1.80	1.30	0.10	30.0	27.0	7.40	4.30
3000.	1405.	0.72	0.92	1.40	1.00	20.0	20.0	1.10	1.50
4000.	1875.	1.00	1.30	1.80	1.10	26.0	24.0	3.00	3.00

$$\Delta\sigma_x = \left| \frac{\sigma_{xa} - \sigma_{xp}}{\sigma_{xa}} \right|$$

$$\Delta\tau_{xy} = \left| \frac{\tau_{xya} - \tau_{xyp}}{\tau_{xya}} \right|$$

$(\sigma_{xa}, \tau_{xya})$ are the applied stresses.

$(\sigma_{xp}, \tau_{xyp})$ are the predicted stresses.

for the first and second linear laws are equal to 500,000 psi (3447 MPa) and 412,000 psi (2841 MPa), respectively. The stresses evaluated using the non-linear law were, in general, closer to experimental results than those found using the linear laws. Only with the second linear law were the results less in error for a few isolated measurements. Nevertheless, the maximun errors on the stresses using the non-linear model were smaller than the errors using the linear models.

2. 2. 2. 6. Newton-Raphson Method

In order to solve the non-linear elastic problem the Newton-Raphson method [25] was implemented in the program. This iterative method is schematicaly explained in Fig. 2.7.

The stiffness matrix S_o is approximated at the origin by its tangent as shown in Fig. 2.7 and the displacement Δd_0 is computed by the equation

$$\{\Delta d_0\} = [K_0]^{-1}\{P^*\} \tag{2.45}$$

The strains $\{\varepsilon_1\}$ are computed from the displacements $\{d_1\} = \{\Delta d_0\}$ and then the stresses $\{\sigma_1\}$ are computed using the the non-linear constitutive law given in section 2.2.2.4. . The load vector $\{P_1\}$ corresponding to the internal work is derived from the gradient of the strain

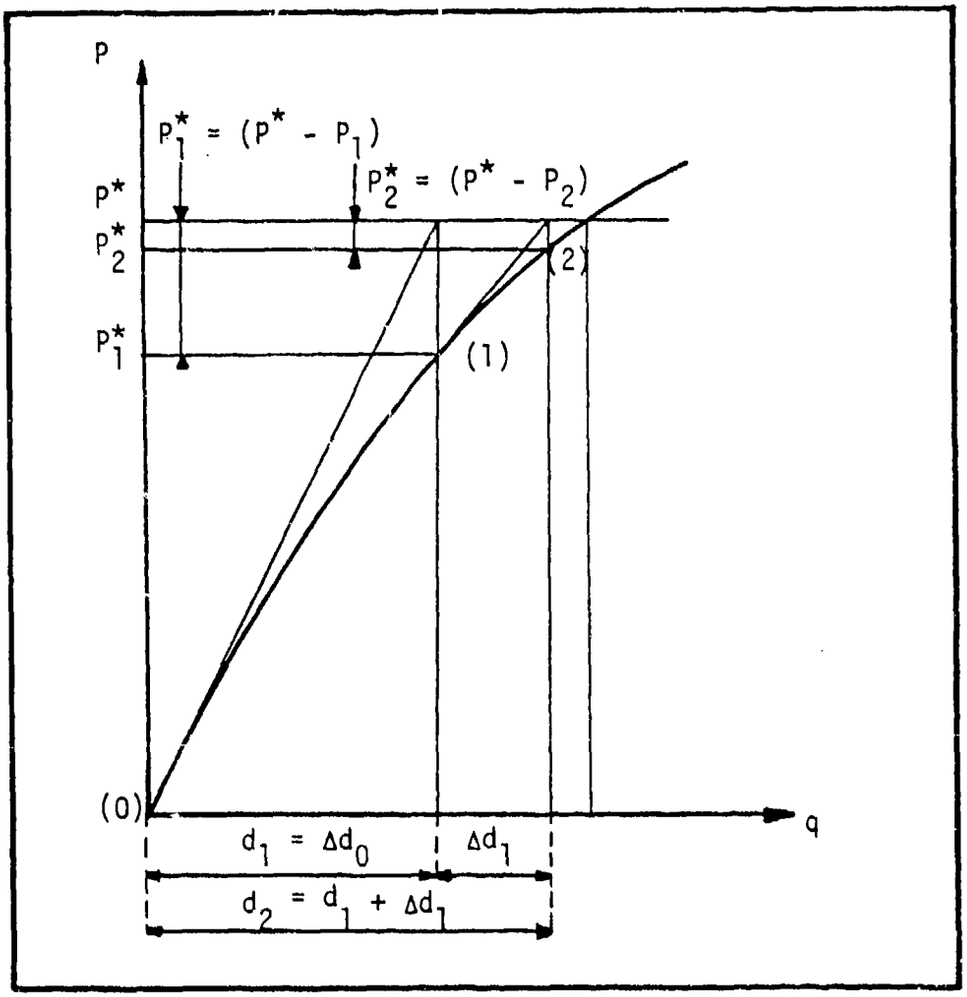

Figure 2.7: Graphical Representation of the Newton-Raphson Method.

energy with respect to the displacement vector. We can express the strain energy gradient as

$$\frac{\partial \Pi}{\partial q} = 0 \quad \rightarrow \frac{\partial U}{\partial q} = -\frac{\partial V}{\partial q} = \{P_i\} \tag{2.46}$$

where U for a non-linear material can be written as

$$U = \int_V \left(\int_0^{\varepsilon} \sigma d\varepsilon \right) dV \tag{2.47}$$

For a corresponding $\{\sigma_1\}$, $\{\varepsilon_1\}$ stress-strain state we can write

$$\frac{\partial U}{\partial q} = \frac{\partial}{\partial q} \left(\int_V \int_0^{\varepsilon_1} \sigma d\varepsilon dV \right) = \{P_1\} \tag{2.48}$$

At the point (1) shown in Fig. 2.7, the same procedure is repeated but $\{P^*\}$ is replaced by $\{P_1^*\} = \{P^* - P_1\}$, a new tangent stiffness matrix $[S_1]$ is derived and $\{\Delta d_1\} = [S_1]^{-1}\{P_1^*\}$. The total displacement at the point (2) is $\{d_2\} = \{d_1\} + \{\Delta d_1\}$. From $\{d_2\}$ we can compute the strains, and the process can be repeated to any desired accuracy.

Two convergence criteria were used in the program. The first was on the norm of the change in the stresses and the second on the norm of the residual load $\{P_i^*\}$. These criteria will be further discussed in section 2.3.3.

2. 3. Finite Element Implementation

This section provides a brief description of the original STAP program as well the modified STAP program including the linear isoparametric element and the non-linear material law. A brief decription of the main routine will be given and the input data will be explained.

2. 3. 1. STAP Computer Code

Because a detailled description of the STAP program can be found in reference [21], it is sufficient to emphasize only the important features here.

1) The STAP program constructs, assembles, and inverts the stiffness matrix in the core of the computer. This procedure increases the speed of the program by eliminating the reading and writing on temporary disks or tapes, but reduces the size of problem that can be solved. Nevertheless the memory space available at VPI&SU was 5000 Kb and was sufficient for the problem analyzed in this study.

2) Nearly all the variables used in the program are stored in a vector A. This method of storage

easily permits an increase or decrease of the storage capacity of the program. Because the vector A is used to store different quantities, an elaborate addressing scheme is required.

Figure 2.8 shows the flow chart of the STAP program.

Explanation of the main routines are given below.

INPUT

* Read and print the title.
* Read and print the control card.
* Set up the memory space.
* Read, generate, and print nodal input.

LOADS

* Read, generate, and print load input.

ELCAL

* Read and print material input.
* Read and print the element input.
* Store information on a temporary disk.

ADDRES

* Set up an allocation vector (MAXA) that addresses the diagonal elements of the assembled stiffness matrix. It is then used in the LDL^t decomposition of the stiffness matrix.

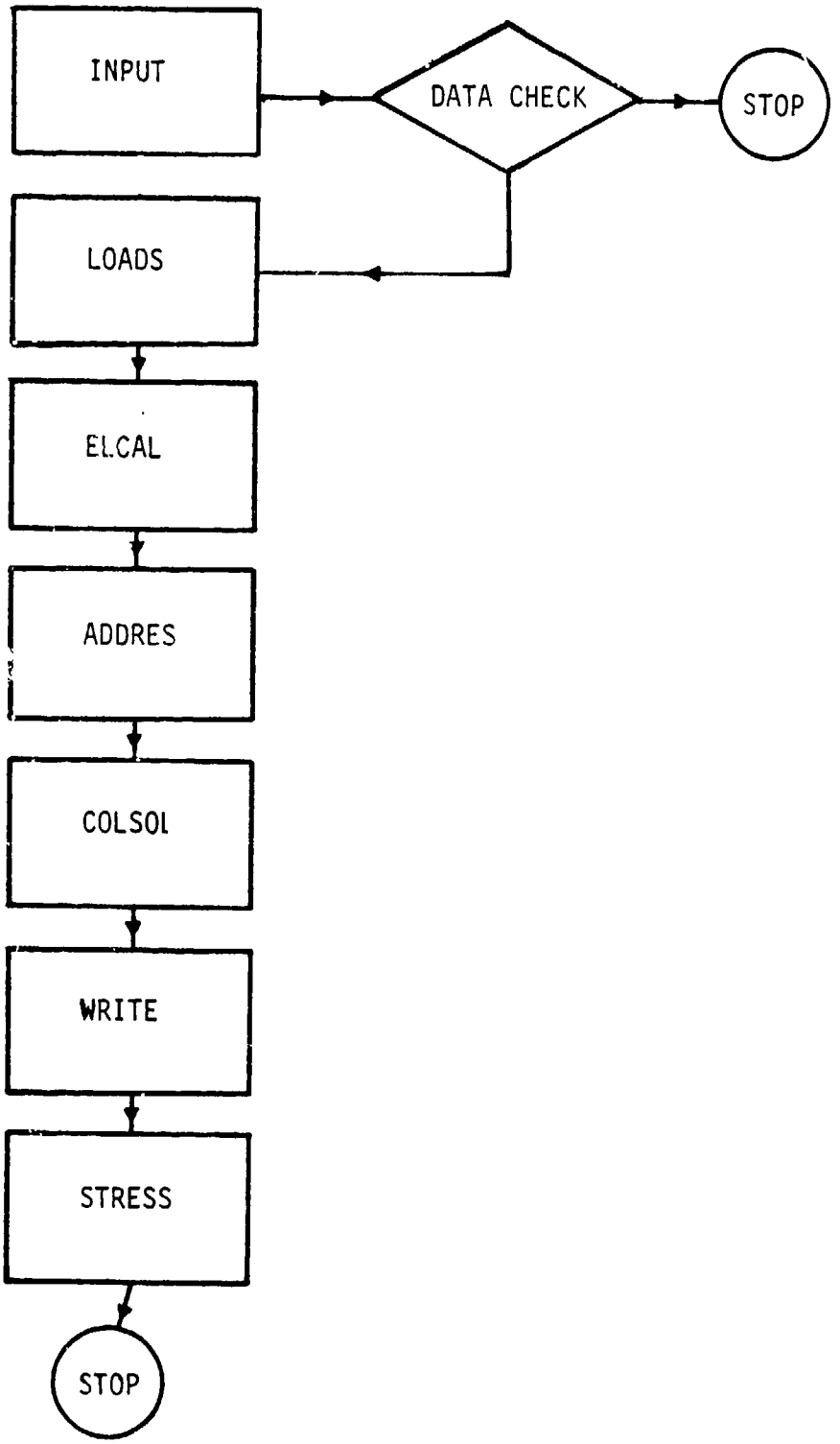

Figure 2.8: Flow Chart of the STAP Program.

ASSEM

* Generate the stiffness matrix for each element.
* Assemble the stiffness matrix for the structure.

COLSOL

* Perform the LDL^t decomposition of the stiffness matrix.
* Perform the forward and the back substitution.

WRITE

* Print the displacements.

STRESS

* Compute the strains from the displacements.
* Compute the stresses from the strains.
* Print the strains and stresses.

Subroutines ELCAL, ASSEM, and STRESS call routine ELEMNT with a parameter ITYP which refers to the element type.

In the original STAP program there was only one element in the library, namely a truss element. The truss element of the original STAP program was replaced by the linear and non-linear eight noded isoparametric element described earlier.

2. Solution Algorithm

Linear Material Behavior

The subroutine associated with the eight noded isoparametric element is called EIGHT2. The main program calls this routine at different times through EIGHT1 and ELEMNT. The routine EIGHT1 sets up the memory space inside the vector A. The EIGHT2 routine is divided into three parts, called by ELCAL, ASSEM, and STRESS, respectively. These different parts are explained below

Part one

* Read and print material input.
* Generate the plane stress or strain matrices.
* Read and print element input.
* Generate connectivity array.

Part two

* Generate and integrate the stiffness matrix for each element.
* Call routine ADBAN (ADBAN routine assembles and stores the stiffness matrix).

Part three

* Compute the strains and stresses at each Gauss point of each element.
* Print the strains and stresses.

2. 3. 3. Solution Algorithm with Non-Linear Material Behavior

The main change in this version of the program resides in part three of the routine EIGTH2. Figure 2.9 shows the algorithm of the non-linear program with the implementation of the Newton Raphson method and the non-linear law.

At first the program constructs the stiffness matrix as if the material were linear, i.e., parameter K in eq. (2.34) is equal to zero. Then it computes the displacements.

When the program reaches part three of subroutine EIGTH2, it computes the strains and the stresses with the non-linear law. The program enters into a loop for the non-linear iterations. The first step is to compute the residual load vector and tests its norm to see if it meets the convergence criterion. The norm used in this program is given in the following equation:

$$P111 = \sum_i \frac{|P_i^0 - P_i^j|}{P_T} \qquad (2.49)$$

where P_i^0 is the initial load corresponding to the i^{th} degree of freedom, P_i^j is the load corresponding to the i^{th} degree of freedom at the iteration j, and

$$P_T = \sum_i |P_i^0|.$$

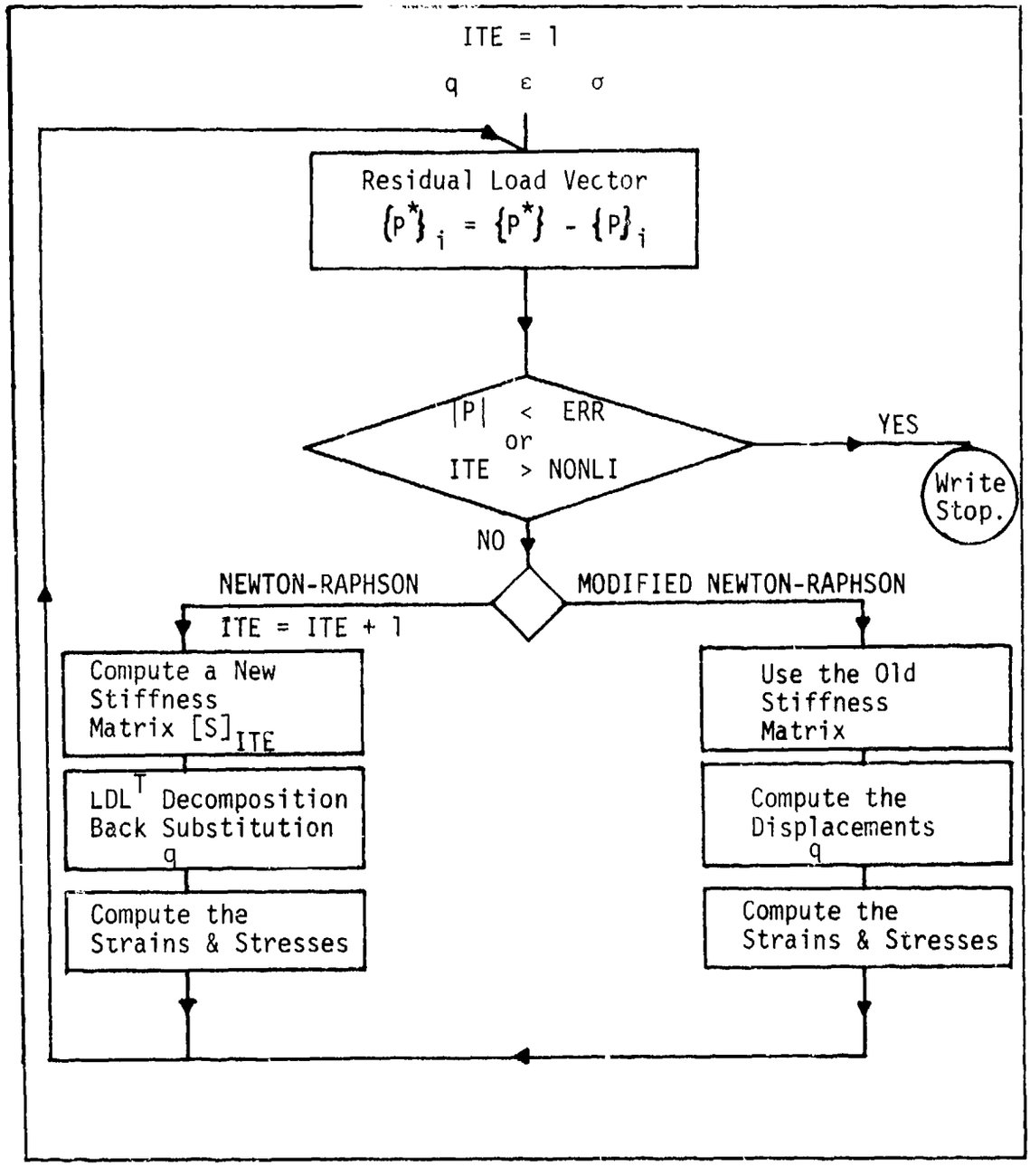

Figure 2.9: Flow-Chart of the Non-Linear Program.

If P111 is smaller than the value ERR specified in the input, the program terminates the iterations and prints the displacements, the strains, and the stresses, and stops. If P111 is larger than ERR, the program will continue until a specified maximum the number of iterations. The term P111 may be interpreted as a norm that measures the satisfication of the equilibrium.

At this point the program has two options that users must specify as input. In the first option, after each iteration the program will compute a new stiffness matrix with the strains of the preceding iteration. Then it will compute the displacements, the strains, and the stresses. This procedure will be repeated until the convergence criterion is satisfied. This procedure is called the Newton Raphson method which was illustrated in Fig.2.7. With the second option, the program uses the old stiffness matrix instead of computing a new one after each iteration. This method is called the modified Newton-Raphson method which is shown in Fig. 2.10. The number of iterations for this method is usually larger than for the first option but the fact that the program does not have to compute the stiffness matrix every time increase the speed of the program.

Figure 2.10 shows a comparison between the two methods.

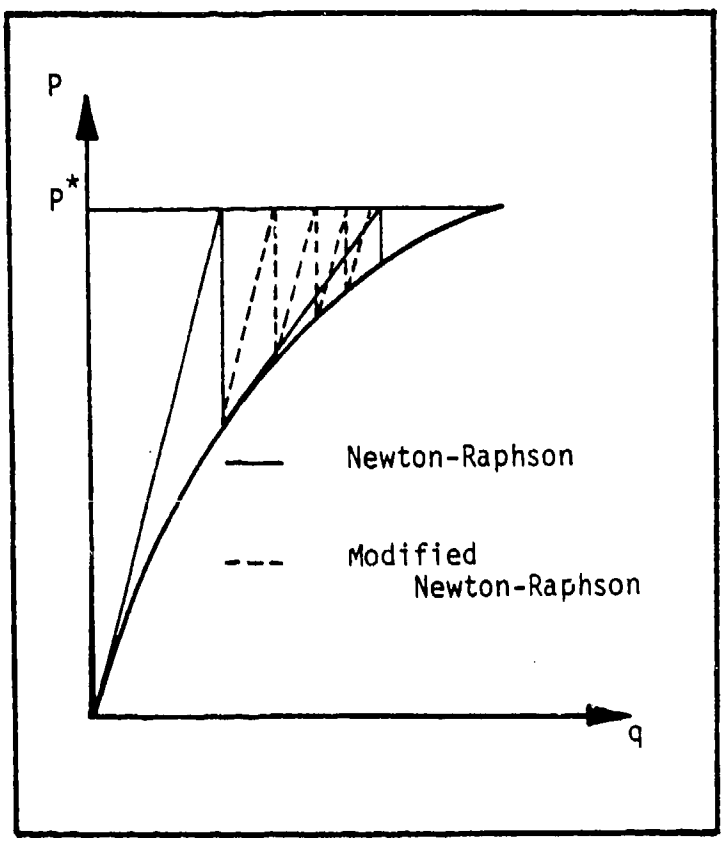

Figure 2.10: Comparison Between Newton-Raphson and Modified Newton-Raphson Methods.

2. 4. Tests of the Program

Several test cases were used in order to verify the program. For clarity of the text, only three of them are presented in this chapter but another one will be present in the next chapter. The purpose of this testing were to compare finite element results and to look at the effects of a change in element configuration (aspect ratio ,midsize node . . .) on the stresses.

2. 4. 1. Effect of the Midside Node Position

In reference [18] the authors show that the eight noded isoparametric element can be used as a singular element. By placing the midside nodes adjacent to a corner at one quarter of the length of the side from the corner as shown in Fig. 2.11, a singularity at the corner can be simulated. With this geometry, the determinant of the Jacobian can be shown to be

$$|J| = f(\frac{1}{r^n}) \quad ,n = 0.5 \tag{2.50}$$

where r is the distance from the corner. This configuration has been used at the reentrant corner of the bonded joints analyzed in the present research.

It appeared appropriate to test the element by

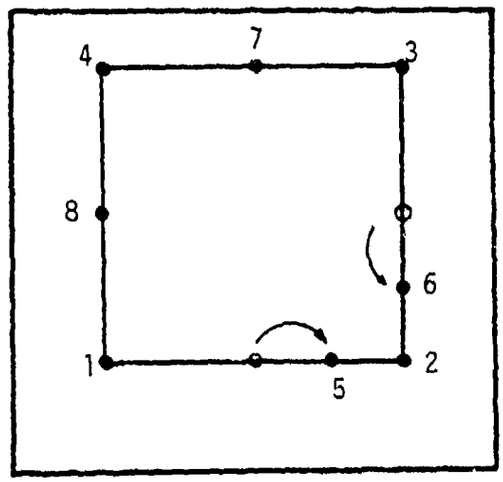

Figure 2.11: Element Configuration With a Singular Jacobien Along the Boundaries 1-2 and 2-3.

displacing the midside nodes and to determine the resulting effects on the stresses. Figure 2.12 shows the element configuration, the boundary conditions, and the loading.

The material properties used were:

$E = 725{,}000$ psi, (4999 MPa),

$\nu = .33$

The midside nodes 5 and 7 were placed in position a, b, c, d, and e, respectively. The loading P was 60 psi (413 MPa) in the x direction. $\{\sigma\}$ and $\{\varepsilon\}$ were constant inside the element and had the exact same value for the different element configurations and were

$$\sigma_x = 60 \text{ psi, (413 KPa)}, \qquad \sigma_y = \tau_{xy} = 0.$$

$$\varepsilon_x = 8.276\ 10^{-5} \qquad \varepsilon_y = -2.731\ 10^{-5} \qquad \gamma_{xy} = 0.$$

which corresponds to the exact solution.

2. 4 .2. Effect of the Aspect Ratio on the Stresses

The aspect ratio of the element can influence the accuracy of the results. Specifically the coefficients of the stiffness matrix are functions of the aspect ratio of the element, and if the aspect ratios are too large, or they are of differing order of magnitude, the stiffness matrix is likely to become ill-conditioned.

To test the influence of the aspect ratio on the

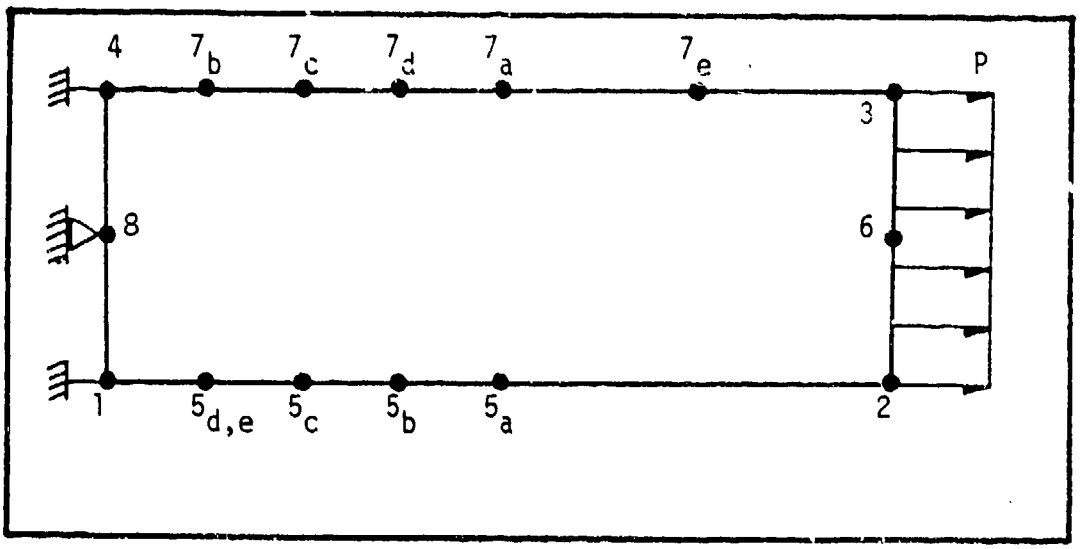

Figure 2.12: Test 1 Element Configuration.

stresses, a cantilever beam was discretized in three different ways by increasing the aspect ratio sequentially from 1/100 to 1/1000. The objective of this test was to determine the loss of precision in the calculated stresses as the aspect ratio of the element is increased. Figure 2.13 shows the three different meshes used, with the boundary conditions and the loading. The three meshes have one element over the length of the beam and one, two, and ten elements across the thickness, respectively. The aspect ratio of the element was 1/100 in the first mesh, 5/1000 for the second mesh, and 1/1000 for the last mesh. The finite element results were compared with a closed form elasticity solution given in reference [26].

Figures 2.14 and 2.15 show a comparison of the stress distributions at the section AA' (Fig. 2.13) between the finite element analysis and the closed form solution. The stresses were non-dimensionalized by dividing them by

$$p = \frac{A}{P}$$

where P is the applied load and A the area cross section of the beam.

The results indicated that even for the third test with an aspect ratio of 1/1000 the results are accurate enough to insure that this configuration can be used in a mesh. However in checking for equilibrium the norm of the residual does appear to be influenced by the aspect ratio.

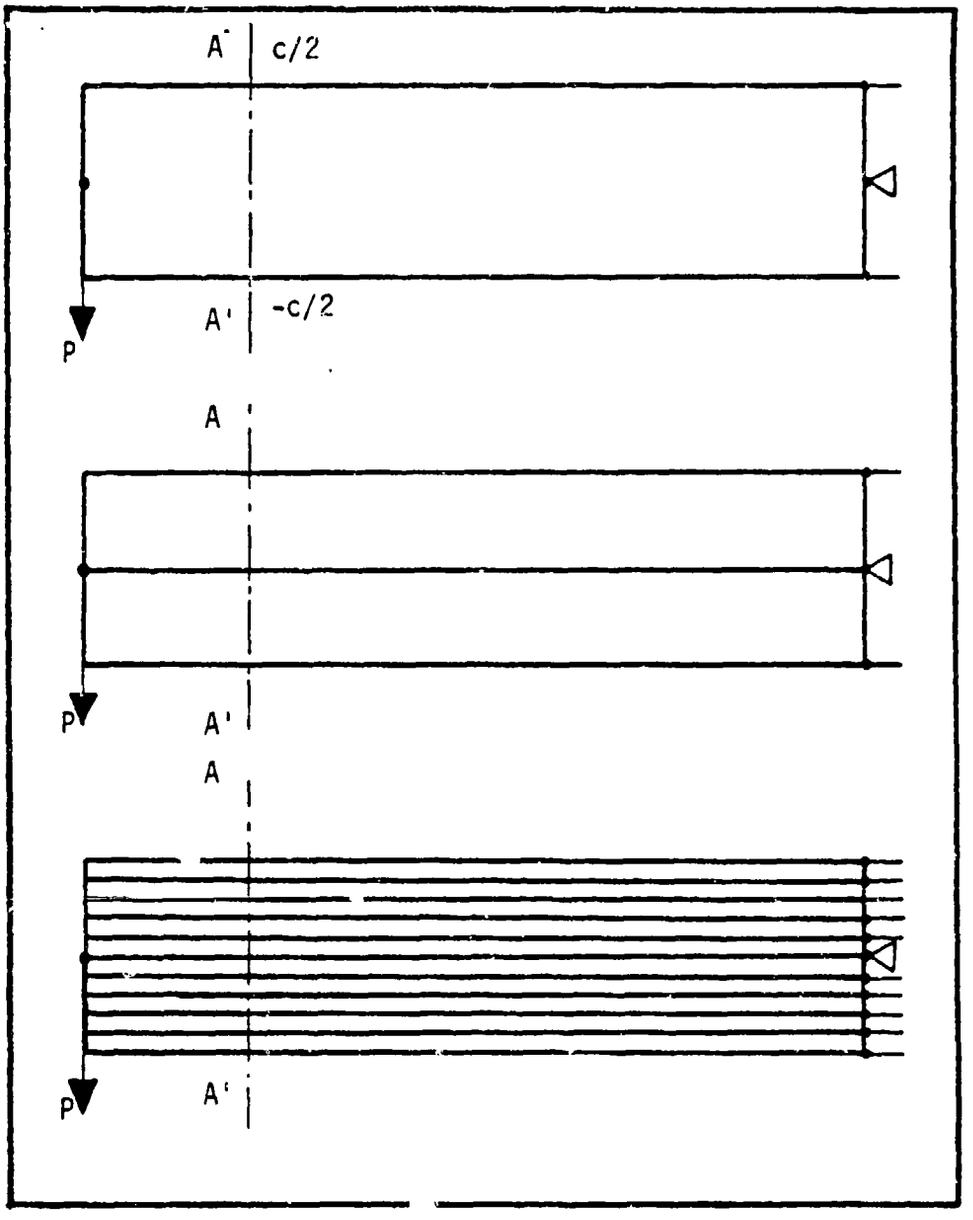

Figure 2.13: Test 2 Element Configuration.

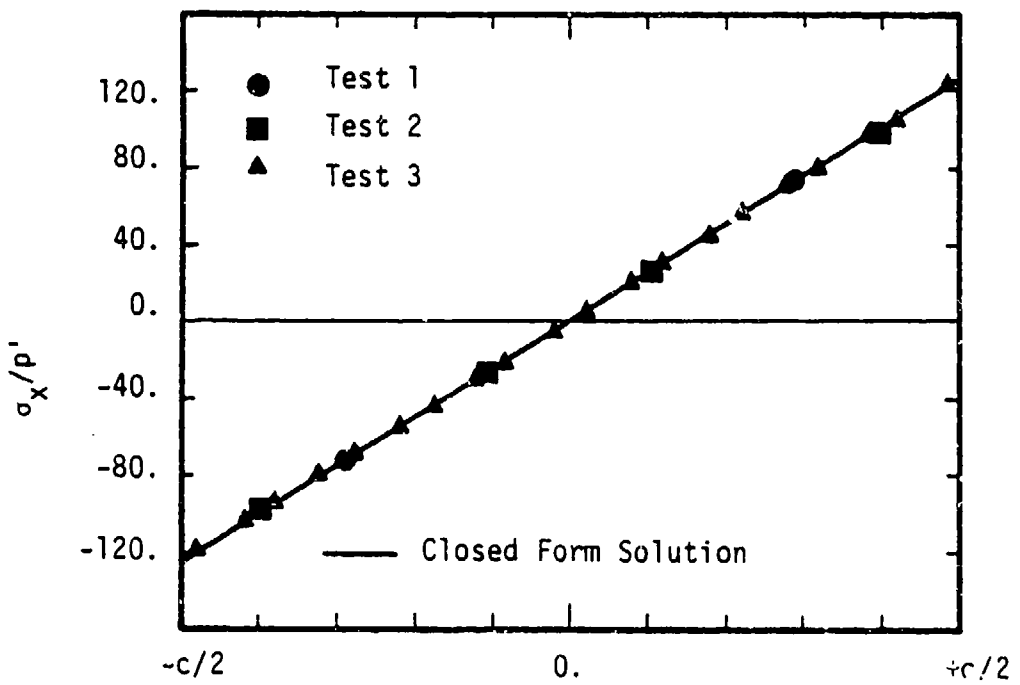

Figure 2.14: σ_x Distribution in Section AA', Comparison Between a Closed Form Solution and a Finite Element Analysis.

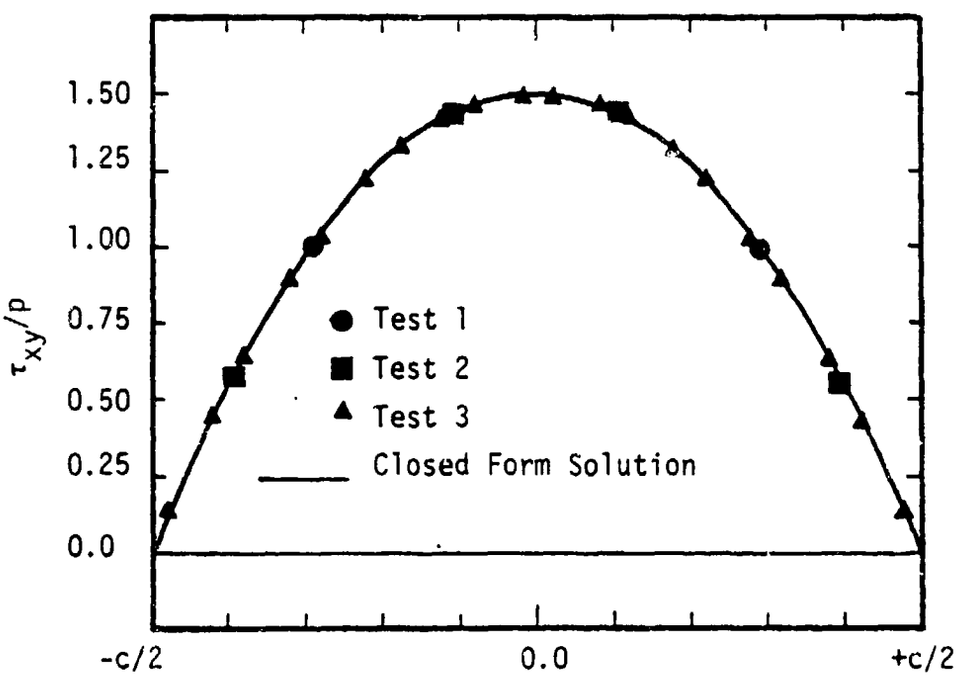

Figure 2.15: τ_{xy} Distribution in Section AA' Comparison Between a Closed Form Solution and a Finite Element Analysis.

Thus, in practice a low aspect ratio should be used if possible.

2. 4 .3. Verification that Equilibrium is Satisfied

The objective of the last test was to verify the satisfaction of the equilibrium inside a structure with linear and non-linear materials. The structure is a plate with a central hole and loaded in the y direction as shown in Fig. 2.16. Due to the symmetry of the problem, we need analyze only one quarter of the plate. The mesh has forty-six elements with one hundred and sixty-nine nodes. The integration of σ_y along the section AA' must be equal to the total load P. Figure 2.17 is the plot of σ_{yl} in the linear case, σ_{ynl} in the non-linear case, and σ_{ya} the average $\sigma_y = \frac{P}{l_1}$ The errors between σ_{ya}, σ_{yl}, and σ_{ynl} are in the range of less than 1/1000.

2. 5. Input of the Program

There are six different sets of input cards which are

1) Title.

2) Control card.

3) Nodal information.

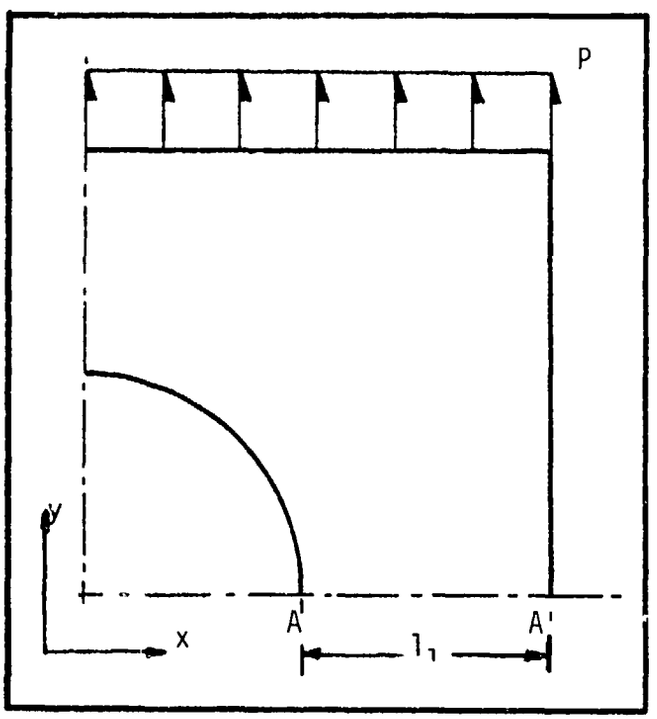

Figure 2.16: Test 3 Geometry and Loading.

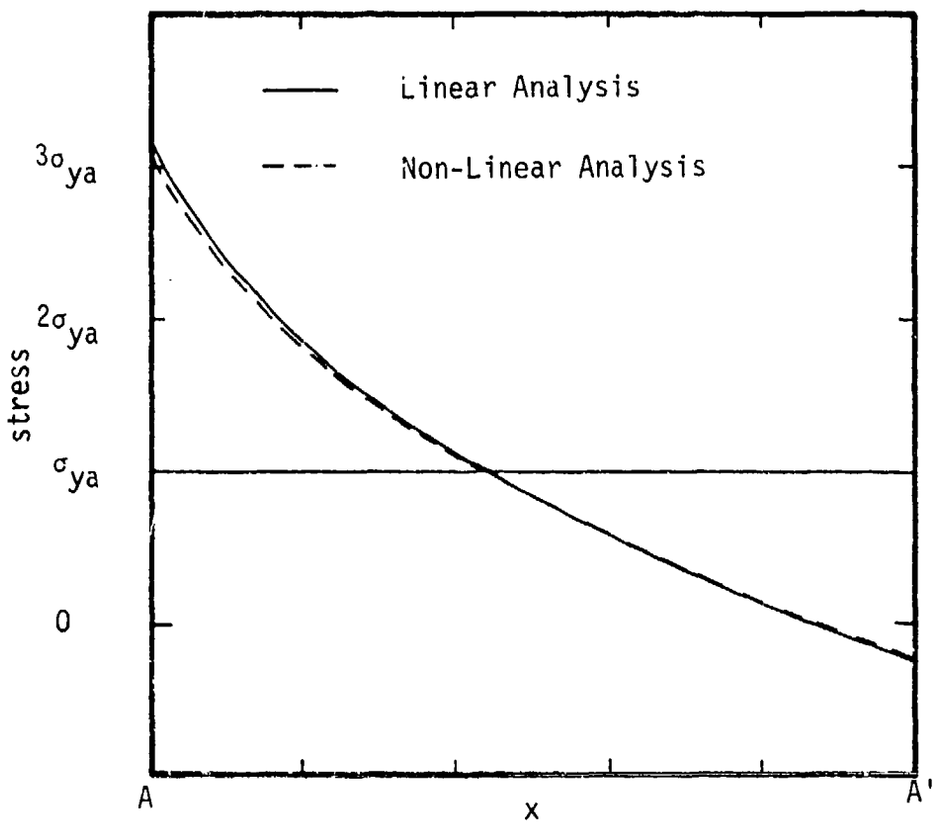

Figure 2.17: σ_y Distribution Along AA' Fig. 2.16 .

4) Load vector.

5) Element description.

6) Element connectivity.

The format type, number of cards, description of the variables are explained as follow

Set 1: 1 time,

variable: HED(20).

20A4 .

HED(20) TITLE (alphanumerique characters.)

Set 2: 1 time,

variables: NUMNP,NUMEG,NLCASE,MODEX,NONLI,INON,ERR.

I5 , I5 , I5 , I5 , I5 , I5 ,F15.0

NUMNP = Total number of nodal points

NUMEG = total number of element group

NLCASE = total number of load case

MODEX = flag if = 0 data check, if = 1 execution of the program

NONLI = maximum number of Newton-Raphson iterations

INON = number of iterations using the same stiffness matrix between to revaluation of the stiffness matrix.

ERR = converge parameters.

Set 3: NUMNP times,

variables: N ,ID(1,N),ID(2,N),ID(3,N),X(N) ,Y(N)

I5, I5 , I5 , I5 ,F15.0,F15.0

N = node number.

ID(i,N)= 0 i^{th} degree of freedom for node N is free.

ID(i,N)= 1 i^{th} degree of freedom for node N is fixed.

X(N) = X coordinate for node N.

Y(N) = Y coordinate for node N.

Set 4: NLCASE times, two different cards.

variables: N,NLOAD (once for each NLCASE)

I5,I5

N = load case number.

NLOAD = number of concentrated loads applied for this case.

variables: NOD,IDIRN,FLOAD (NLOAD times each NLCASE)

I5 ,I5 ,F10.0

NOD = node number.

IDIRN = direction of the load 1=x,2=y,and 3=z.

FLOAD = magnitude of the load.

Set 5: NUMEG times, three different cards.

variables: NPAR(1),NUME,IGROUP

I5 , I5 , I5

NPAR(1)= 1

NUME = number of elements in the group.

IGROUP = number of different sets of materials in

the group.

linear material

variables: N ,ITE1,ITE2, E1 ,E2 , E3 , ν_{12},ν_{13},ν_{23},G_{12}

format 3I5,6F10.0/F10.0 (IGROUP times)

N = material number

ITE1 = (1 or 2) = (plane stress or plane strain)

ITE2 = (1 or 2) = (isotropic or anisotropic)

E1,E2,E3= Young's modulus in the x, y, and z directions, respectively. ν_{12},ν_{13},ν_{23}= Poisson ratio in the xy, xz,and yz planes, respectively.

G_{12} = Shear modulus in the xy plane.

non-linear material

variables: N ,ITE1,ITE2, E , K , N , ν_{12}

format 3I5,3F10.0 (ICROUP TIMES)

N = material number

ITE1 = (1 or 2) = (plane stress or plane strain)

ITE2 = no meaning.

E,K,N = parameters of the non-linear law.

ν_{12} = Poisson ratio.

Set 6: NUME times,

variables: M ,I1,I2,I3,I4,I5,I6,I7,I8,MTYP

I5,I5,I5,I5,I5,I5,I5,I5,I5,I5.

M = element number.

I1...I8= connectivity.

MTYP = material type.

CHAPTER 3 ANALYTICAL, EXPERIMENTAL, AND FINITE ELEMENT COMPARISON

3. 1. Introduction

Having tested the finite element program (Chapter 2) on relatively simple structures, it was decided to test it on single-lap joint and compare the results with analytical and experimental methods. This evaluation was intended to verify whether the element used was capable of accomodating high stress and strain gradients. This validation also provides some indications on the type of discretization to be used for bonded joints that would be tested later (crack-lap and thick-adherend specimens).

In the first part of this chapter the single-lap joint have been analyzed with our finite element program and the results have been compared with Goland and Reissner's solution [12]. The object was to assess the influence of the method of Gaussian quadrature integration on the solution. The finite element results have been also evaluated by comparison with the experimental results of reference [27].

3. 2. Comparison Between Goland and Reissner, and the Finite Element Solution

3. 2. 1. Description of the Joint

Figure 3.1 shows the geometry of the single-lap joint used in this comparison. The Young's modulus and Poisson's ratio for the adherends were

E = 10,300,000 psi, (71,018 MPa),

ν = 0.33

and for the adhesive were

E_c = 130,000 psi, (710.18 MPa),

ν_c = 0.33

Adherends and adhesive were considered to be linear elastic and isotropic. The loading was P = 1423 psi (9810 KPa). The single-lap geometry and the material properties used for the adhesive and adherends classified this joint of flexible adhesive layer in the Goland and Reissner theory [12].

3. 2. 2. Description of Finite Element Analysis

The single-lap joint of Fig. 3.1 was modeled using three different finite element meshes, and the stress

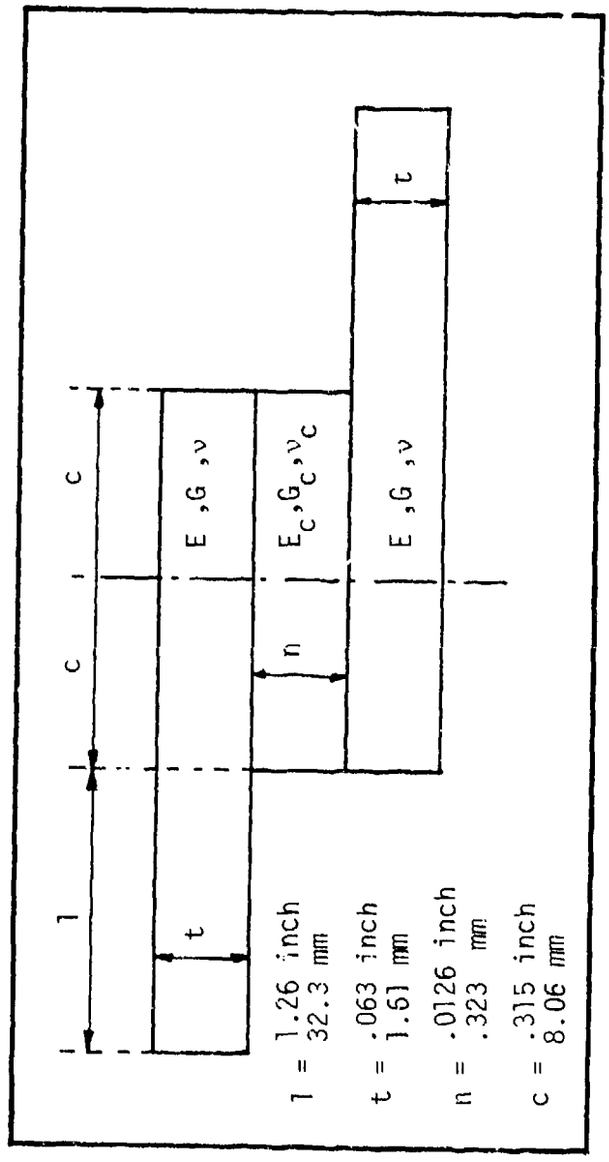

Figure 3.1: Geometry of the Single-Lap.

results are compared in this section with Goland and Reissner's solution. The difference between the first two models is in the integration of the stiffness matrix. Each discretization has the same number of elements (three hundred and fourteen), but for the first model nine Gauss points are used for the integration of the stiffness matrix, whereas the second model uses only four Gauss points. The third analysis uses a discretization with three hundred and eighty six elements and a four Gauss points integration scheme. Figure 3.2 shows the discretization, loading, and boundary conditions used in the third analysis. There are five elements across the thickness of each adherend, eight elements through the thickness of the adhesive layer, and nineteen elements over the length of the overlap.

3. 2. 3. Comparison of the Results

Figures 3.3 and 3.4 give a comparison between the first two finite element analyses. As we decrease the Gauss point number, stress distributions become smoother. The most likely explanation is that too high an order of integration of the stiffness matrix results in a more rigid structure. These results suggest the use of 4 Gauss points to integrate the stiffness matrix in the rest of the

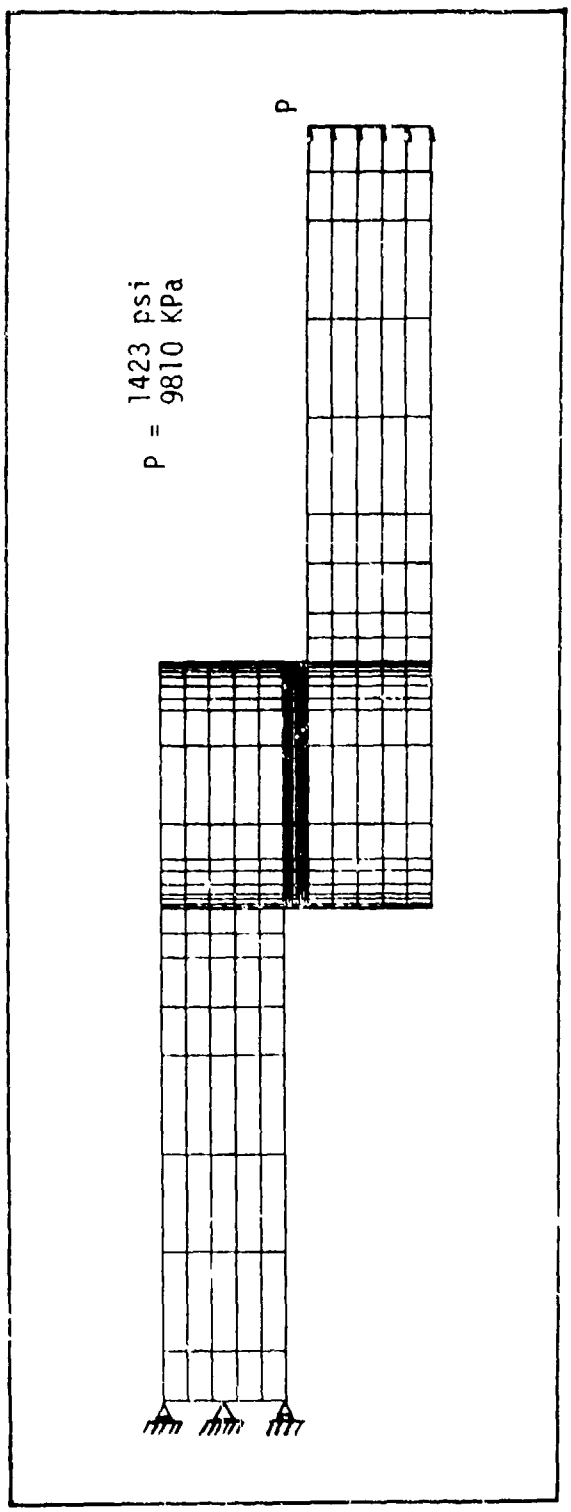

Figure 3.2: Finite Element Discretization of the Single-Lap Joint, Loading, and Boundary Conditions.

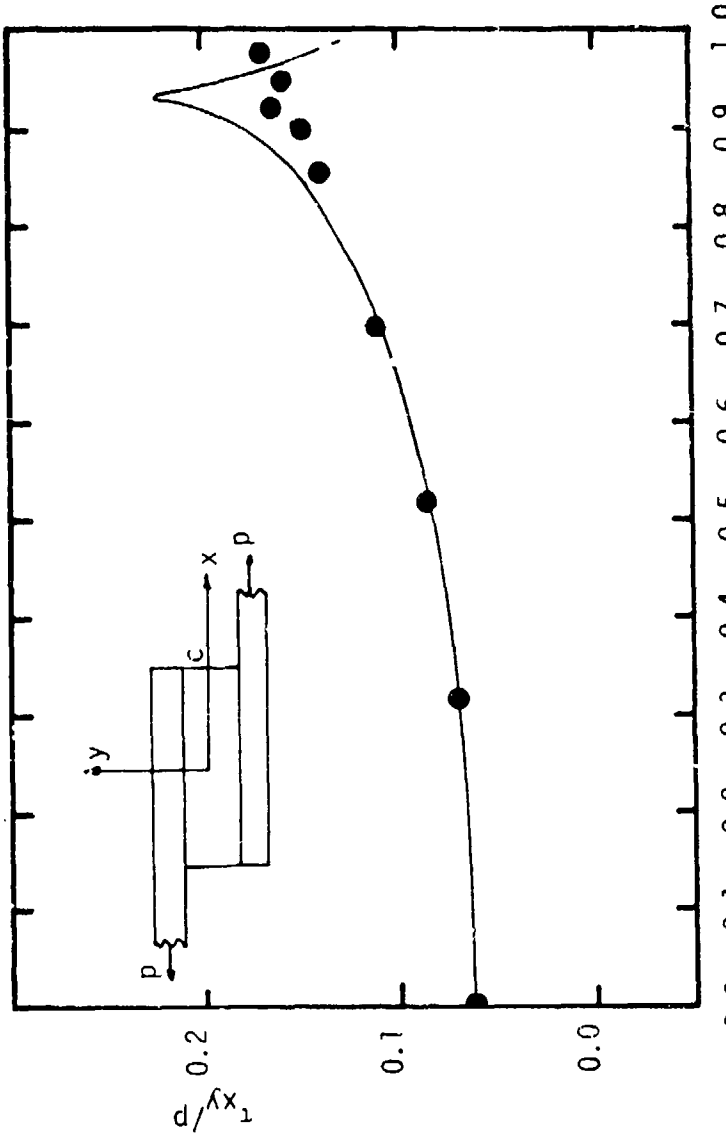

Figure 3.3: Normalized Shear Stress Distribution Along x Axis at y = 0,
● : Finite Element Output for 314 Elements and 9 Gauss Points,
— : Finite Element Output for 314 Elements and 4 Gauss Points.

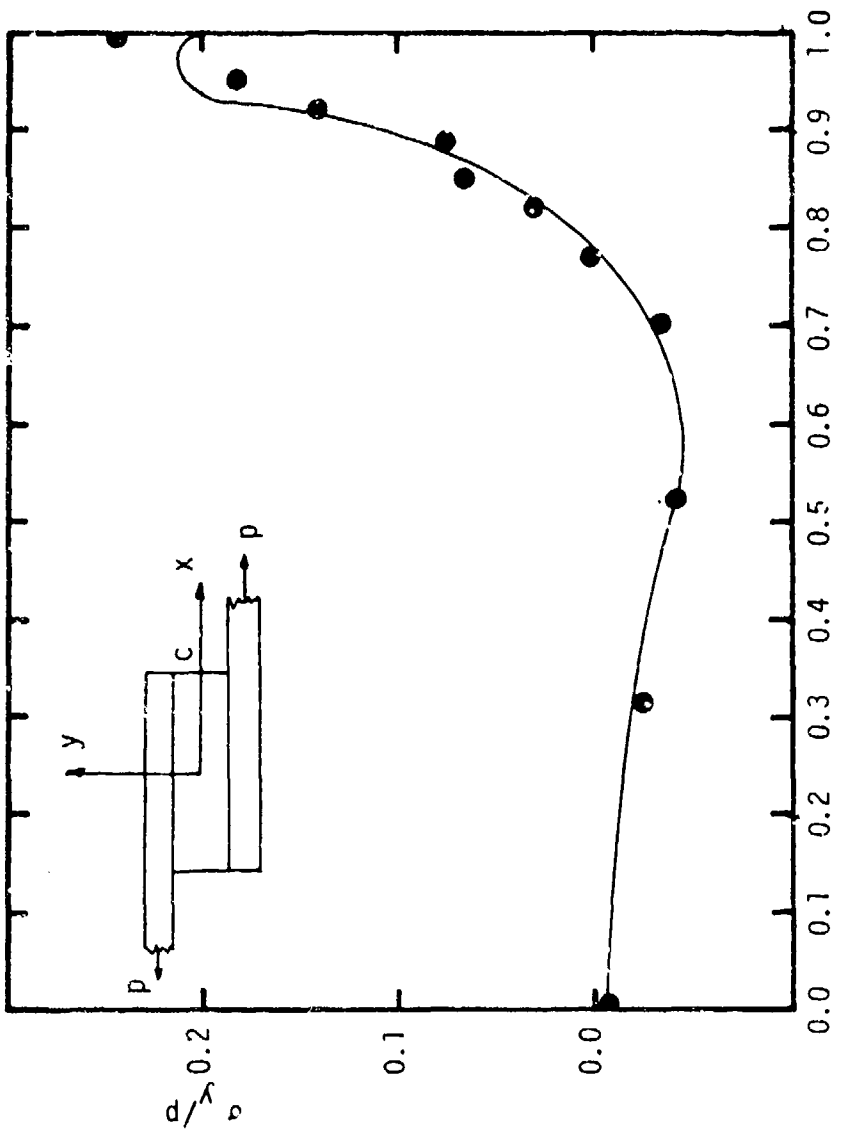

Figure 3.4: Normalized Peel Stress Distribution Along x Axis at y = 0,
● : Finite Element Output for 314 Elements and 9 Gauss Points,
— : Finite Element Output for 314 Elements and 4 Gauss Points.

research.

Figures 3.5 and 3.6 show the comparison between the results of Goland and Reissner and the third finite element analysis to be in very close agreement. However, the shear stress prediction from their method gives a non-zero stress at the free boundary whereas the finite-element solution has a vanishing stress at the corresponding location. For the peel stress, the finite element results show the maximum to occur slightly inside the free edge whereas Goland and Reissner's solution predicts the the maximum peel stress to occur at the edge. The main difference is that Goland and Reissner assume that no axial stress exists in the joint while the finite element method shows that an axial stress does exit and is of the same order of magnitude as the other stresses with its maximum at the same location.

3. 3. Comparison Between Experimental and Finite Element Results

The finite element results will next be compared with experimental measurements obtained by embedding a resistance foil strain gage within a single-lap joint [27]. The dominant loading modes within an adhesive bond are the transverse shear and peel stresses. The transverse and peel

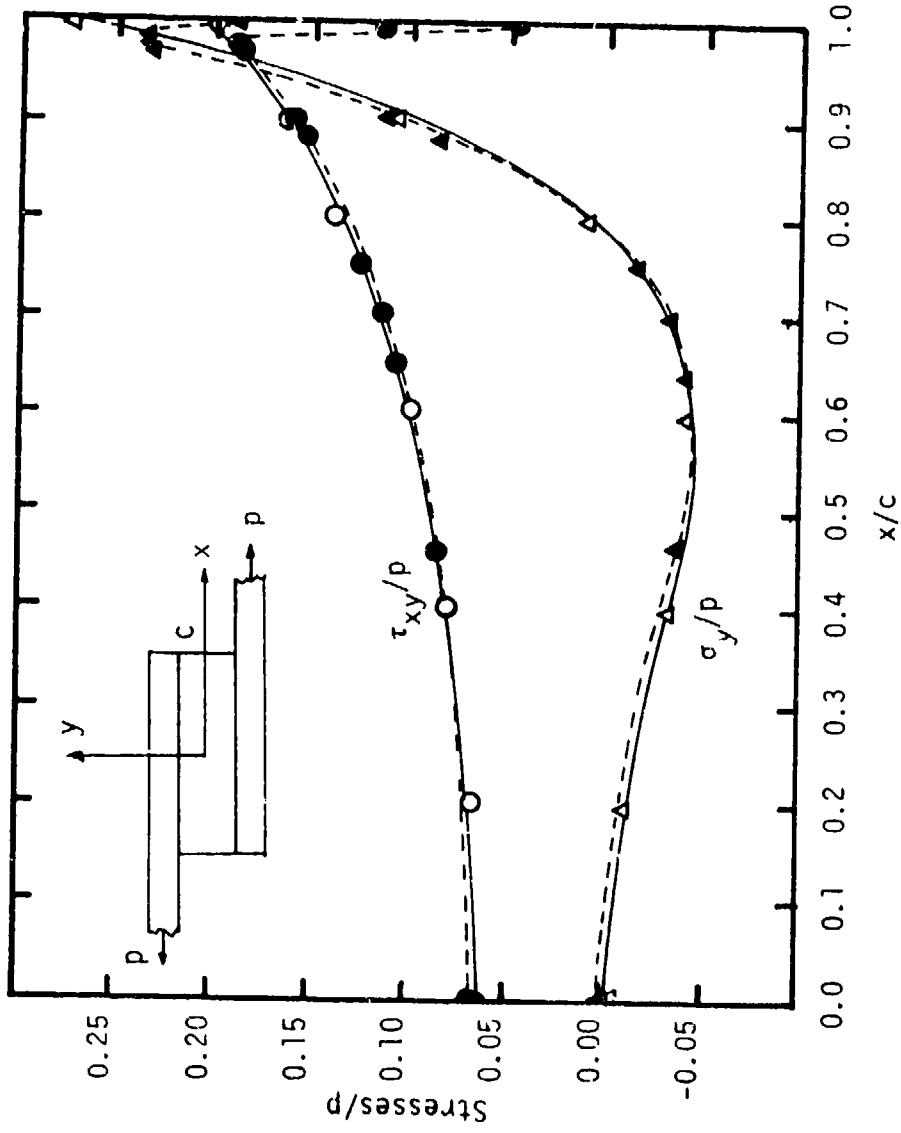

Figure 3.5: Normalized Peel and Shear Stress Distribution Inside the Adhesive Layer of a Single-Lap Joint Along the x Axis at y = 0. Comparison Between Analytical and Numerical Results, (○ , Δ) = (τ/p, σ_y/p) From Goland and Reissner (● , ▲) = (τ/p, σ_y/p) From Finite Element Analysis (386 Elements).

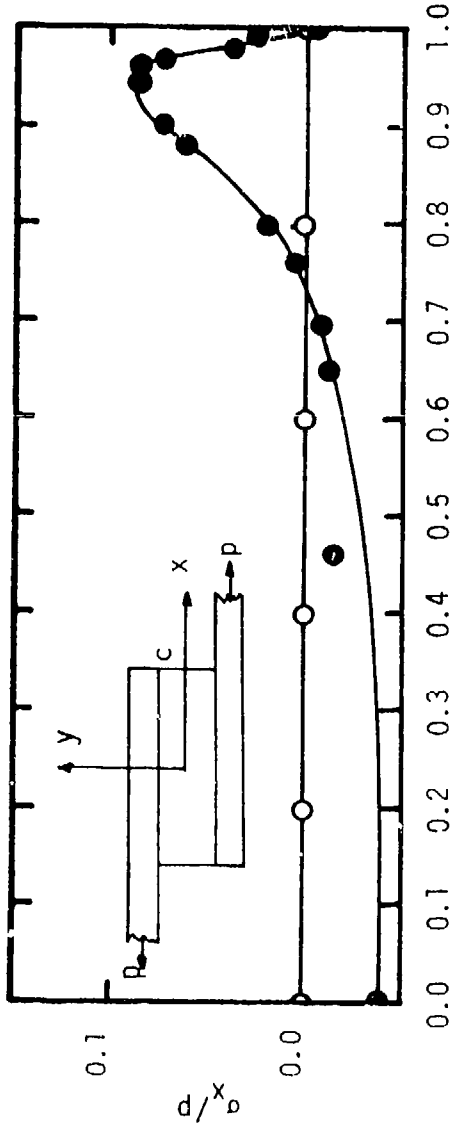

Figure 3.6: Normalized Axial Stress Distribution Inside the Adhesive Layer of a Single-Lap Joint Along the x Axis at y = 0, Comparison Between Analytical and Numerical Results,
(○) = (σ_x/p) From Goland and Reissner
(●) = (σ_x/p) Form Finite Element Analysis (386 Elements).

strains induced by these stresses cannot be directly measured using in-plane embedded foil strain gages, since such gages measure only in-plane normal strains. Perhaps the reason that embedded strain gages have not been used in the experimental analysis of joints previously is because the analytical solutions which most people utilize such as that of Goland and Reissner neglect or ignore axial stresses within the bondline.

The intent herein is to confirm the numerical analysis of the single-lap joint as obtained with the finite element program. An important feature to keep in mind is that the needed adhesive properties (E, ν) for the finite element program were found from tensile tests on neat resin coupons [9]. As a result, as will be shown, this comparison tends to confirm that neat resin properties can be safely used in lap joint analyses, contrary to earlier expectations [16].

The measured in-plane normal strains will be compared to the in-plane normal strains predicted by the finite element analysis. A good comparison will serve to increase confidence in the transverse shear and peel stress distribution predicted by the finite element analysis. Such a marriage between experimental and finite element techniques has been suggested in the literature as a hybrid stress analysis tool [28].

3. 3. 1. Preparation of the Specimens

A schematic representation of the single lap specimen used is given in Fig. 3.7. The nominal dimensions of the titanium Ti-6-4 adherends were 0.05 X 1.0 X 5.0 inch (0.13 X 2.5 X 12.7 cm). The adherend overlap was 1.0 inch (2.5 cm), resulting in a 1.0 in^2 (6.5 cm^2) adhesively bonded area FM-300 structural adhesive was used to bond the joint.

Prior to bonding, the adherends were subjected to a phosphate/fluoride pretreatment which was intended to produce a uniform oxide layer suitable for adhesive bonding. The pretreatment is itemized below:

* light surface abrasion using a belt sander with a 60-grit belt to remove excessive oxide formations or adhesive from previous use
* grit blasting using fine sand at approximately 90 psi
* solvent wipe using methylethyl ketone
* soak in an alkaline SPREX-AN9 solution for 15 minutes at 80C (176F)
* rinse in deionized water

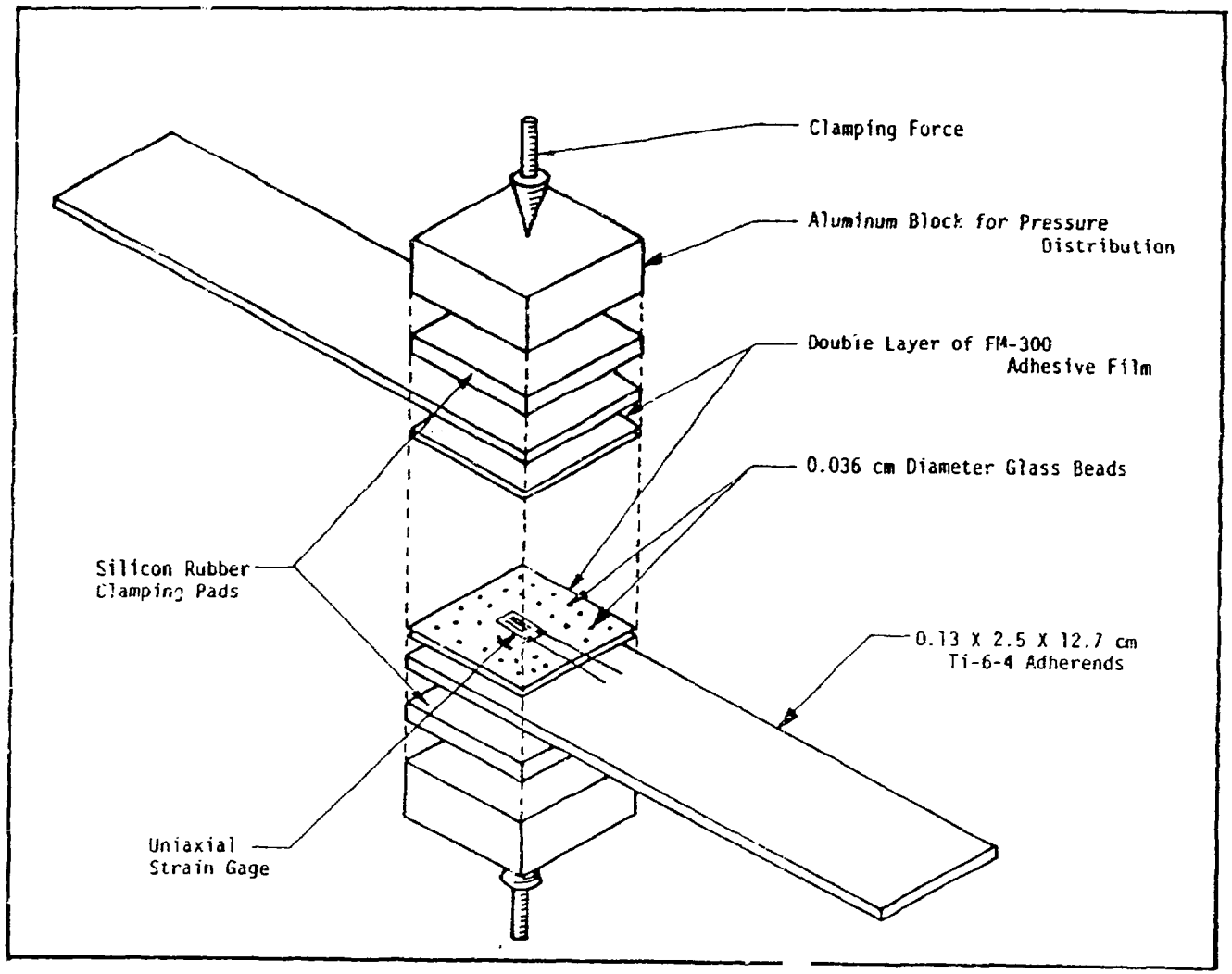

Figure 3.7: Exploded View of Single-Lap Joint Fabrication.

* soak in pickling solution consisting of 31 ml/liter hydrofluoric acid (HF) and 213 ml/liter nitric acid (HNO_3) for 2 minutes at room temperature

* rinse in deionized water

* soak in the phosphate/fluoride solution consisting of 50.3 gm/liter sodium phosphate (Na_3PO_4), 20.5 gm/liter potassium fluoride (KF), and 29.1 ml/liter HF for 2 minutes at room temperature

* rinse in deionized water

* soak in deionized water for 15 minutes at 65C (149F)

* rinse in deionized water

* dry in dry nitrogen

The adherend pairs were placed in a desiccator immediately after surface pretreatment, and all joints were cured within 24 hours of the treatment.

As shown in Fig. 3.7, a double layer of FM-300 adhesive film was placed immediately adjacent to each adherend surface, and a Micro-Measurment EA-06-060CD-350 uniaxial strain gage with preattached leadwires and polyimide encapsulation was centered within the 1.0 X 1.0 inch (2.5 X 2.5 cm) bond area. The gage backing was trimmed

to within about 0.02 inch (0.05 cm) of the gage grid area prior to gage installation, which produced a nominal gage area of 0.16 X 0.22 inch (0.40 X 0.55 cm). In addition, the preattached leadwires were coated with Micro-Measurement M-Coat D to provide leadwire insulation and prevent shorting of the leadwires against the titanium adherends. No additional strain gage surface preparation was performed.

During initial efforts it was very difficult to obtain a uniform bondline thickness. From industrial sources it was learned that bondline thickness is often controlled by impregnating the adhesive with small glass beads prior to cure. Therefore glass beads with nominal diameter of 0.014 inch (0.036 cm) were distributed throughout the adhesive joint area, resulting in a uniform bondline.

The specimens were cured for 4 hours at 350F (177c). A clamping pressure of 20 psi (0.14MPa) was maintained during the cure cycle, and silicon rubber pads were used to assure that a uniform pressure was applied throughout the bonded area. This clamping pressure is near the lower limit of the manufacturers recommended pressures of 15-100 psi (0.10-0.69 MPa). High clamping pressures were used during initial efforts, but it was found that clamping pressures higher than about 20 psi would crush both the glass beads and the leadwire coating, resulting in irregular bondline thickness and often causing the leadwires to short against

the titanium substrate. Another difficulty encountered was that in two cases the uniaxial gage rotated away from the intended axial alignment during cure. In these cases a clamping pressure greater than 50 psi (0.35 MPa) was applied. It was postulated that this gage rotation occurred because the adhesive was forced out from between the adherends to a greater extent during cure at the higher clamping pressures. At lower pressures gage rotation did not occur. Gage rotation could only be detected by inspection following testing of the bond to failure.

Strain gage temperature compensation was achieved by preparing two identical specimens and using one as an active specimen and one as a dummy specimen in a standard 2-arm Wheatstone bridge configuration. A constant bridge excitation voltage of 2.0 volts was used, resulting in a grid power density of 0.50 watt/in^2 (0.78 watt/m^2). Excellent gage stability was observed throughout the testing program.

A total of three specimens with embedded strain gages have been fabricated as described above. A concern was that the presence of the strain gage would adversely affect the performance of the bonded joint. Therefore, additional three specimens have been fabricated without an embedded strain gage and were used as control specimens. That is, the average ultimate shear strength of the gaged specimens

was compared to the average ultimate shear strength of the control specimens.

3. 3. 2. Results

A comparison of the ultimate bond shear strengths of the specimens containing an embedded strain gage and the control specimens is given in Table 3.1. All tests were conducted at room temperature. As indicated, the average ultimate shear strength of the gaged specimens and control specimens was 2327 psi (16.1 MPa) and 2047 psi (14.1 MPa), respectively. While the number of specimens tested cannot be considered a statistically valid sample size, results obtained indicate that the strain gage has not reduced bond performance, at least in terms of ultimate bond strength. In order to measure the strain gage effect on the stress and strain field inside the adhesive layer, finite-element analyses of the single-lap joint with strain-gage inside the joint were run. Due to the lack of knowledge of the Young's modulus of the strain gage, three different tests were run. For the first test, the strain gage Young's modulus was equal to the adhesive Young's modulus, for the second one it was 10 times larger, and for the last test 10 times smaller. The stress fields were locally affected by the strain gage modulus, but

Table 3.1: Comparison of Ultimate Bond Shear Strengths of Joints With and Without an Embedded Strain Gage.

Specimen Number	Embedded Gage?	Ultimate Shear Strength MPa	Psi	Average Ultimate Shear Strength
1	YES	15.1	2187	
2	YES	16.9	2449	16.1 MPa (2327 psi)
3	YES	16.2	2344	
4	NO	15.8	2292	
5	NO	13.3	1924	14.1 MPa (2047 psi)
6	NO	13.3	1924	

no significant effect could be seen for the strain field. These results indicated that ıe axial strain was little disturbed by the introduction of the strain gage. Details of the finite-element analysis will be presented in a later publication [29].

The specimens were mounted in a dead-weight testing frame and subjected to several load levels up to bond failure. For applied loads less than about 2100 lbs (9340 N) a completely elastic response was observed. That is, the same strain reading was obtained for repeated loading/unloading cycles, and the strain reading would return to zero following unloading. At load levels greater than about 2100 lbs, a time-dependent response was observed. This was attributed to the combined effects of a viscoelastic response of the adhesive and an accumulation of damage within the adhesive layer. Upon unloading from these higher load levels a permanent strain reading on the order of 30-50 μin/in was observed. Also, at stress levels very near ultimate the strain readings steadily decreased for a constant load. his phenomenon is not understood at present but will be addressed in a later publication [29].

The strain measurments for specimens 1 and 2 were in agreement to within 10% at all elastic load levels, while the elastic strains for specimen 3 were about 40% higher. Upon inspection of specimen 3 after bond failure, a void was

discovered in the adhesive layer immediately adjacent to the embedded strain gage. This void was apparently responsible for the higher strain levels recorded for specimen 3, although it did not appreciably effect the ultimate bond strength as indicated in Table 3.1.

The average strain recorded for specimens 1 and 2 are compared with the results from a finite-element analysis in Fig. 3.8. As discussed above, the strains measured for specimen 3 were approximately 40% higher than those indicated in Fig. 3.8, due to a void within the adhesive layer. Although further testing is in progress, the excellent correlation exhibited thus far between theory and experiment is very encouraging.

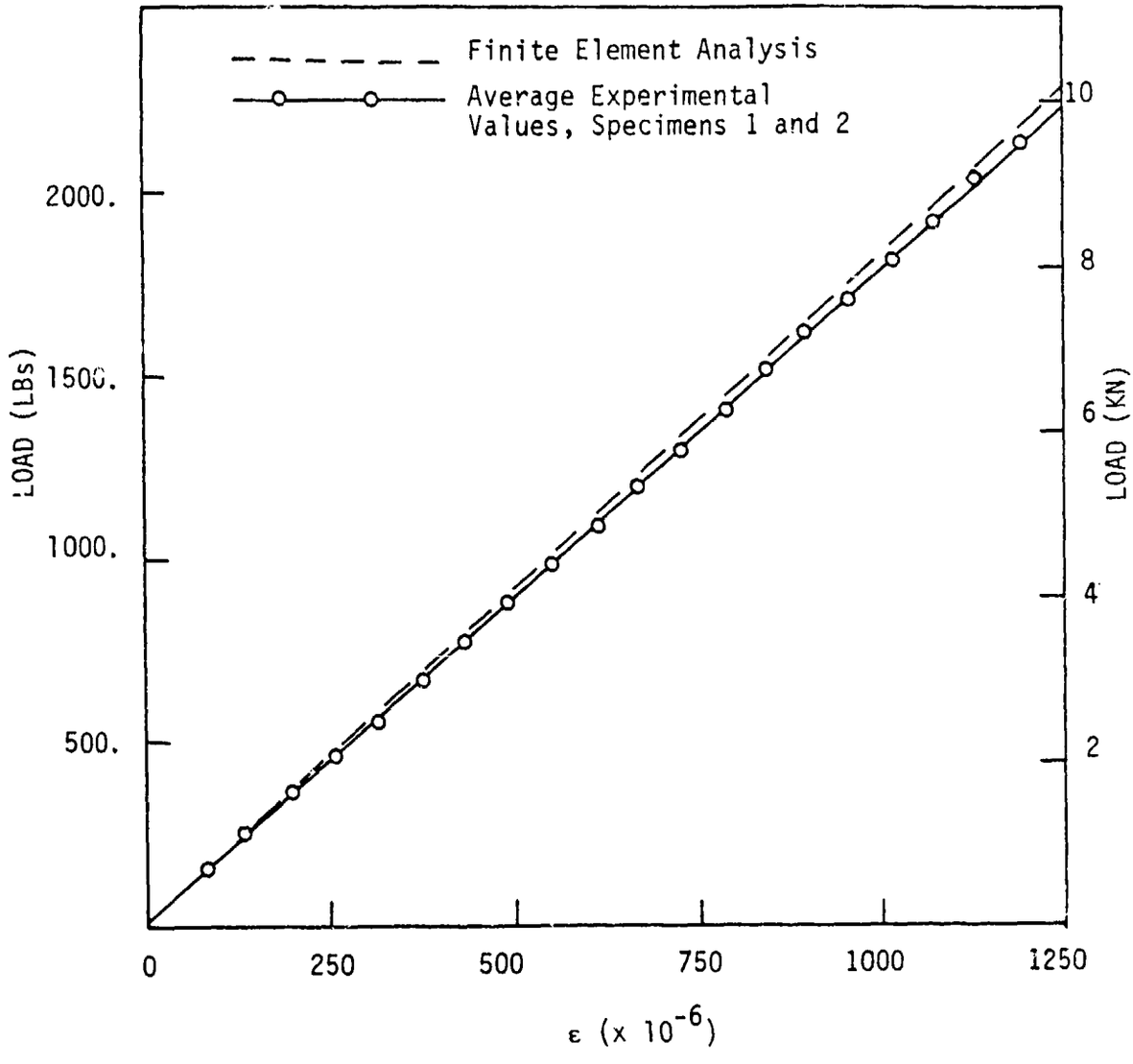

Figure 3.8: Comparison of Experimental and Finite Element Results.

CHAPTER 4 FINITE ELEMENT ANALYSIS OF BONDED JOINTS

4. 1. Introduction

The three different adhesive joints studied in this section are the single-lap, thick-adherend, and crack-lap joints. These specimens are often used in experimental analyses to evaluate adhesive properties. Such studies are difficult for the following two reasons. First, testing of bonded joints gives little information on the deformation of the adhesive layer. Second, the bonded joint is in a three-dimensional state of stress. Shear, peel, and axial stresses are present and are not constant along the bond line or even across the adhesive layer. The two reentrant corners existing near each end of the adhesive layer (Fig. 4.1) introduce singularities in the analytical solution. This causes great difficulty in attempts to either predict or measure stress distributions or ultimate strengths.

The bonded joints studied in this section are often used to quantify shear stress-strain properties, but for the above reasons the specimens cannot be considered to be in a pure shear stress field. However, it is worth noting that better alternatives are lacking and for this reason a good

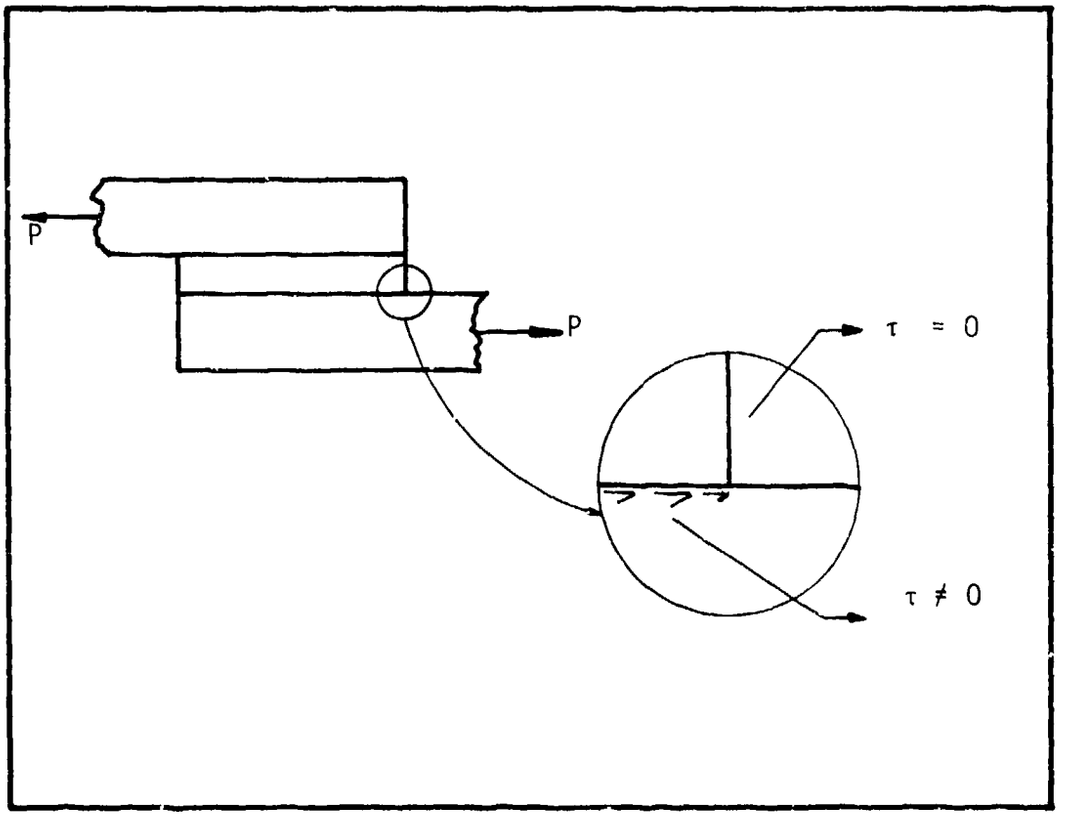

Figure 4.1: Singular Geometry, Discontinuity in the Shear Stress at the Free Edge Due to a Reentrant Corner.

analysis of these geometries would be invaluable in properly understanding laboratory observations.

For the single-lap joint, the intensity of the shear, peel, and axial stresses are functions of the aspect ratio of the joint geometry and the material used for the adhesive and the adherends. The thick-adherend specimen has been designed to minimize the peeling effects while maximizing the shearing effects. But for this joint , the aspect ratio determines the intensity of the shear response also [17].

4. 2. Single-Lap Joint

4. 2. 1. Geometry, Boundary Conditions, and Material

The single-lap joint has been analysed by many people including Nagaraja, et al. [30] and Botha, et al. [16].The geometry to be considered is given in Fig. 4.2. The adherends are aluminum and the adhesive is a linear viscoelastic material. Nagaraja, et al. [30] used Schapery's direct method to model a linear viscoelastic adhesive. Botha, et al., on the other hand, used Schapery's quasi-elastic method in which the viscoelastic modulus at time t_i is replaced by the apparent Young's modulus at the same time. This method was also used in the present

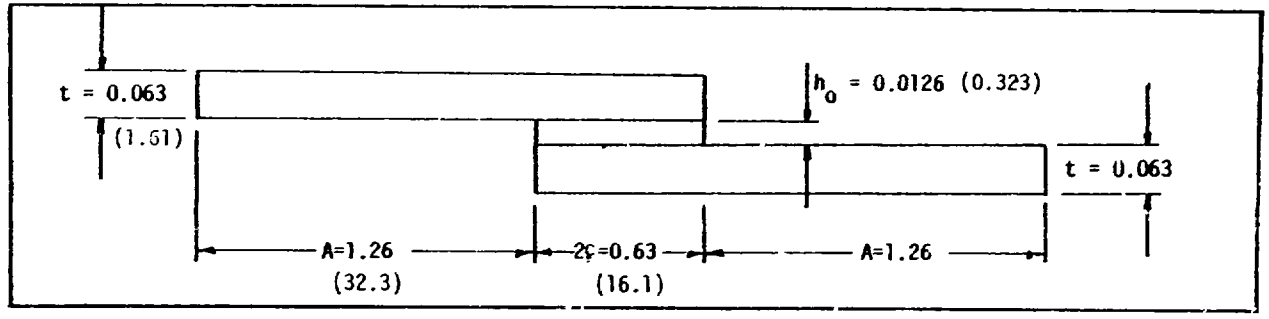

Figure 4.2: Geometry of the Single-Lap Joint as Used by Nagaraja and Alwar [30], Botha et al. [16], and the Present Analysis. Dimension in Inches, (Dimension in Millimaters).

analysis. Table 4.1 shows the Young's modulus of the adherends and the time dependent material properties of the adhesive layer.

4. 2. 2. Discretization of the Single-Lap Joint

Figures 4.3 and 4.4 show the meshes used in the two previous analyses while Fig. 4.5 shows the discretization used in the present case. The elements used in the two earlier analyses were an eighteen degrees of freedom triangle with three nodes and an eight degrees of freedom quadrilateral with four nodes. Our element was an isoparametric with sixteen degrees of freedom eight nodes.

In the present analysis five elements were used across the thickness of each adherend and eight across the thickness of the adhesive layer. Seventeen elements were used along the length of the bonded overlap and six elements along the length of the unbonded adherends. The aspect ratio of the smallest element was 3 (the length was 0.006 inch (0.1524 mm)).

Table 4.1: Time Dependent Material Properties Used for the Single-Lap Joint by Nagaraja and Alwar [30], Botha et al. [16], and in the Present Analysis

		Young's Modulus E (psi)	Poisson's Ratio ν
Aluminum Adherends		10.3×10^6*	0.30
	Time (days)	Relaxation Modulus $E_r(t)$ (psi)	Poisson's Ratio ν
Araldite Adhesive	10	8.194×10^6	0.33
	100	3.073×10^6	0.33
	1000	1.138×10^6	0.33

*This value assumed

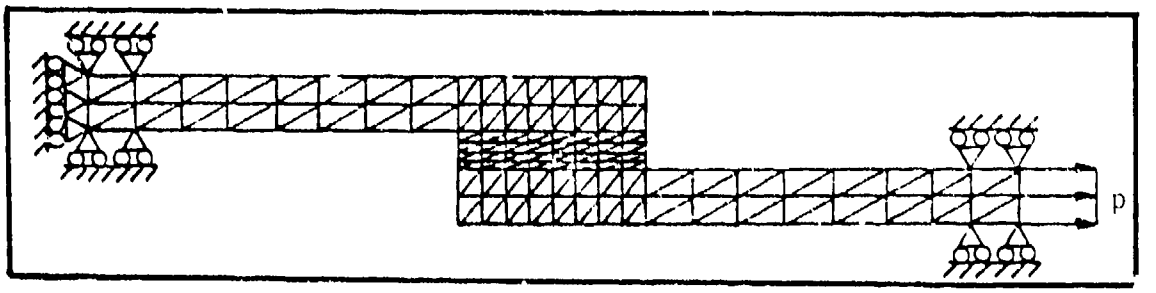

Figure 4.3: Finite Element Discretization and boundary Conditions as Used by Nagaraja and Alwar [30] for the Single-Lap Joint.

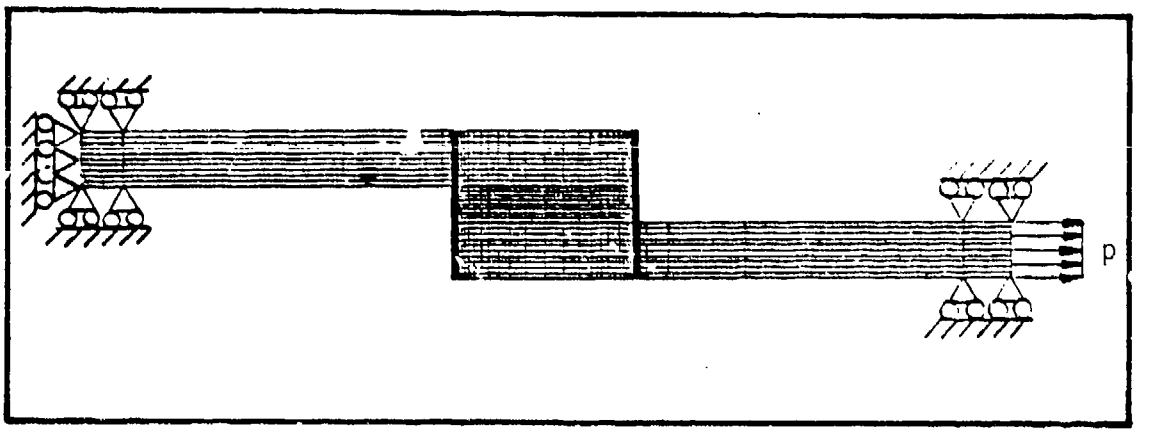

Figure 4.4: Finite Element Discretizations and Boundary Conditions as Used by Botha et al. [16] for the Single-Lap Joint.

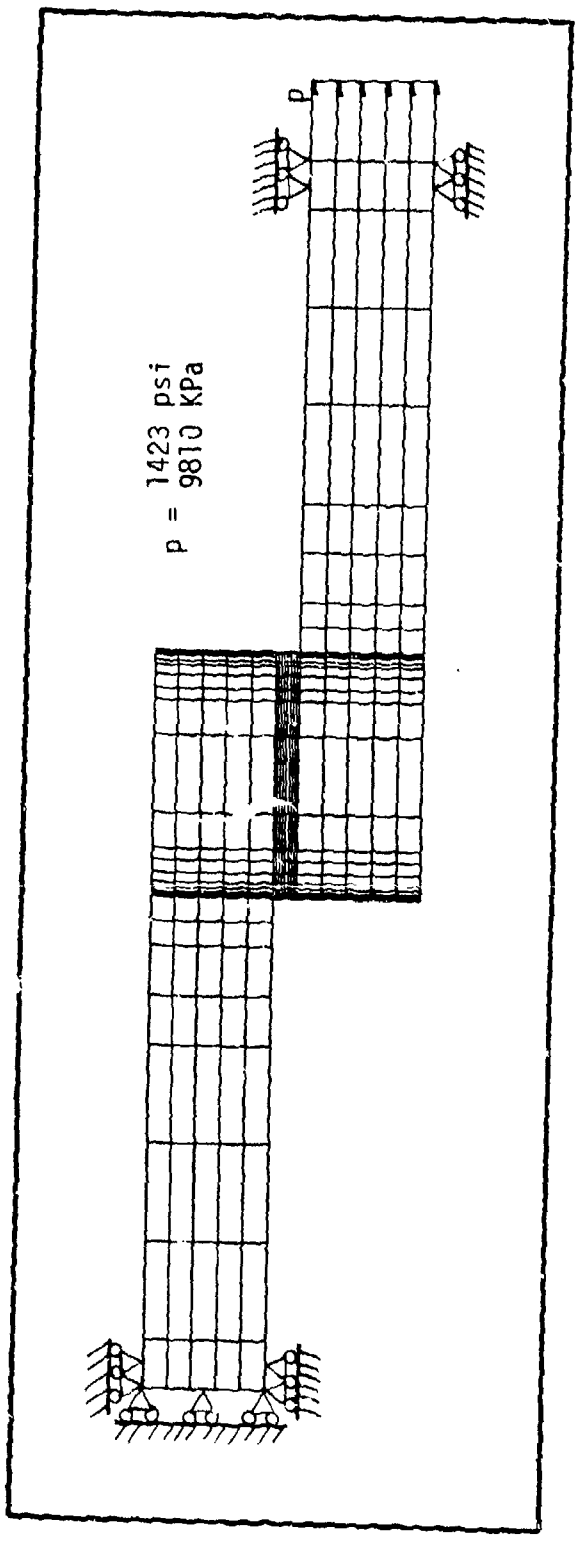

Figure 4.5: Finite Element Discretization, Boundary Conditions, and Loading Used in the Present Analysis.

4. 2. 3. Finite Element Results

In all cases the analyses of the single-lap joint were linear and the calculated stresses were non-dimensionalized by the applied stress

$$p = \frac{P}{A}$$

where P is the load and A is the area cross section of the adherends. The results shown in Figs. 4.6 and 4.7 are the shear and peel stresses along the adhesive layer, near the middle of the joint for the three analyses. The results of Nagaraja, et al. do not show stresses decreasing near the free edges, but show them increasing instead. However, their results appear symmetric. In the analysis of Botha, et al., the shear and peel stresses tend to satisfy the boundary conditions for some of the edges, but their results are quite unsymmetric. In the present analysis, the results are symmetric and at both ends the stresses tend to satisfy the condition of the free edges.

Figures 4.8, 4.9, and 4.10 are the shear, peel, and axial stress distributions obtained along the bottom interface at three different times, using the modified STAP program. At the left free edge, away from the singularity, the three stresses are nearly equal to zero. Slightly inside the joint, the stresses reach a maximum, caused by the stress singularity induced at the top left edge of the

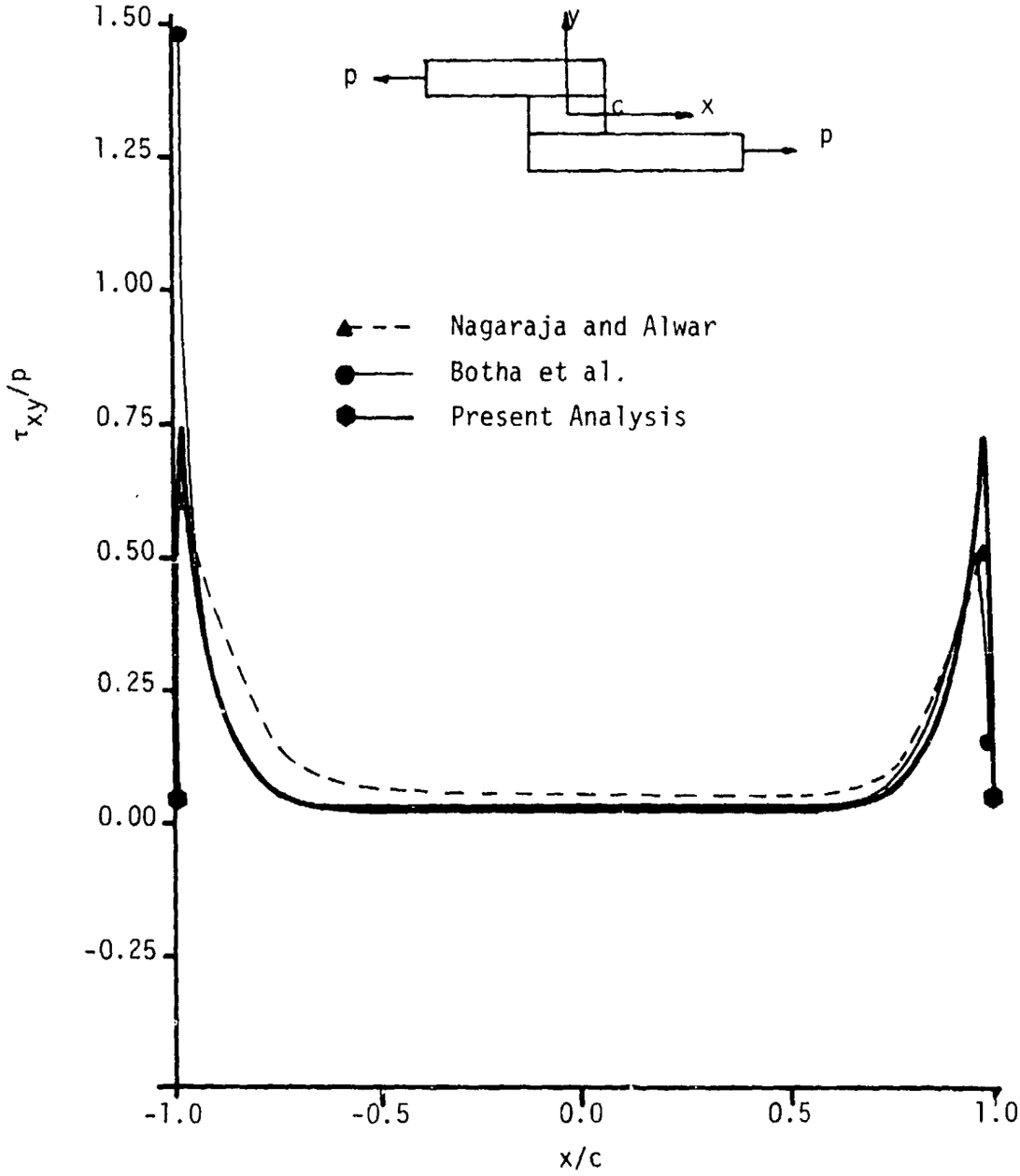

Figure 4.6: Shear Stress Distribution near the Middle of the Adhesive Layer, Comparison Between the Results of Nagaraja and Alwar [30], Botha et al. [16], and the Present Analysis.

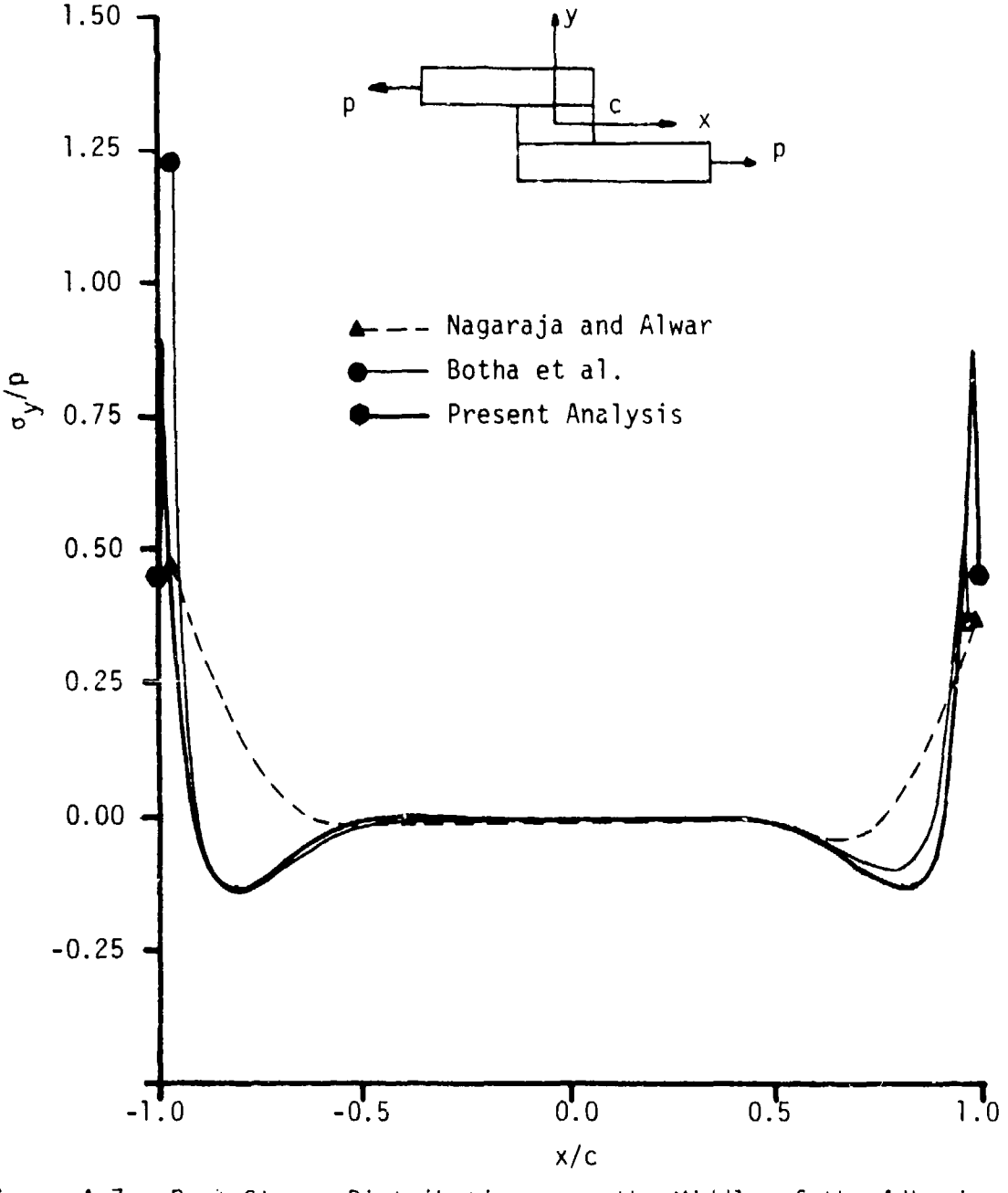

Figure 4.7: Peel Stress Distribution near the Middle of the Adhesive Layer, Comparison Between the Results of Nagaraja and Alwar [30], Botha et al. [16], and the Present Analysis.

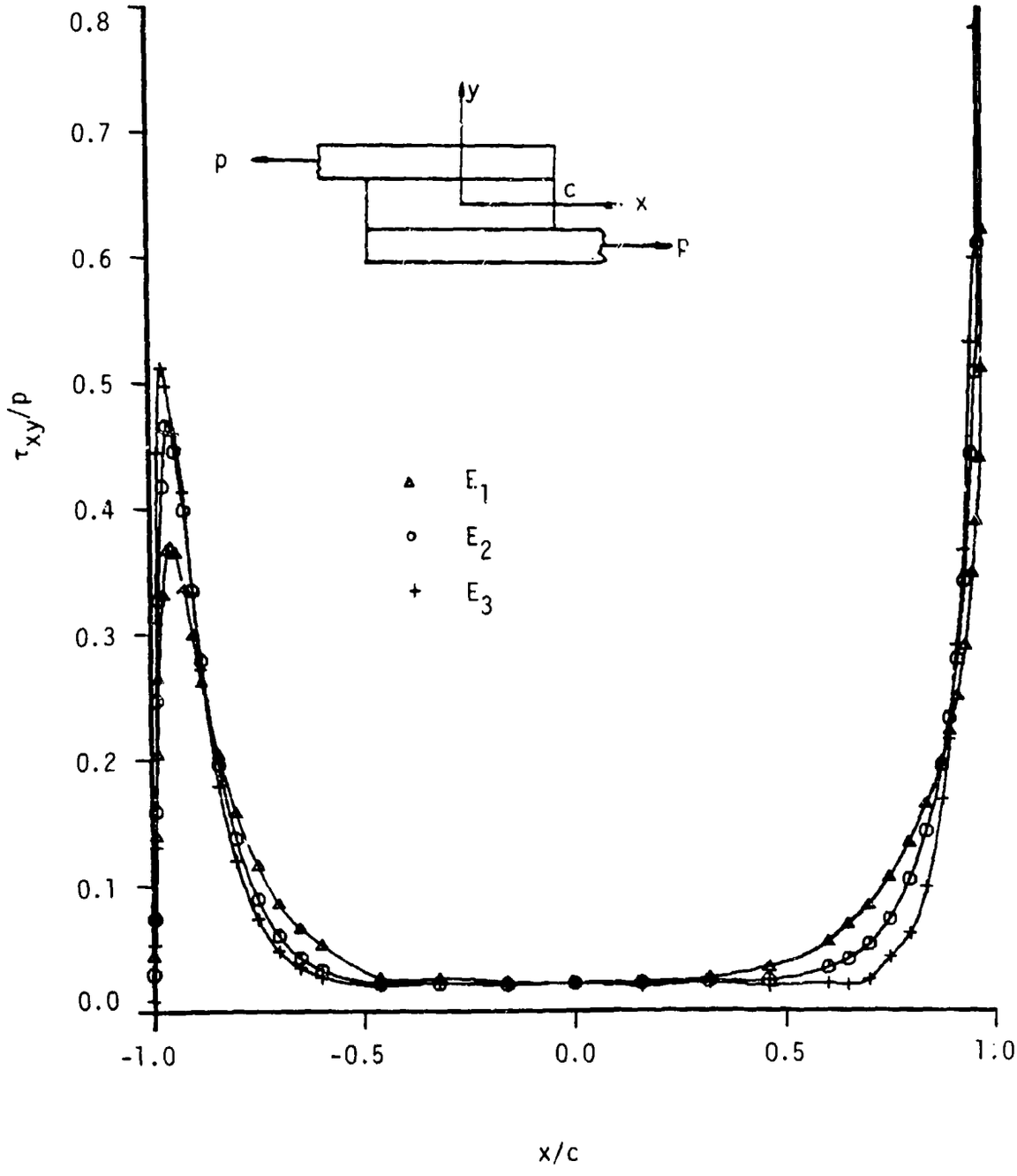

Figure 4.8: Shear Stress Distribution at the Bottom Interface for the Three Different Apparent Young's Modulus Table 4.2.

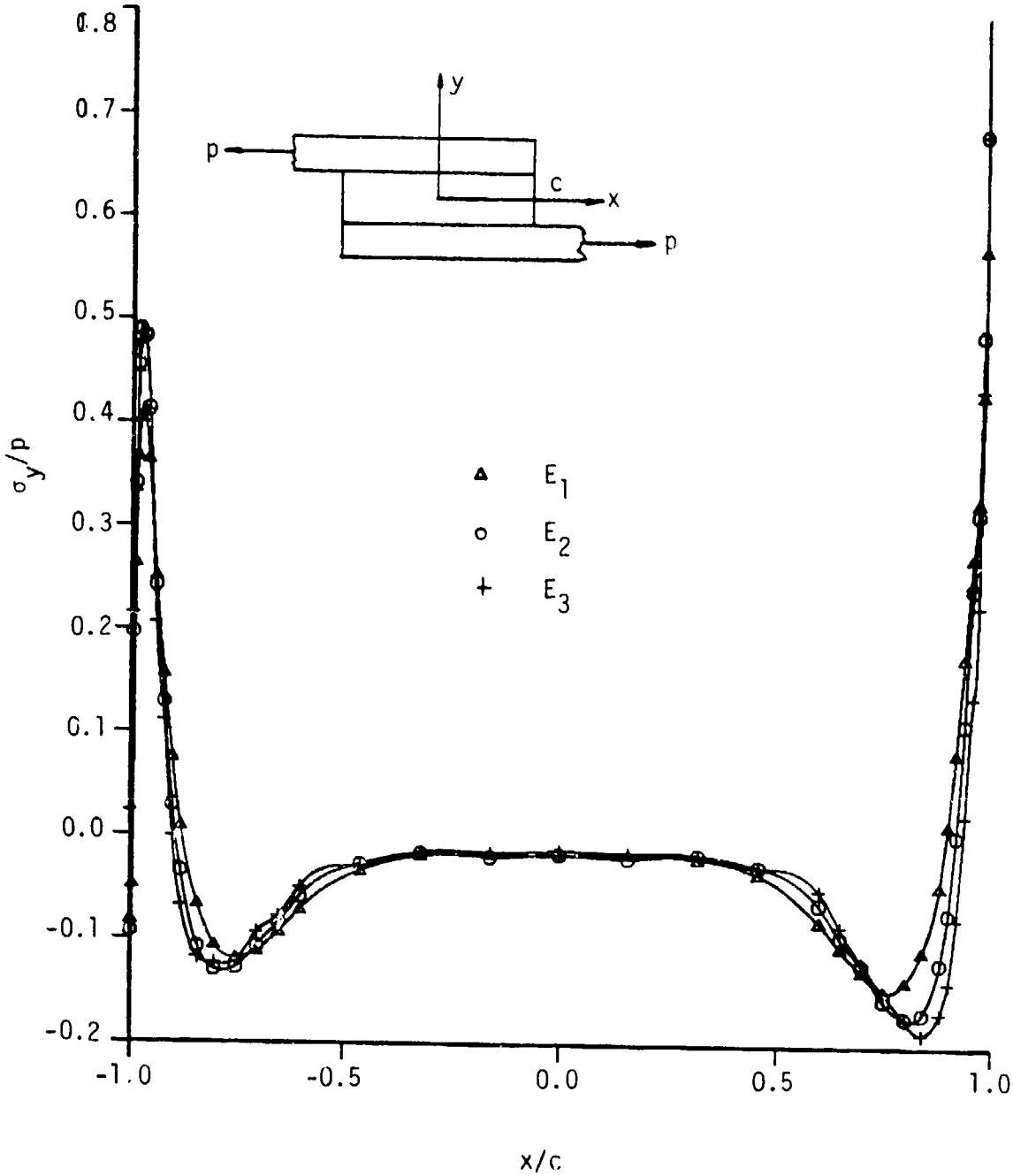

Figure 4.9: Peel Stress Distribution at the Bottom Interface for the Three Different Apparent Young's Modulus Table 4.2.

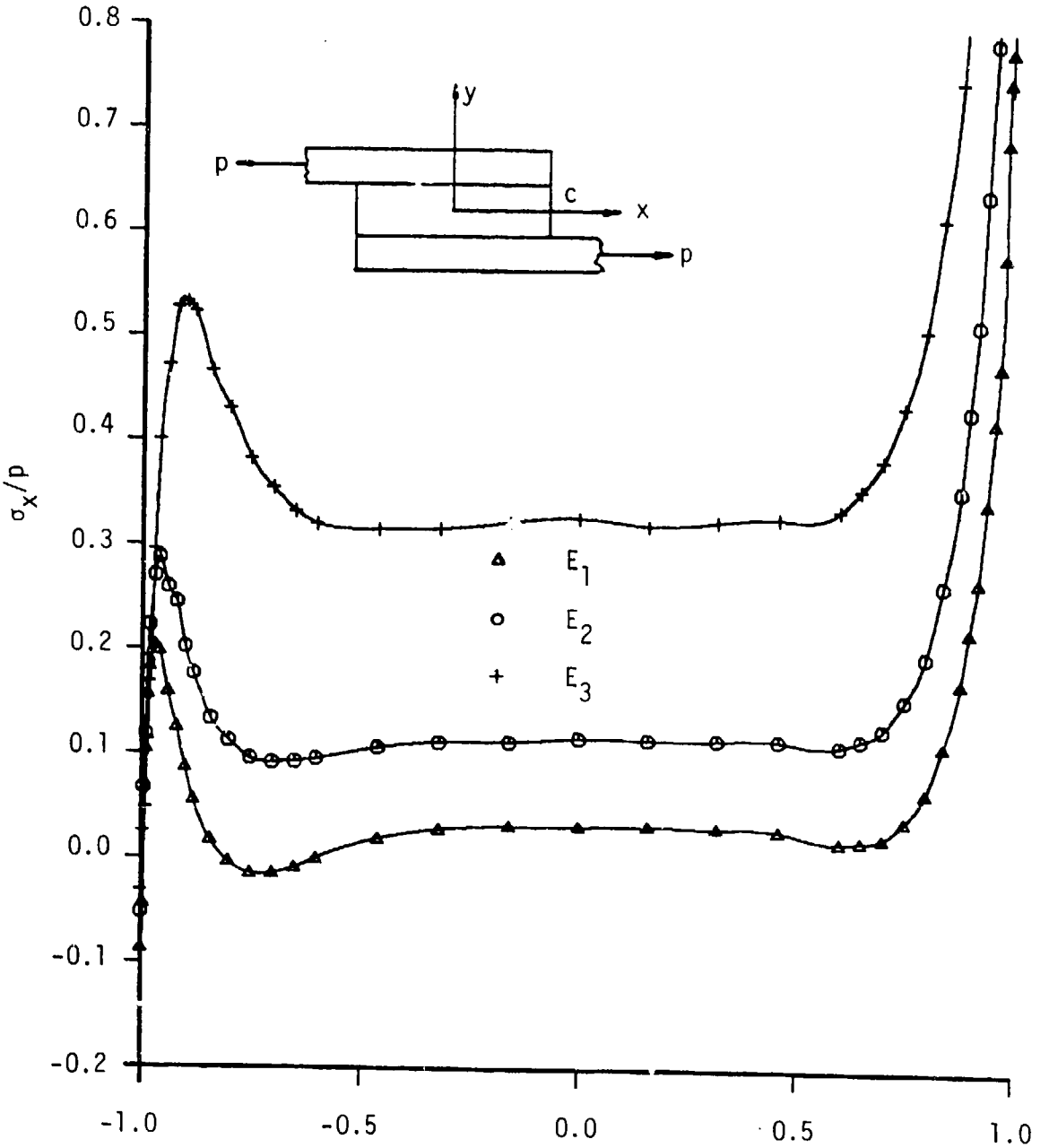

Figure 4.10: Axial Stress Distribution at the Bottom Interface for the Three Different Apparent Young's Modulus Table 4.2.

adhesive layer. Over nearly fifty percent of the overlap length the stresses are constant, but over the remaining portion the stress distributions are dramatically influenced by the stress singularity induced at the bottom right edge. Hence significant stress gradients exist within the adhesive layer.

The central part of the shear and peel distributions do not seem to be significantly influenced by the adhesive Young's modulus. The near constant shear stress is slightly positive while the peel stress is slightly negative. Only at the region of high stress gradients are the values of the shear and peel stresses functions of the adhesive Young's modulus. However, the sensitivity of the axial stress to the adhesive Young's modulus is present all along the joint. In addition, the order of magnitude of this stress is much higher than the order of magnitude of the other two stresses.

4. 3. Thick-Adherend Specimen

The thick-adherend specimen was a joint originally designed to test the adhesives in a shear state minimizing the peeling. But due to the geometry, the peel stress is still very large near the free edges. The shear stress,

however, is much more constant along the bond line than the other stresses.

Four different analyses of this joint have been performed. The first one used a linear elastic constitutive law to model the adhesive with the main interest being to compare the stress distributions at the bottom interface and in the middle of the adhesive layer. The three other analyses used non-linear elastic constitutive laws to model the adhesive layer. The interest here was to determine the sensitivity of the stress ditributions inside the adhesive layer for a change in its Young's modulus.

All the stress distributions were non-dimensionalyzed by dividing them with p which is defined by

$$p = \frac{P}{2*A}$$

where P is the applied load, and A the area cross section of one adherend.

4. 3. 1. Geometry, Material, and Discretization

The geometry of the thick-adherend specimen analysed in this section is given in Fig. 4.11. The adherends of the specimen were made of aluminum. The adhesive layer was modeled with a linear material for the first test, then with different non-linear elastic materials. Figure 4.12 is a

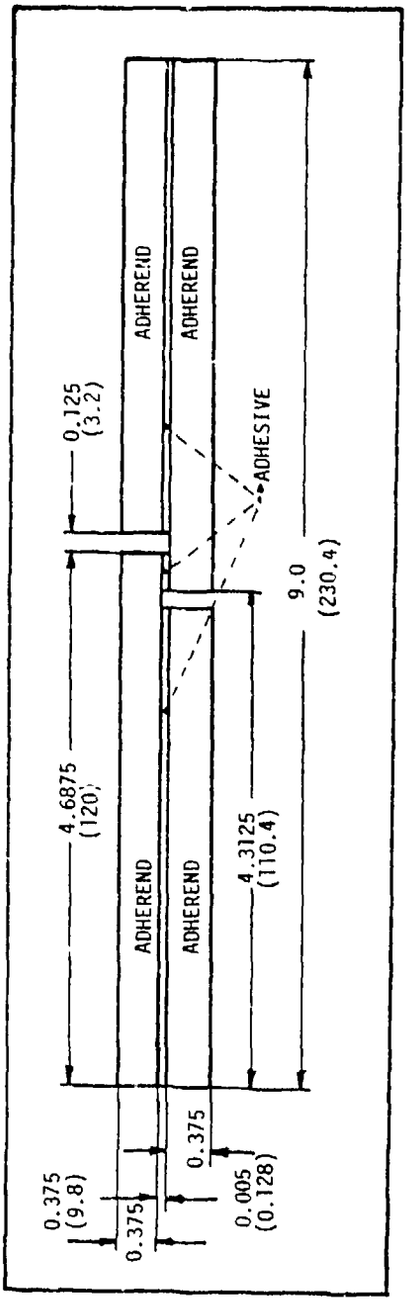

Figure 4.11: Geometry of the Thick-Adherend Specimen, Dimension in Inches, (Dimension in millimeters).

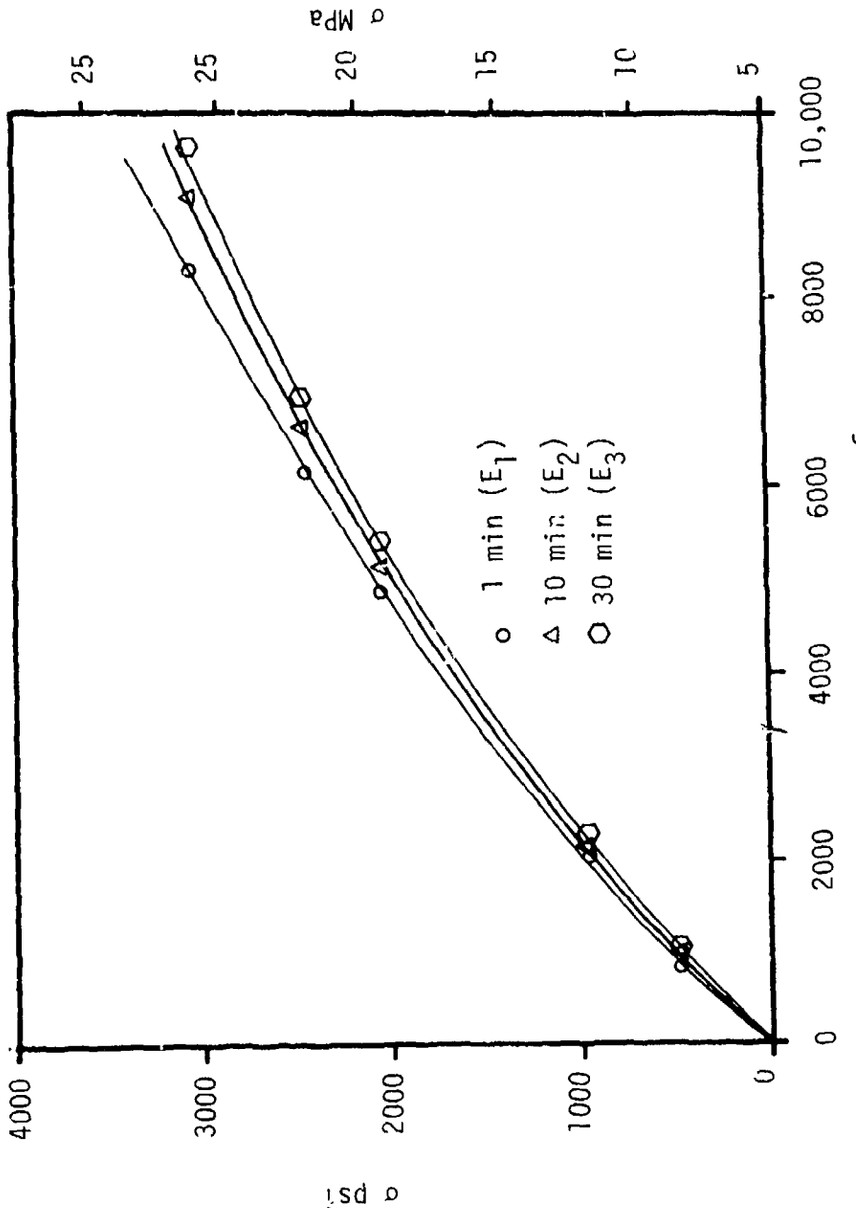

Figure 4.12: Uniaxial Stress Strain Curve for FM-73 Adhesive, Creep Data Points From Rochefort et al. [9], Apparent Young's Moduli after 1. 10, and 30 Minutes.

plot of the non-linear stress-strain uniaxial relationship for the adhesive [9]. They correspond to the apparent Young's modulus of FM-73 after one, ten, and thirty minutes for a creep test. Table 4.2 presents the properties of the linear adherend and adhesive, and the parameters of the non-linear adhesive (eq. 2.35).

The discretization of the joint is given in Fig. 4.13. The adhesive layer in the central part of the bond was discretized with ten elements through the thickness and twenty-two elements over the length.

The boundary conditions were as follows. The middle point of the left edge of the specimen was fixed in the x and y directions. At the right edge, the y displacement of the middle point was fixed, and a load of 1200 lbs (5345 N) was applied at this point in the x direction.

4. 3. 2. Finite Element Results

Figures 4.14 and 4.15 represent the stress distributions for the linear case at the bottom interface and in the middle of the adhesive layer. The dot, triangle, and cross points correspond to the axial, peel, and shear stresses, respectively. The main difference in the results is due to the effect of the stress singularity. The

Table 4.2: Material Propreties of the Aluminum and FM-73 Adhesive Used for the Thick-Adherend and Crack-Lap Joints Analyses.

MATERIAL	E	ν
Aluminum	$10.3 \times 10^{+6}$ psi 71,000 MPa	0.33 } Linear Material
Adhesive FM-73	481,700 psi 3,321 MPa	0.32 } Linear Material

Parameters for the Non-Linear Elastic Law eq. (2.35).

TIME	E	n	K
1 Minute	481,700 psi 3,321 MPa	1.218	$0.0442\ (psi)^{-.218}$ $0.0064\ (Pa)^{-.218}$
10 Minutes	463,800 psi 3,198 MPa	1.175	$0.0766\ (psi)^{-.175}$ $0.0163\ (Pa)^{-.175}$
30 Minutes	439,400 psi 3,030 MPa	1.180	$0.0735\ (psi)^{-.180}$ $0.0150\ (Pa)^{-.180}$

} Non-Linear Material, $\nu = 0.32$

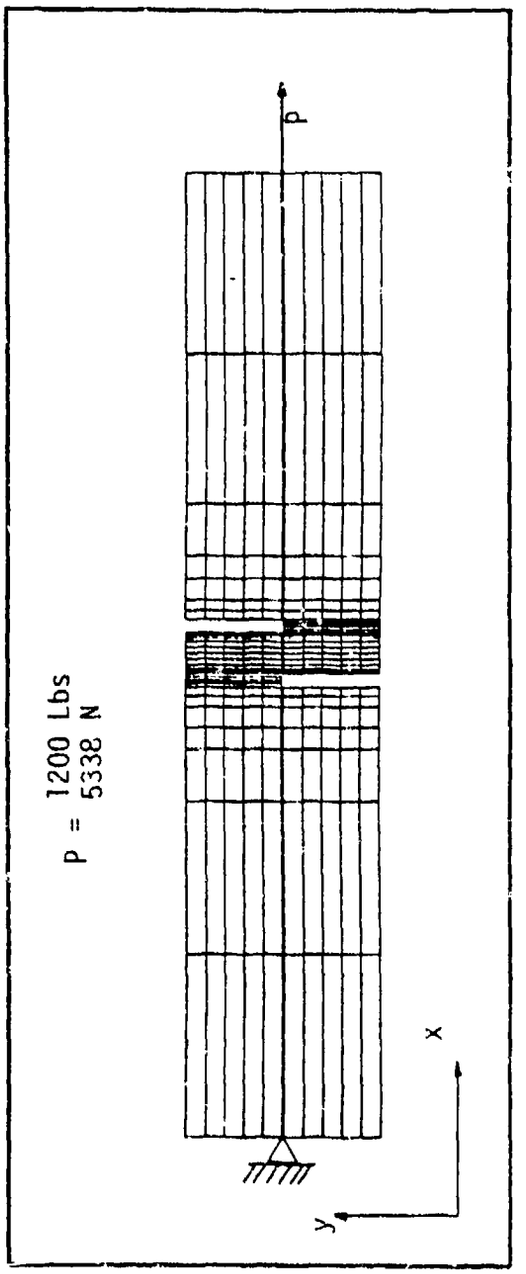

Figure 4.13: Discretization of the Thick-Adherend Specimen, Boundary Conditions, and Loading.

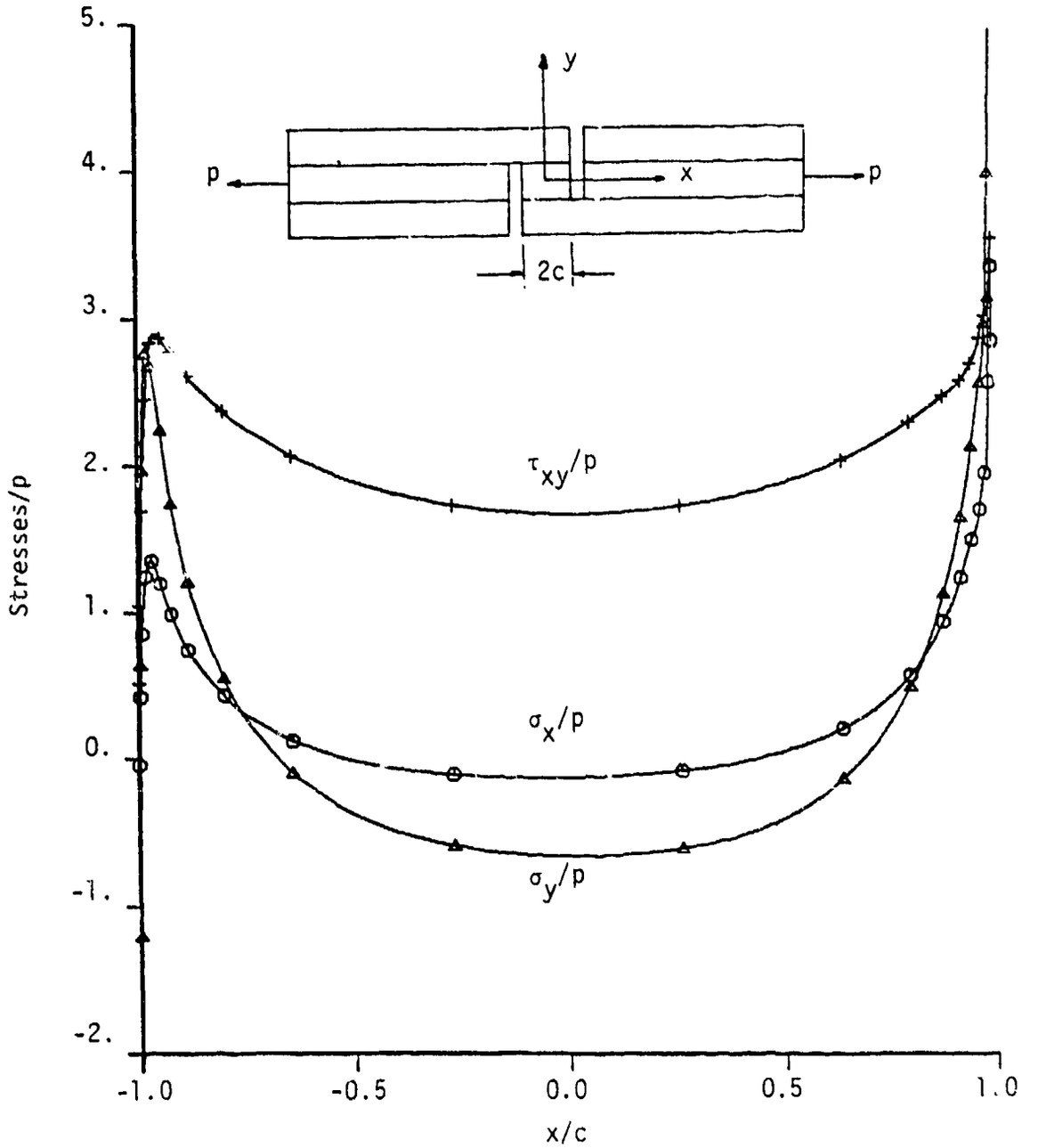

Figure 4.14: Stress Distribution at the Bottom Interface Layer .

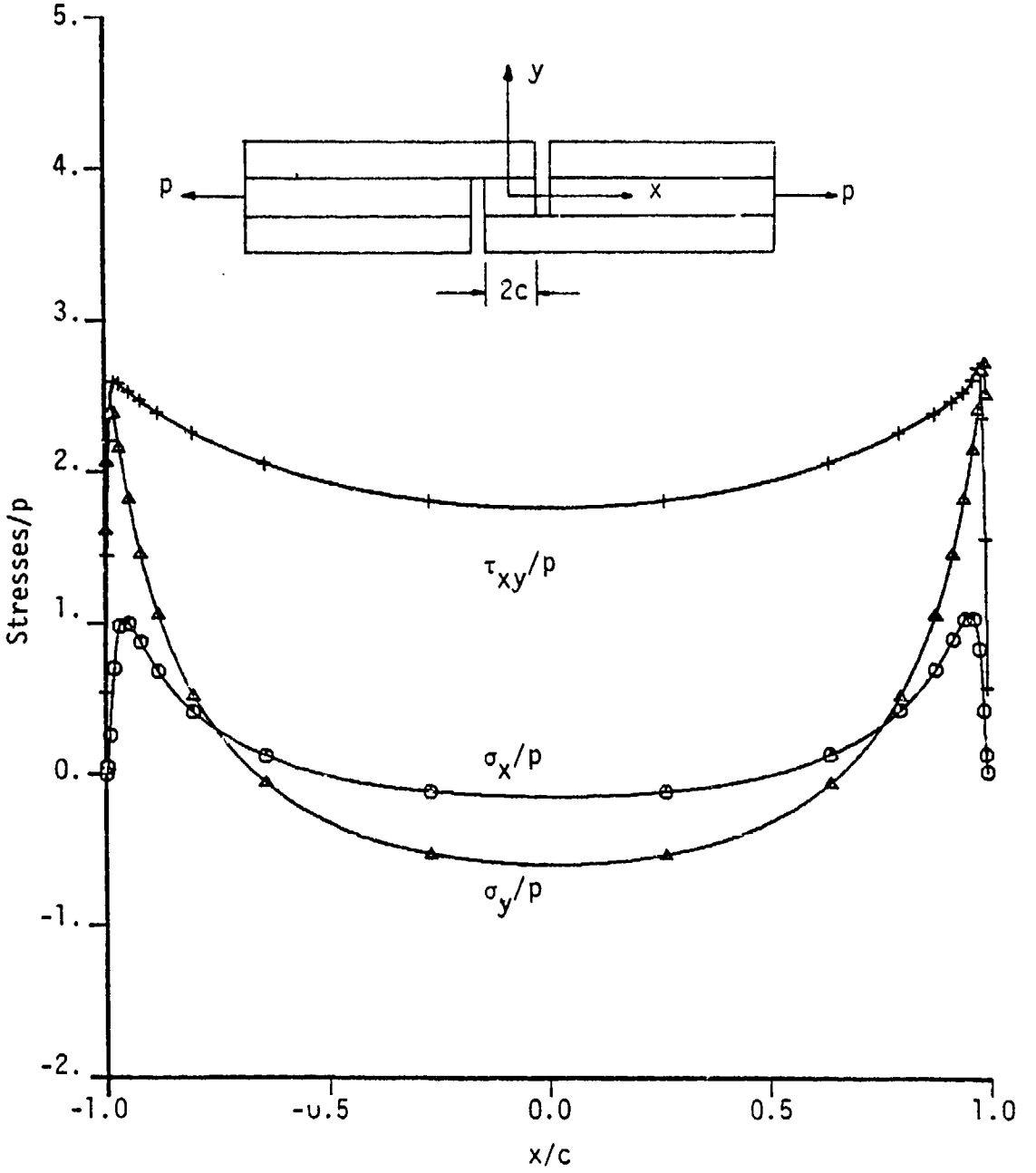

Figure 4.15: Stress Distribution in the Middle of the Adhesive Layer.

stresses along the bottom interface increase dramatically near the right free edge, and do not satisfy the boundary conditions at this edge due to the singularity. The stresses at the middle of the adhesive are decreasing at both ends.

Figures 4.16, 4.17, and 4.18 are the stresses along the interface layer for three different non-linear adhesive materials. It appears that the stresses inside the thick-adherend specimen are less sensitive to a change in the Young's modulus of the adhesive than in the case of the single-lap joint discussed earlier, or the crack-lap joint which will be discussed subsequently. At the singularity, the shear stress decreases slightly. This effect is due to the formulation of the non-linear law.

Figures 4.19, 4.20, and 4.21 are the stress distributions across the thickness of the adhesive layer at different distances from the right free edge. The adhesive Young's modulus corresponds to the first non-linear modulus given in Table 4.2. The 0. and 1. abscissa values correspond to the top and bottom interface, respectively. Each curve is plotted for x constant values, given in each figure. The singularity effect is localized near the end of the bond line.

Figures 4.22 and 4.23 is a comparison of the shear and peel stress distributions obtained by Botha, et al. [16] and

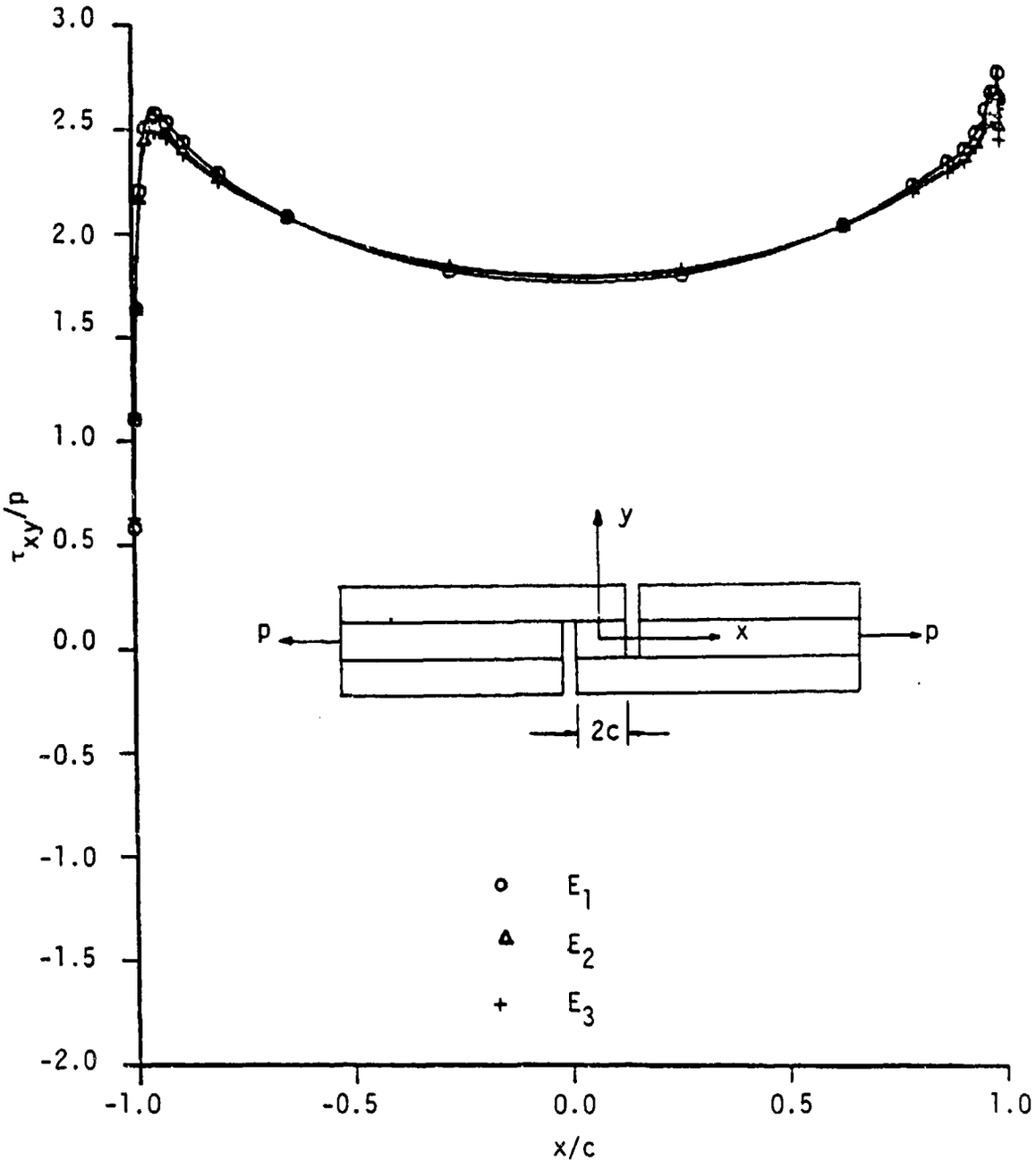

Figure 4.16: Shear Stress Distribution at the Bottom Interface for Three Different Non-Linear Young's Moduli.

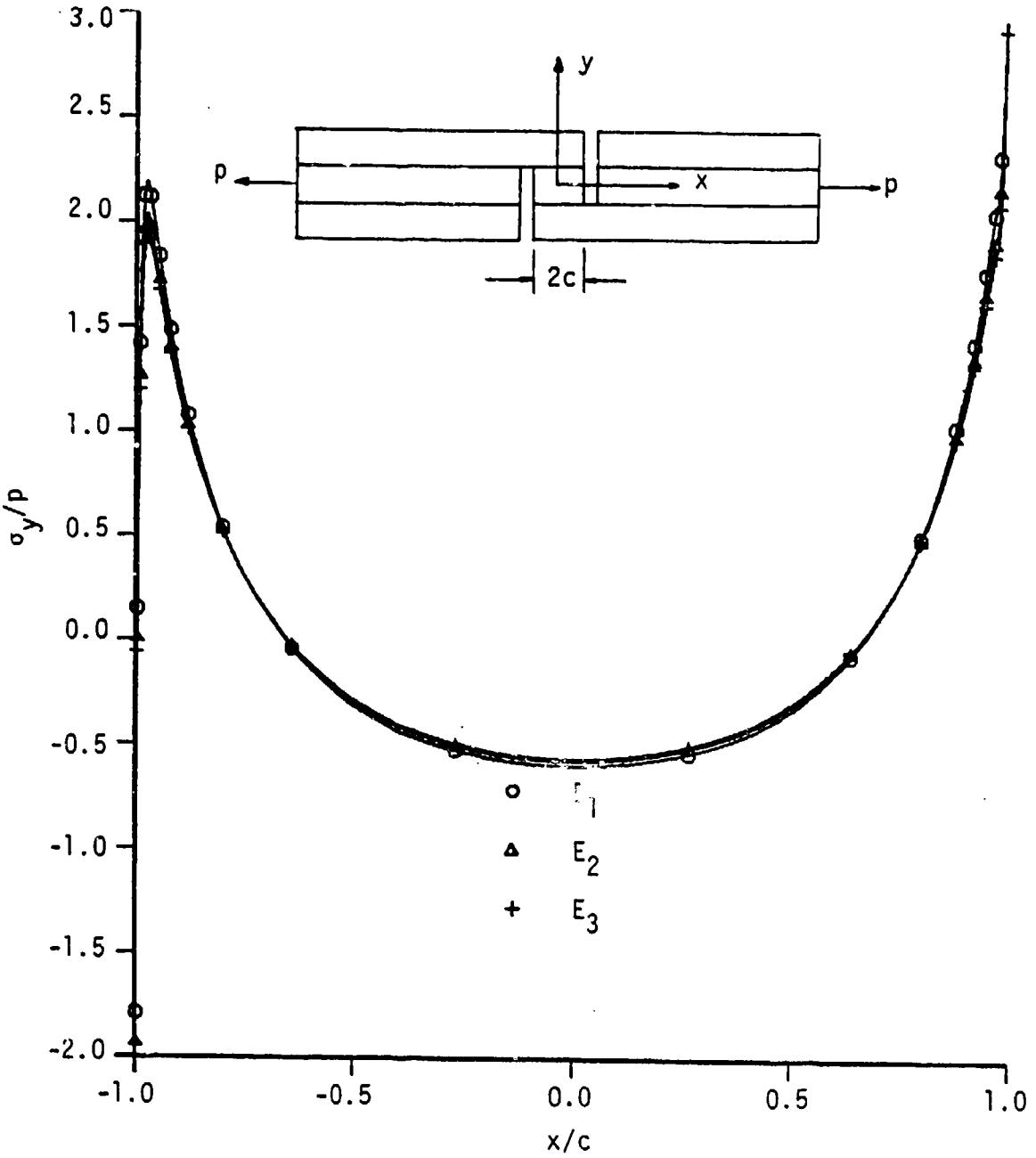

Figure 4.17: Peel Stress Distribution at the Bottom Interface for Three Different Non-Linear Young's Moduli.

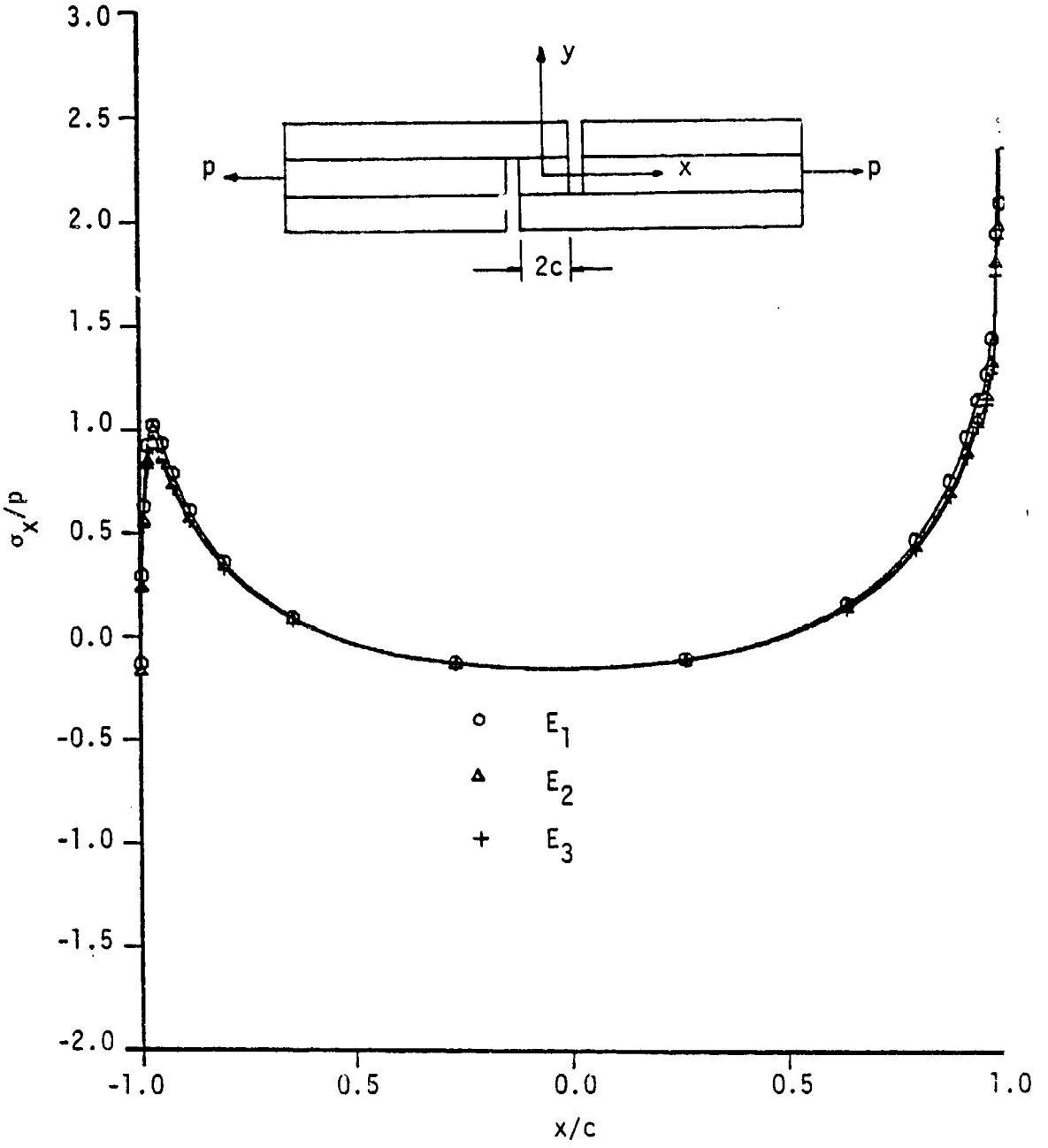

Figure 4.18: Axial Stress Distribution at the Bottom Interface for Three Different Non-Linear Young's Moduli.

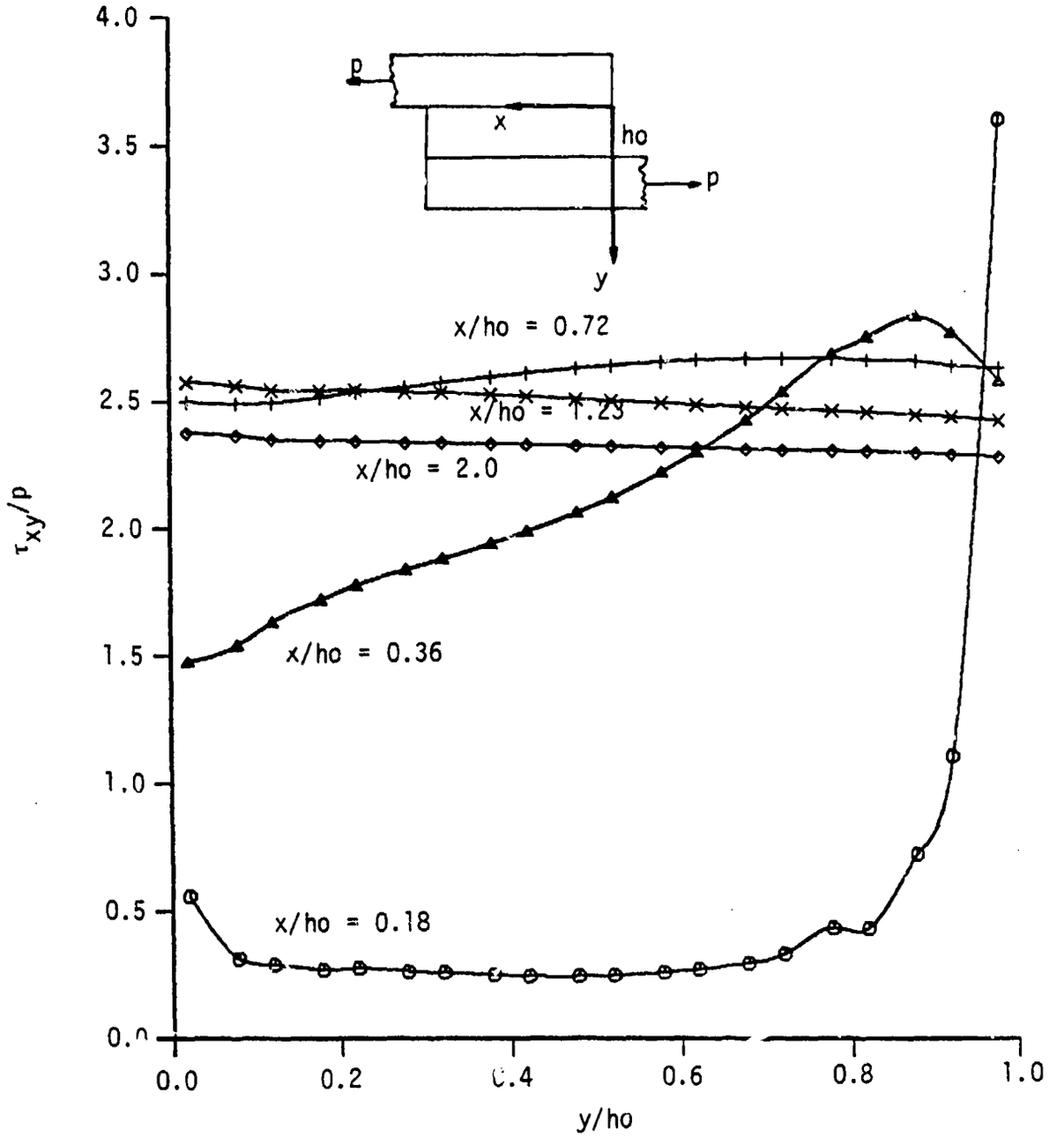

Figure 4.19: Stress Distribution across the Adhesive Layer Near the Right Edge, Results for the First Non-Linear Adhesive.

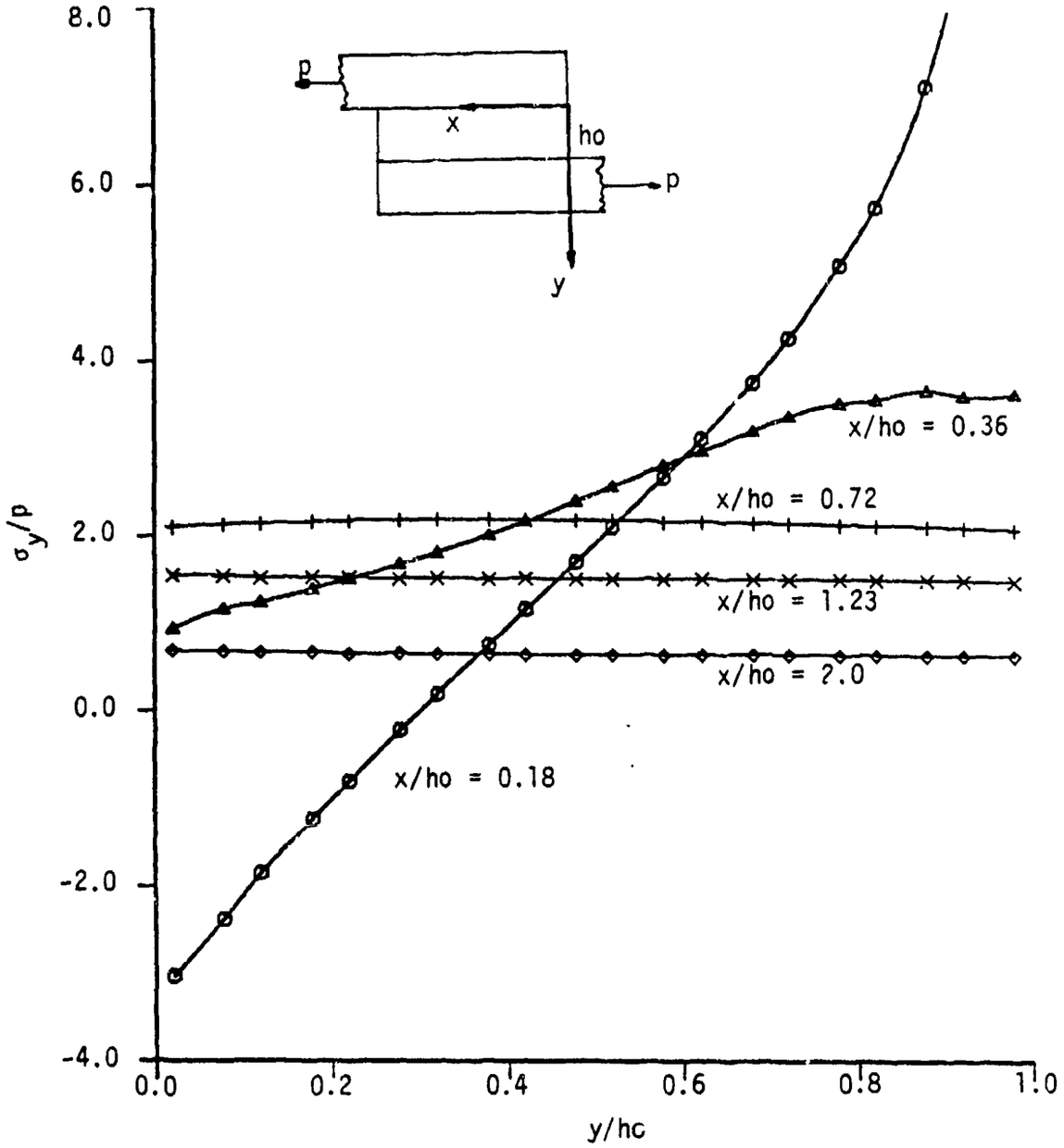

Figure 4.20: Peel Stress Distribution Across the Adhesive Layer Near the Right Edge, Results for the First Non-Linear Adhesive.

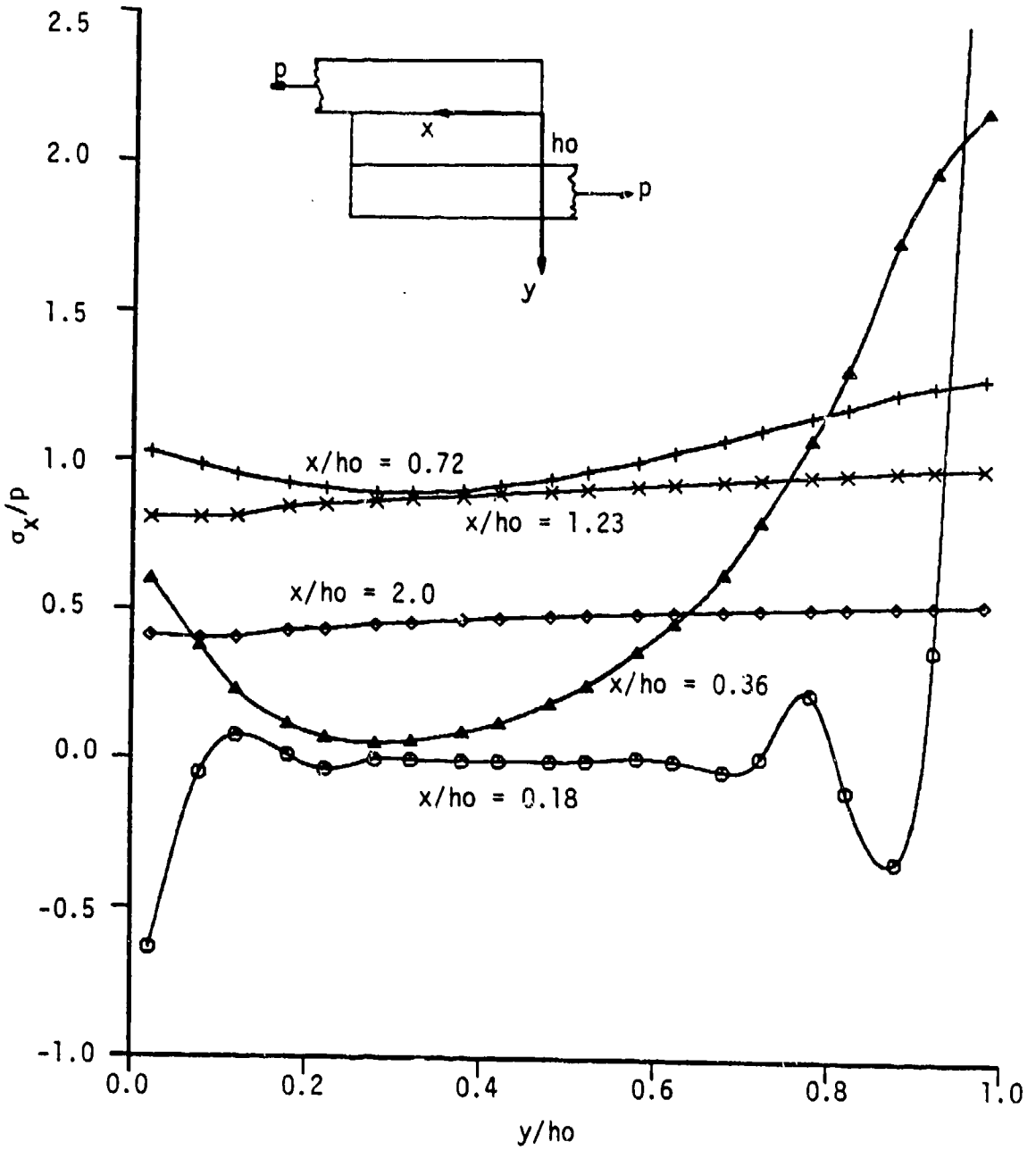

Figure 4.21: Axial Stress Distribution Across the Adhesive Layer Near the Right Edge, Results for the First Non-Linear Adhesive.

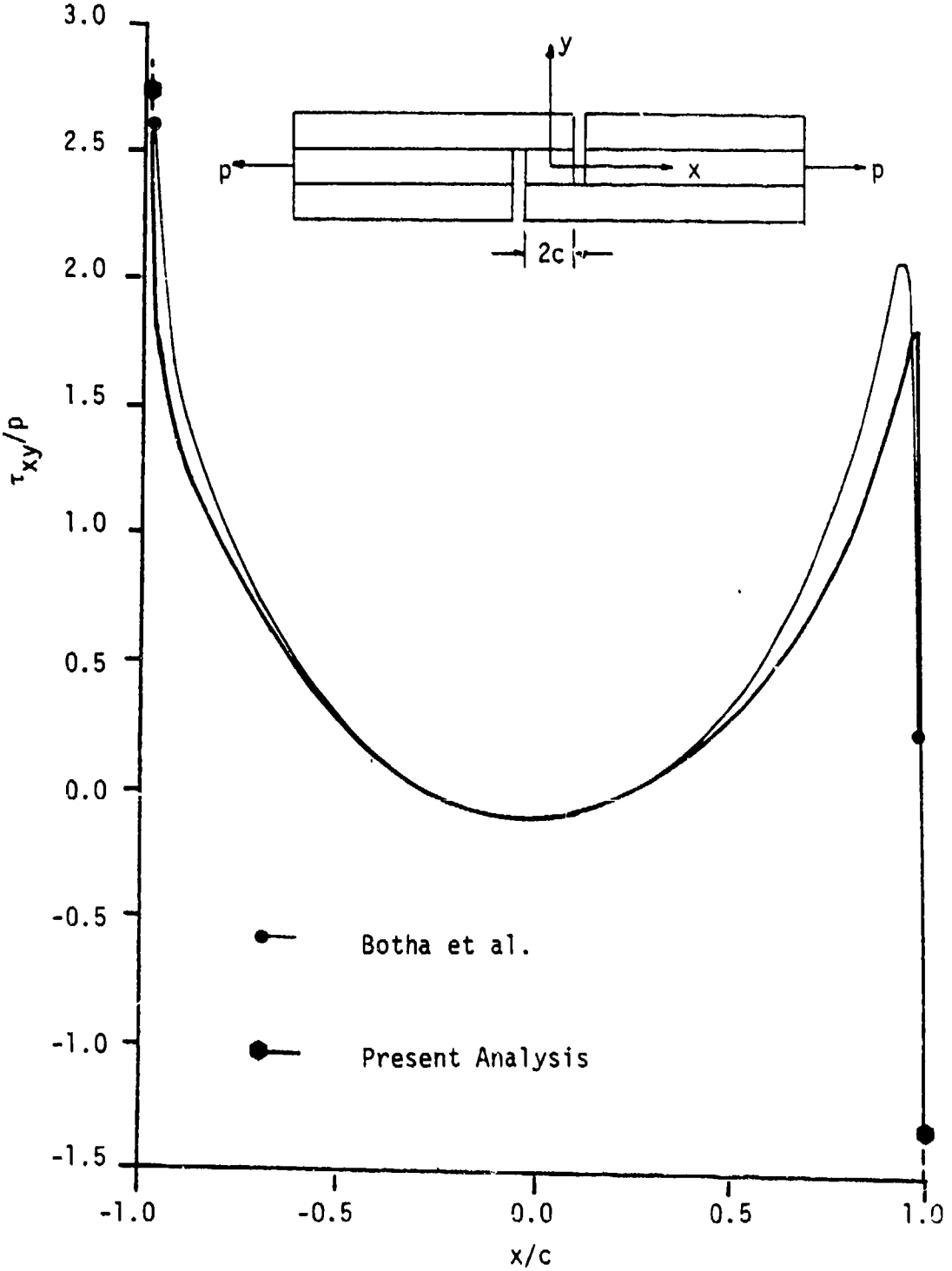

Figure 4.22: Shear Stress Distribution at the Top Interface, Comparison Between Botha [16] and the Present Analysis.

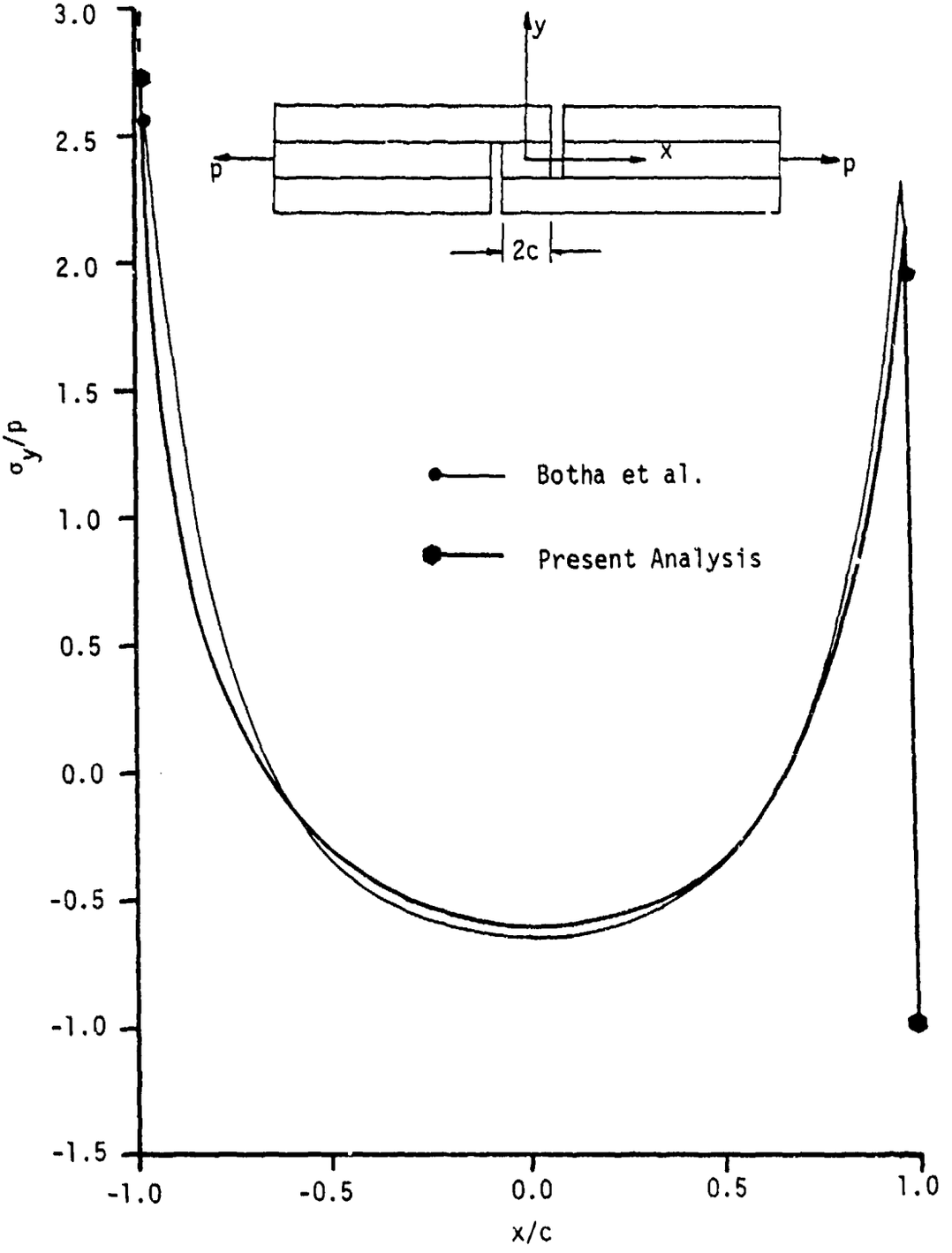

Figure 4.23: Peel Stress Distribution at the Top Interface, Comparison Between Botha [16] and the Present Analysis.

the present analysis. The main differences are at the point of maximum stresses and near the singularity.

4. 4. Crack-Lap Joint

4. 4. 1. Geometry and Discretization

The crack-lap joint configuration is often used for fracture analysis of adhesive. This joint is currently used at NASA Langley for the study of the G_I, G_{II}, and G_{III} coefficients of an adhesive. These coefficients are related to the strain energy released in a crack propagation for the first, second, and third opening modes. This study [31] should lead to design criteria of bonded joints. In our study we were interested in the stress distributions inside the adhesive layer, and the sensitivity of these stress distributions to a change in the Young's modulus of the adhesive.

The geometry of joint studied in this section is given in Fig. 4.24. As indicated, it had an equal adherends thickness of 0.125 inch (3.18 mm), and a width of 1. inch (25.4 mm). The adhesive thickness was 0.005 inch (0.127 mm). The total length of the joint was 12 inch (305 mm), and the overlap was 10 inch (254 mm).

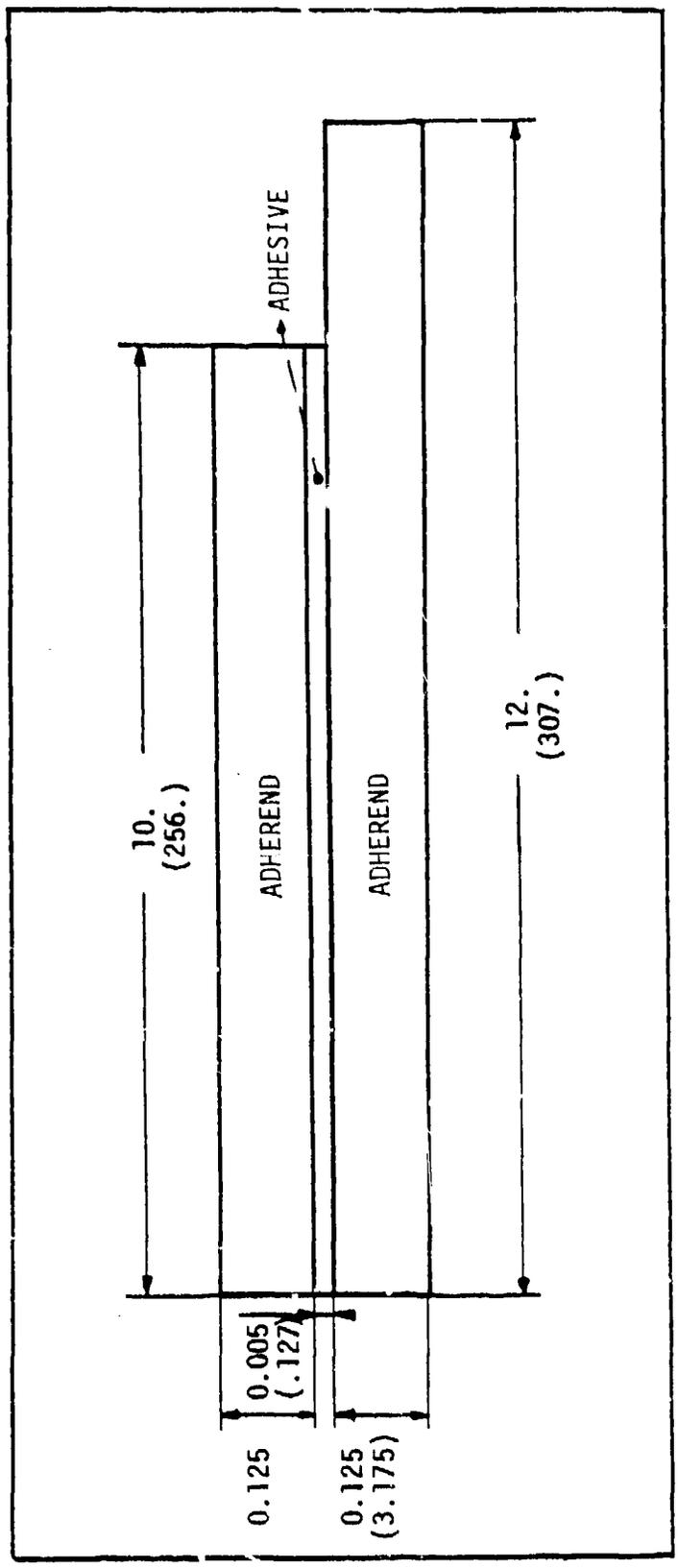

Figure 4.24: Geometry of the Crack-Lap Joint Analyzed in this Section, Dimension in Inches, (Dimension in Millimeters)

The materials used for both adherends and adhesive are the same as previously given in Table 4.2, used for the for the thick adherend analyses.

The discretization of the structure is given in Fig. 4.25. A total of four hundred and fifty elements and fourteen hundred and fifty one nodes were used. Five and ten elements were used over the thickness of the adherends and adhesive layer, respectively. Twenty elements were used to model the overlap part of the joint.

4. 4. 2. Loading and Boundary Condition Effects

The specimen was loaded at 128 lbs (570 N) at the right edge of the bottom adherend. Two different boundary conditions were used to analyze the problem. The first condition was a clamping of the left end of the specimen, fixing all the x and y displacements. In the second condition all x displacements were fixed but only one point at the left edge was fixed for the y displacement (to avoid any rigid body motion). In these analyses the Young's modulus of the adhesive was linear, and corresponded to the first adhesive Young's modulus of Table 4.2. Figures 4.26, 4.27, and 4.28 show the comparison for the shear, peel and axial stress distributions under the two different boundary

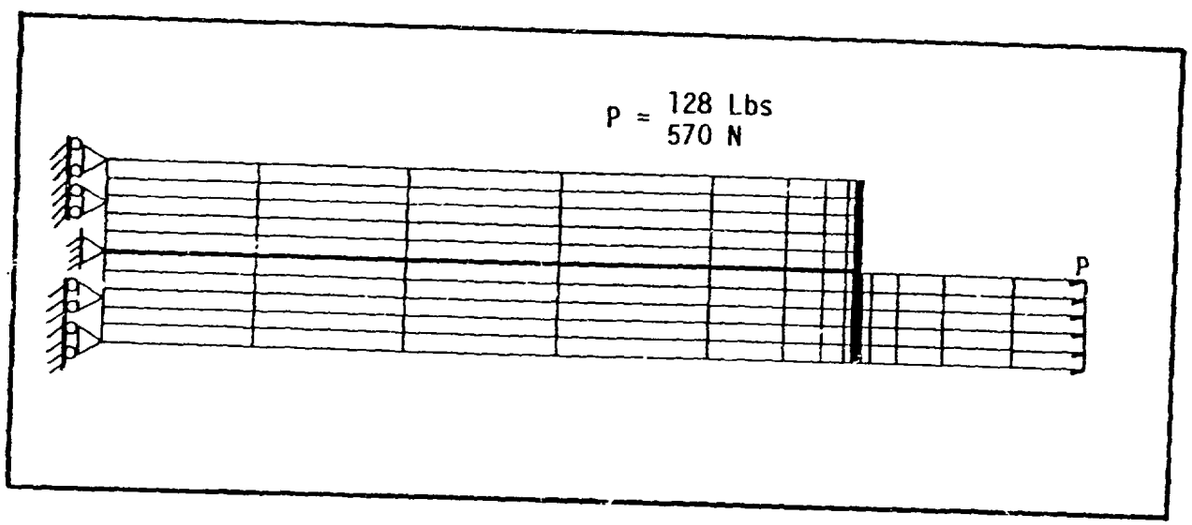

Figure 4.25: Discretization, Boundary Conditions, and Loading of the Crack-Lap Joint Analyzed in this Section.

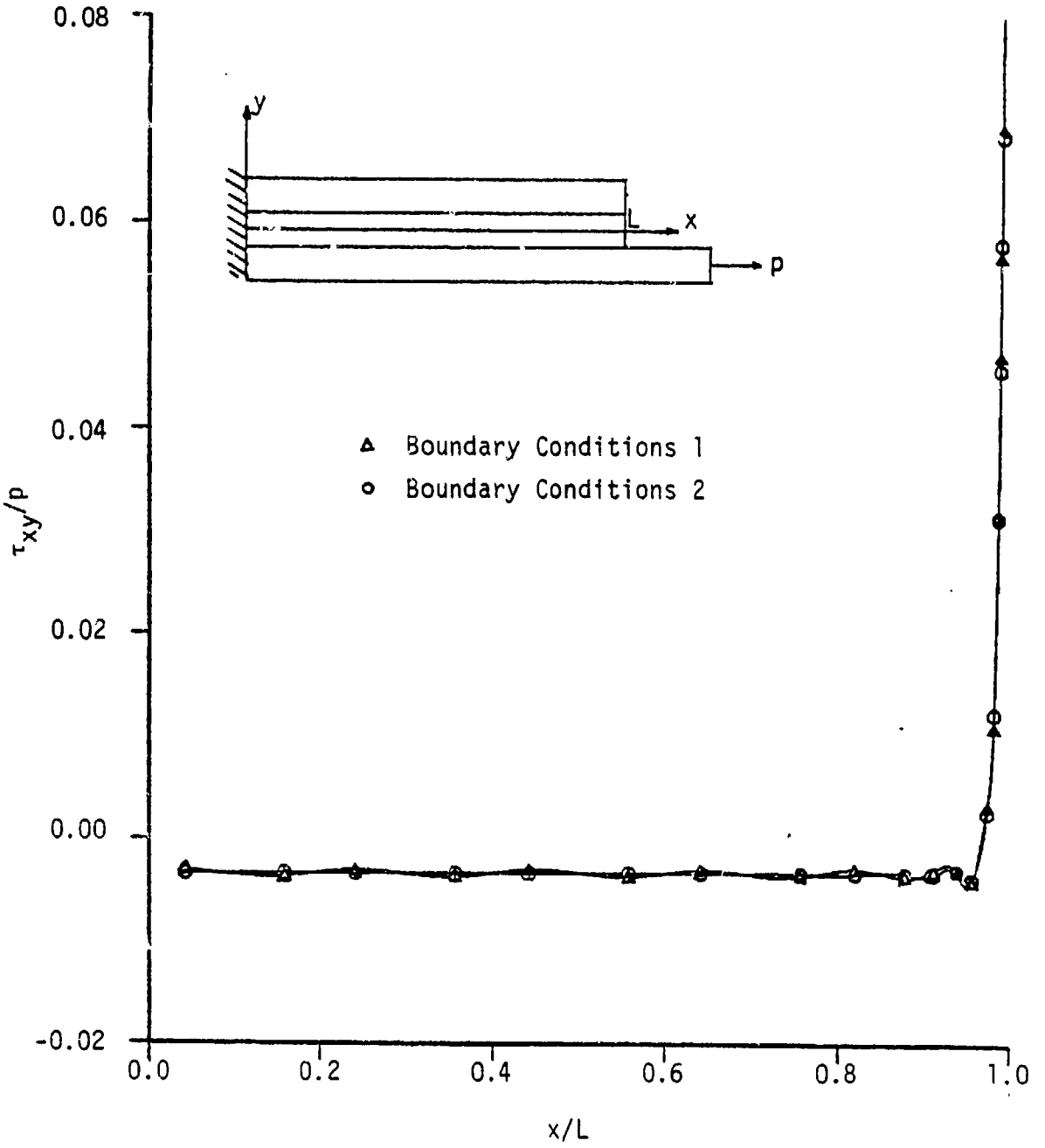

Figure 4.26: Effect of the Boundary Conditions on the Shear Stress at the Bottom Interface.

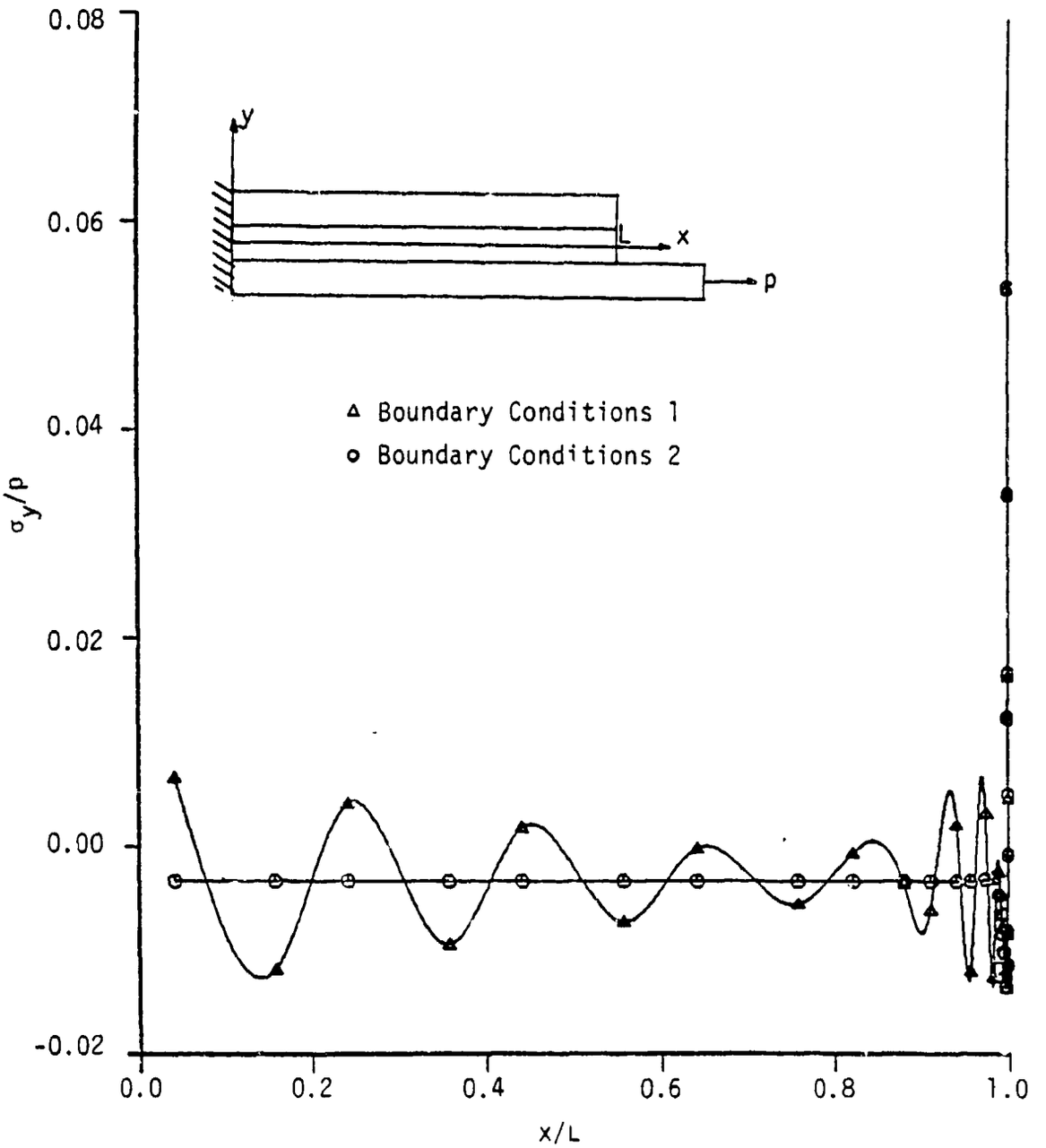

Figure 4.27: Effect of the Boundary Conditions on the Peel Stress at the Bottom Interface.

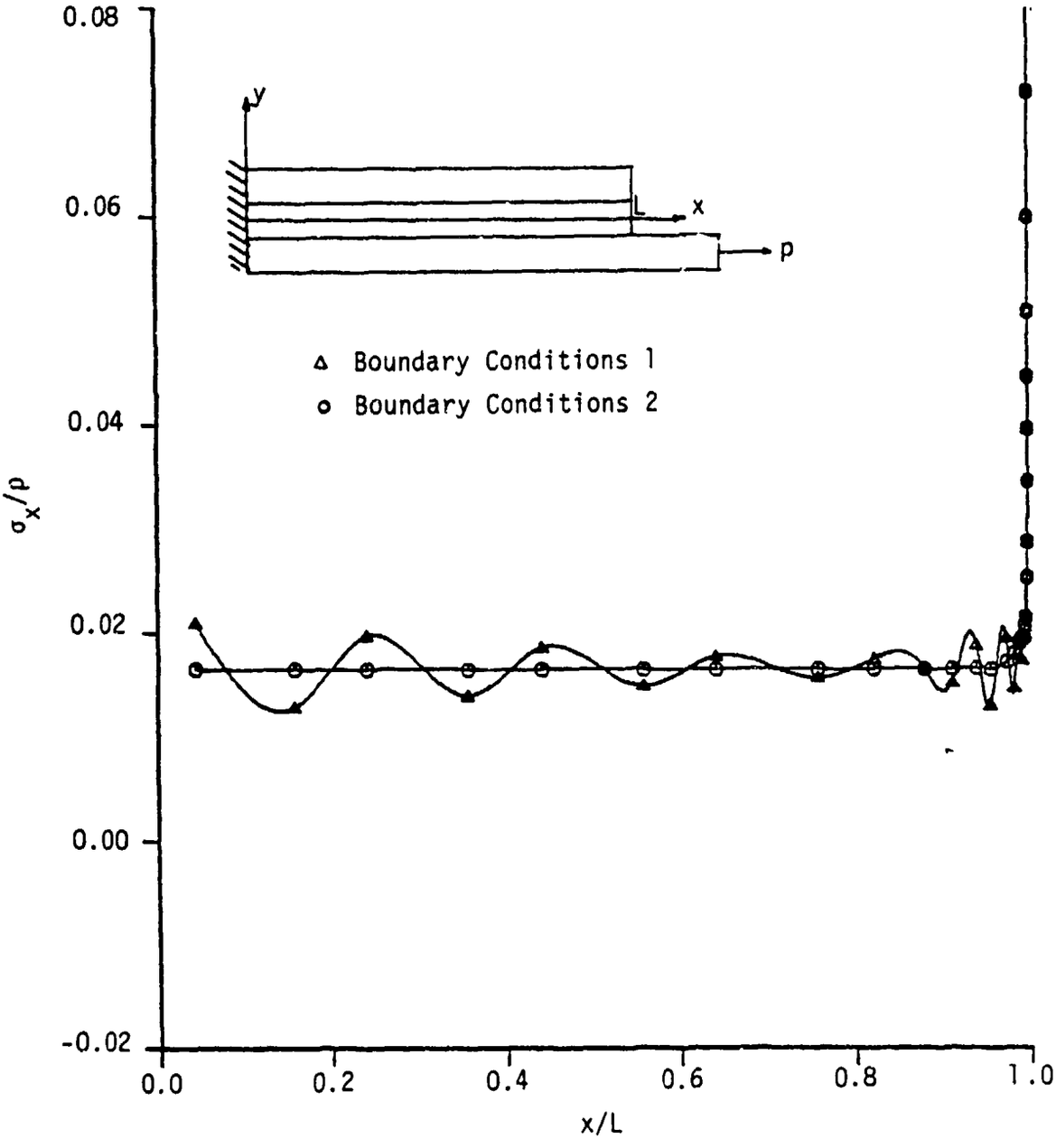

Figure 4.28: Effect of the Boundary Conditions on the Axial Stress at the Bottom Interface.

conditions. The stress results were non-dimensionalized by the factor

$$p = \frac{P}{A}$$

where P is the applied load P=128 lbs(570 N), and A is the area of the cross section of the bottom adherend. The oscillation in the results for the first boundary condition was due to the fact that the adhesive layer could not shrink under Poisson's effect at the left boundary.

4. 4. 3. Results for the Non-linear Analysis

Figures 4.29, 4.30, and 4.31 show the shear, peel, and axial stresses of the crack-lap joint at the bottom interface for the last two inches of the overlap. The three different curves correspond to the three different Young's moduli used for the adhesive layer. The shear and peel distributions are less sensitive than the axial stress distribution to a change in the Young's modulus of the adhesive. As indicated, the singularity of the geometry has a different effect on the shear stress than on the peel or the axial stress. It appears that the shear stress is affected by this singularity at a distance of 0.5 inch (12.5 mm) before the edge, whereas the peel and axial stresses start to increase at a very small distance from the free

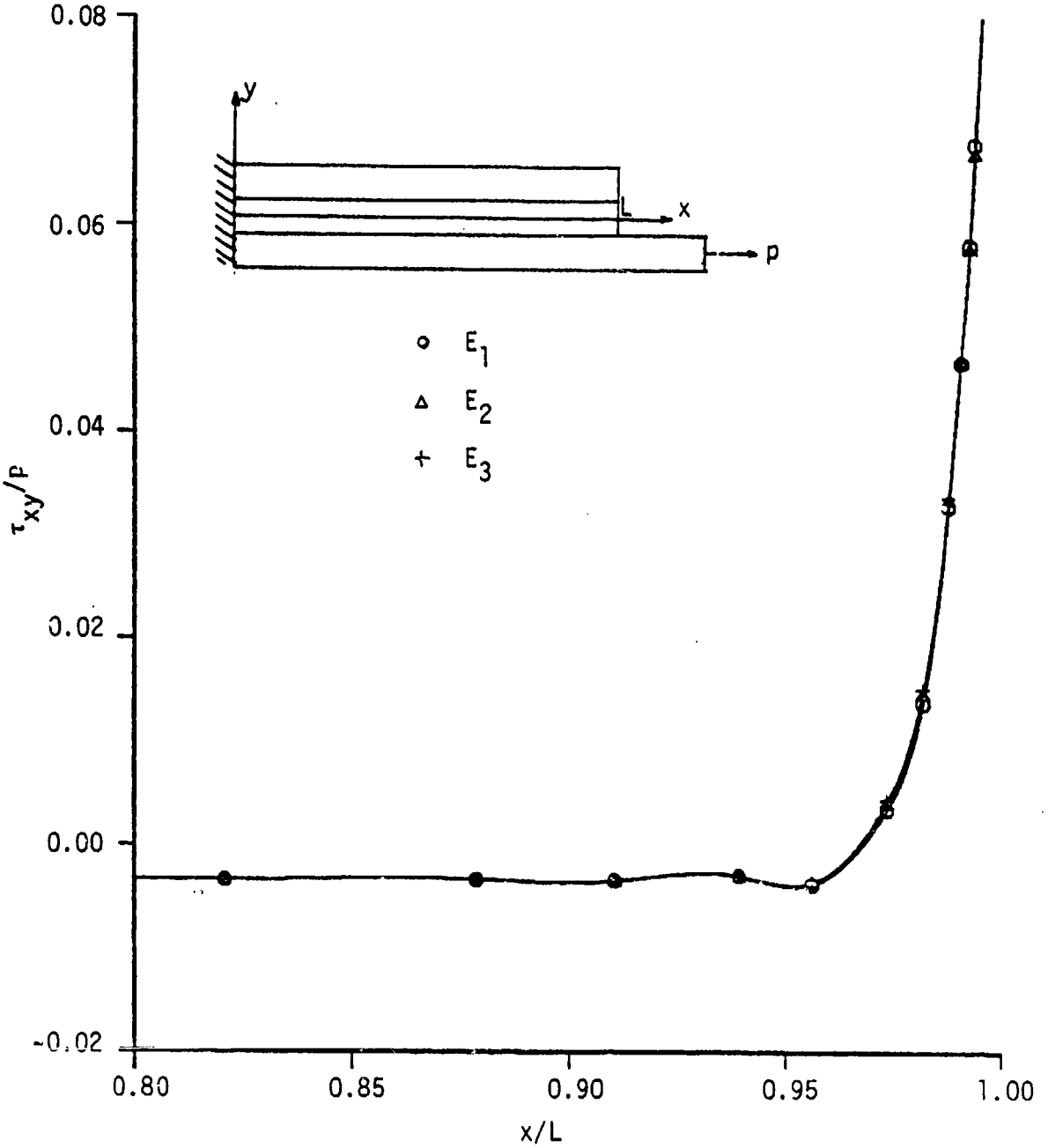

Figure 4.29: Shear Stress Distribution at the Bottom Interface for Different Non-Linear Adhesive.

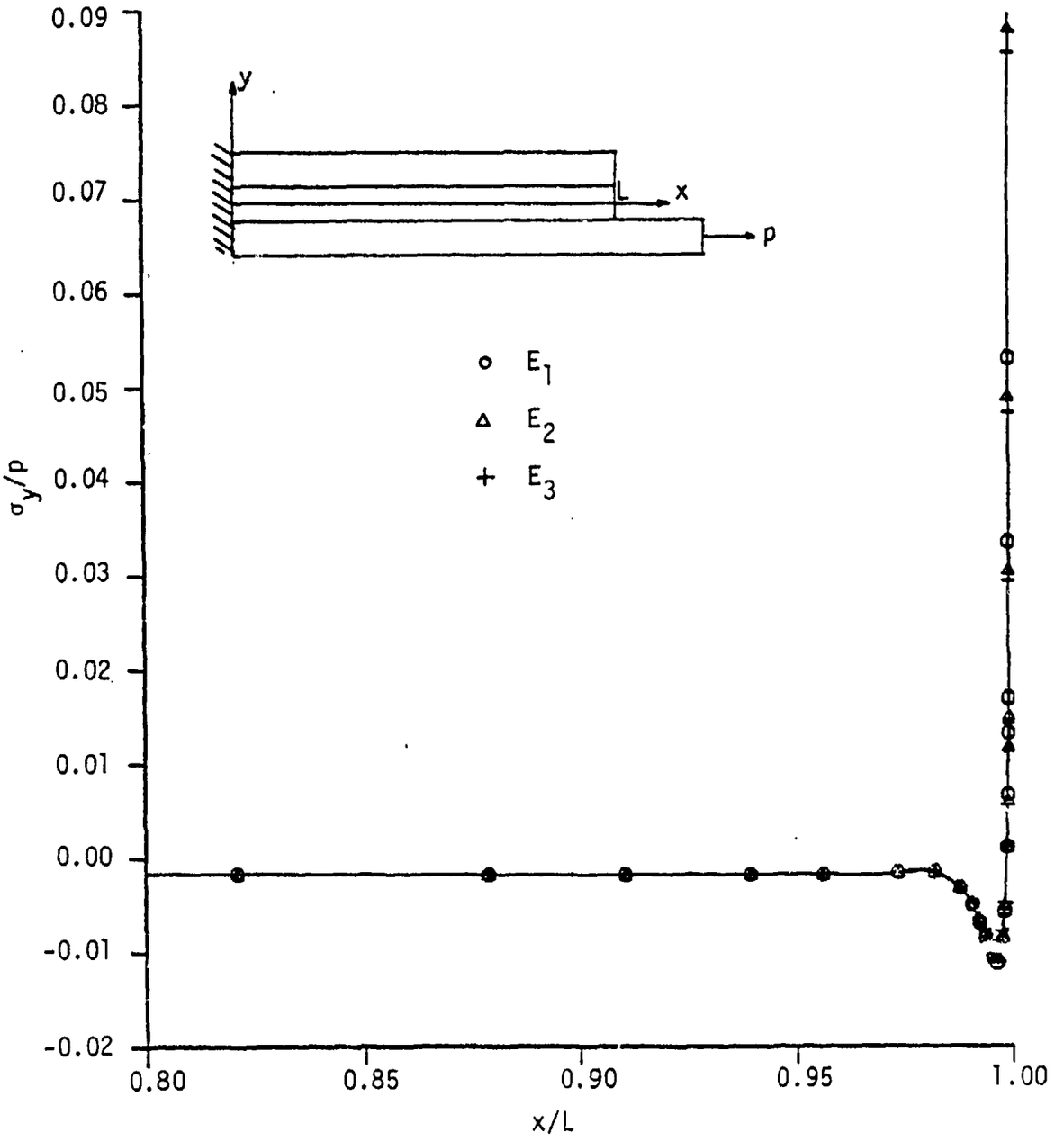

Figure 4.30: Peel Stress Distribution at the Bottom Interface for Different Non-Linear Adhesive.

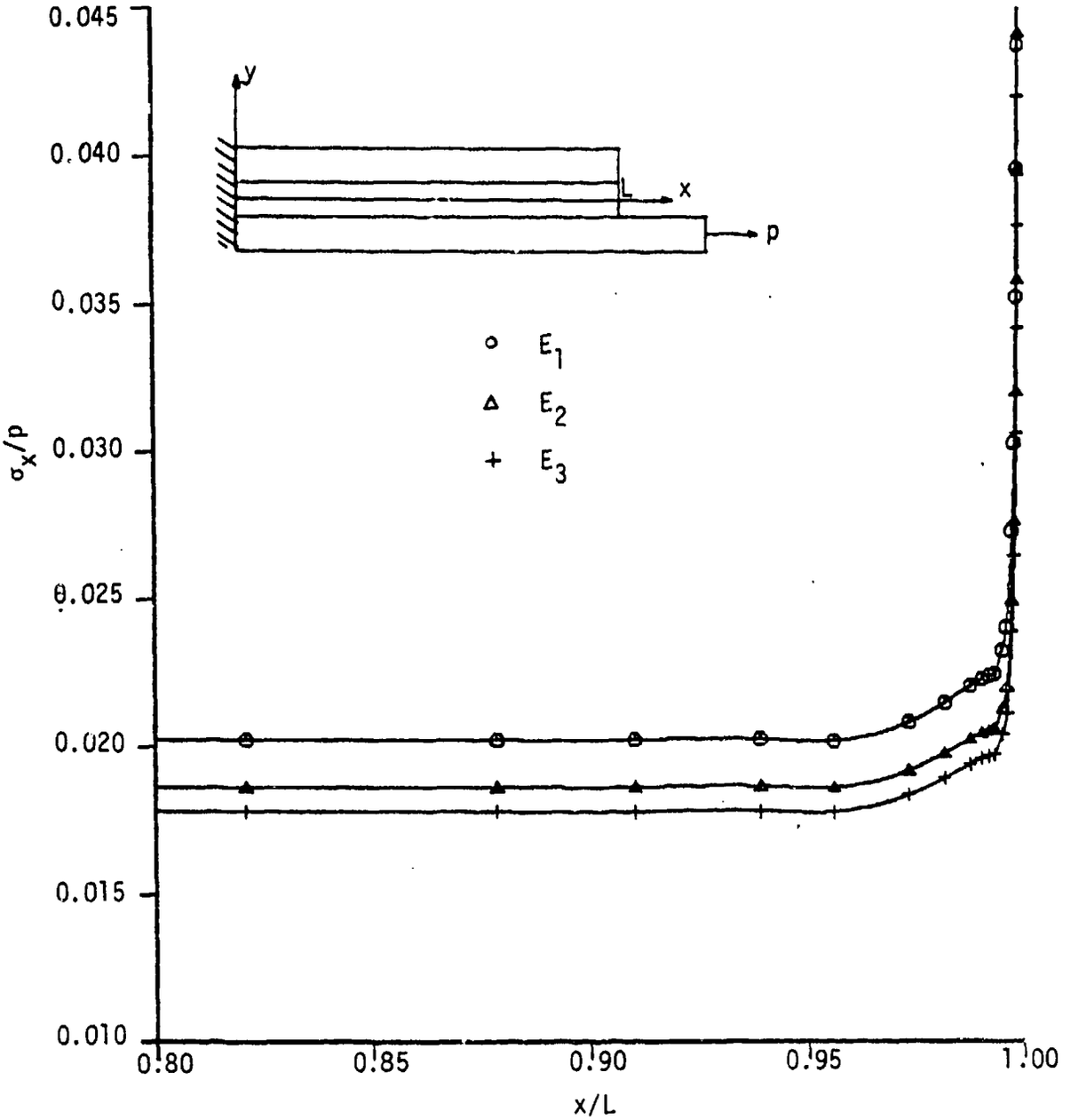

Figure 4.31: Axial Stress Distribution at the Bottom Interface for Different Non-Linear Adhesive.

edge.

Figures 4.32, 4.33, and 4.34 present the stress distributions through the thickness of the adhesive layer at different distances from the free edge. The Young's modulus of the adhesive corresponds to the first non-linear modulus Table 4.2. The 0. and 1. abscissa values correspond to the top and bottom interface, respectively. Each curve is plotted for x constant given in the figures. The singularity affects the stress distributions near the end of the bond line, but this effect damps out rapidly.

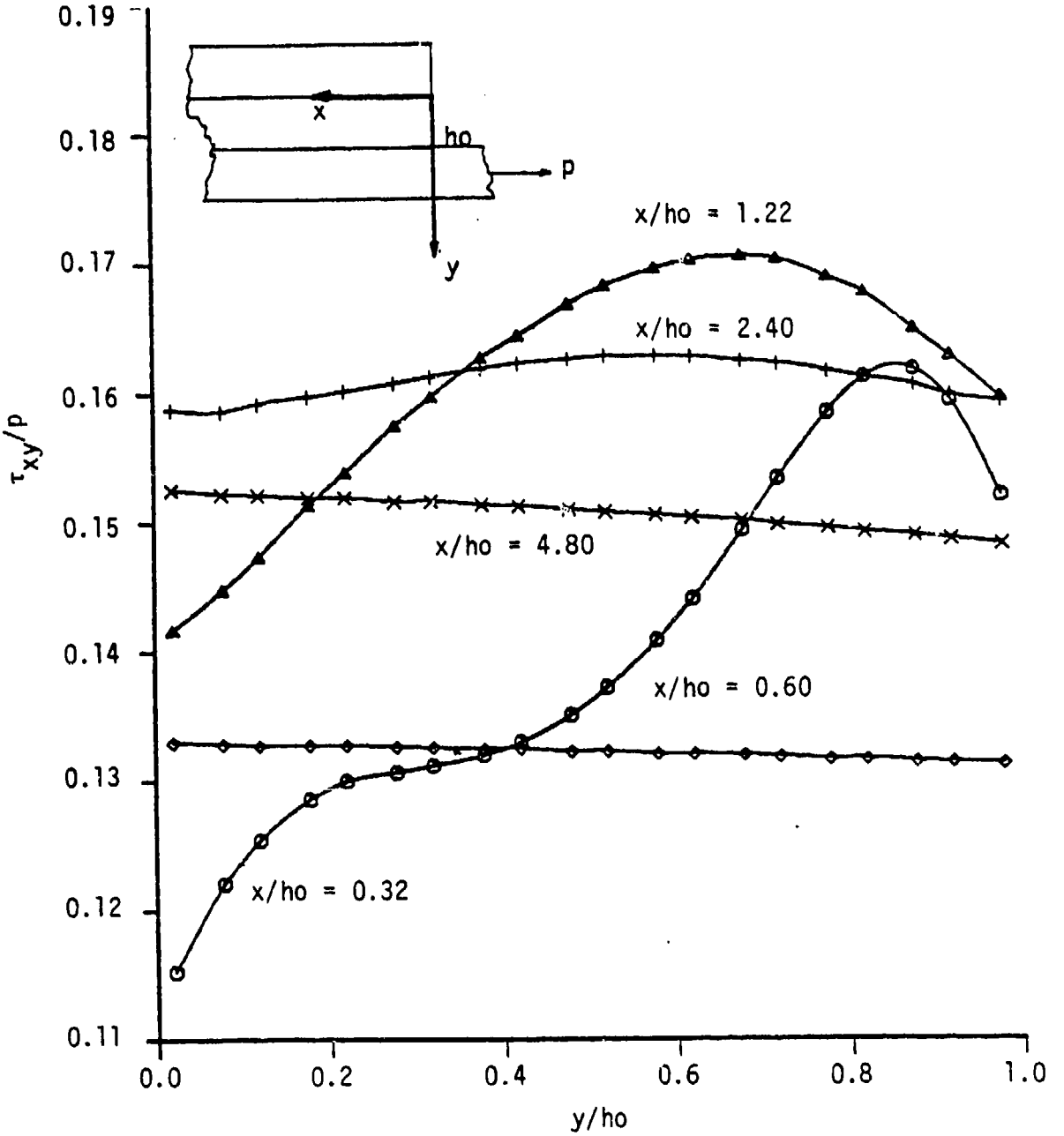

Figure 4.32: Shear Stress Gradient Across the Adhesive Layer for the First Non-Linear Case (E1).

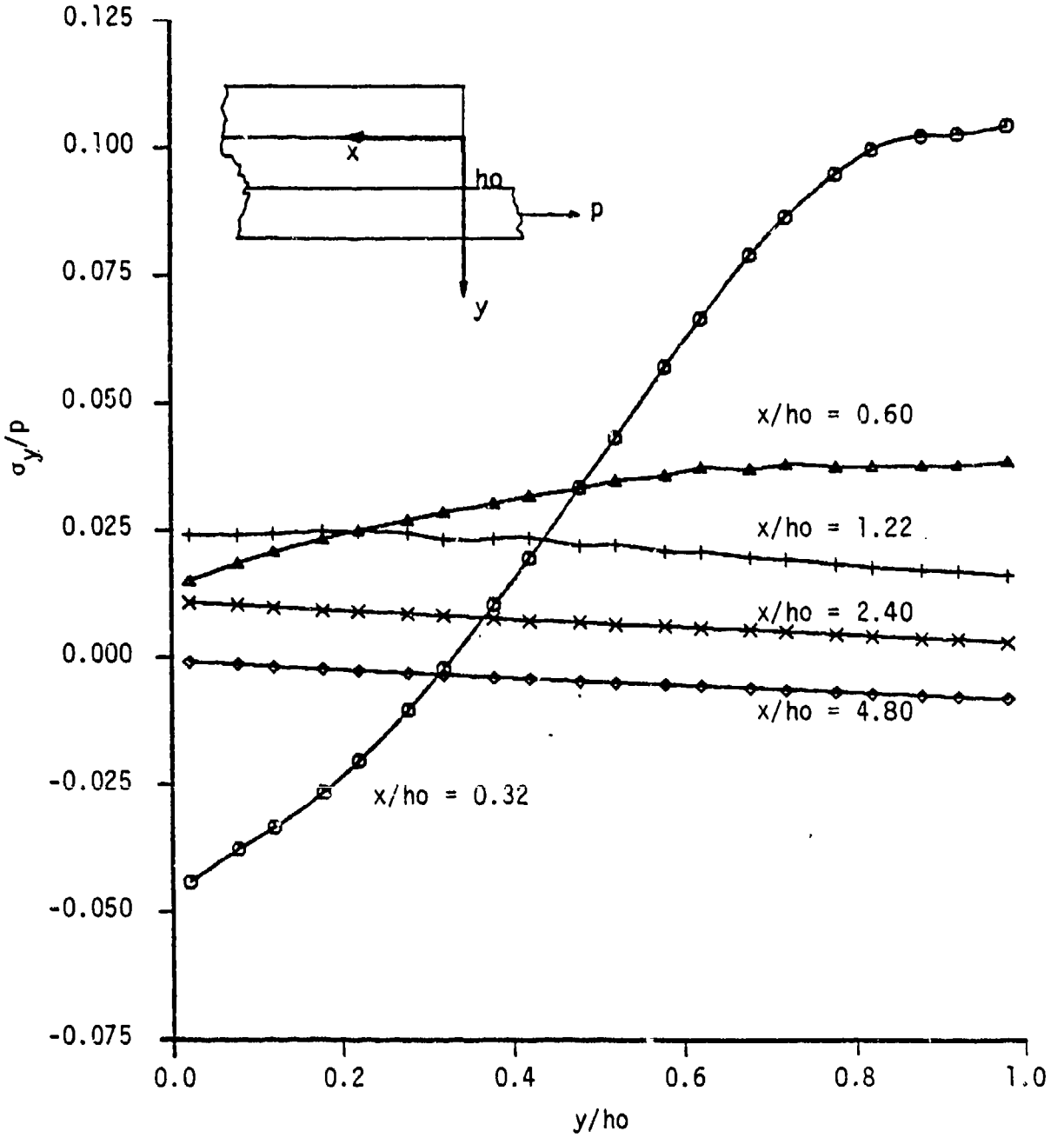

Figure 4.33: Peel Stress Gradient Across the Adhesive Layer for the First Non-Linear Case (E_1).

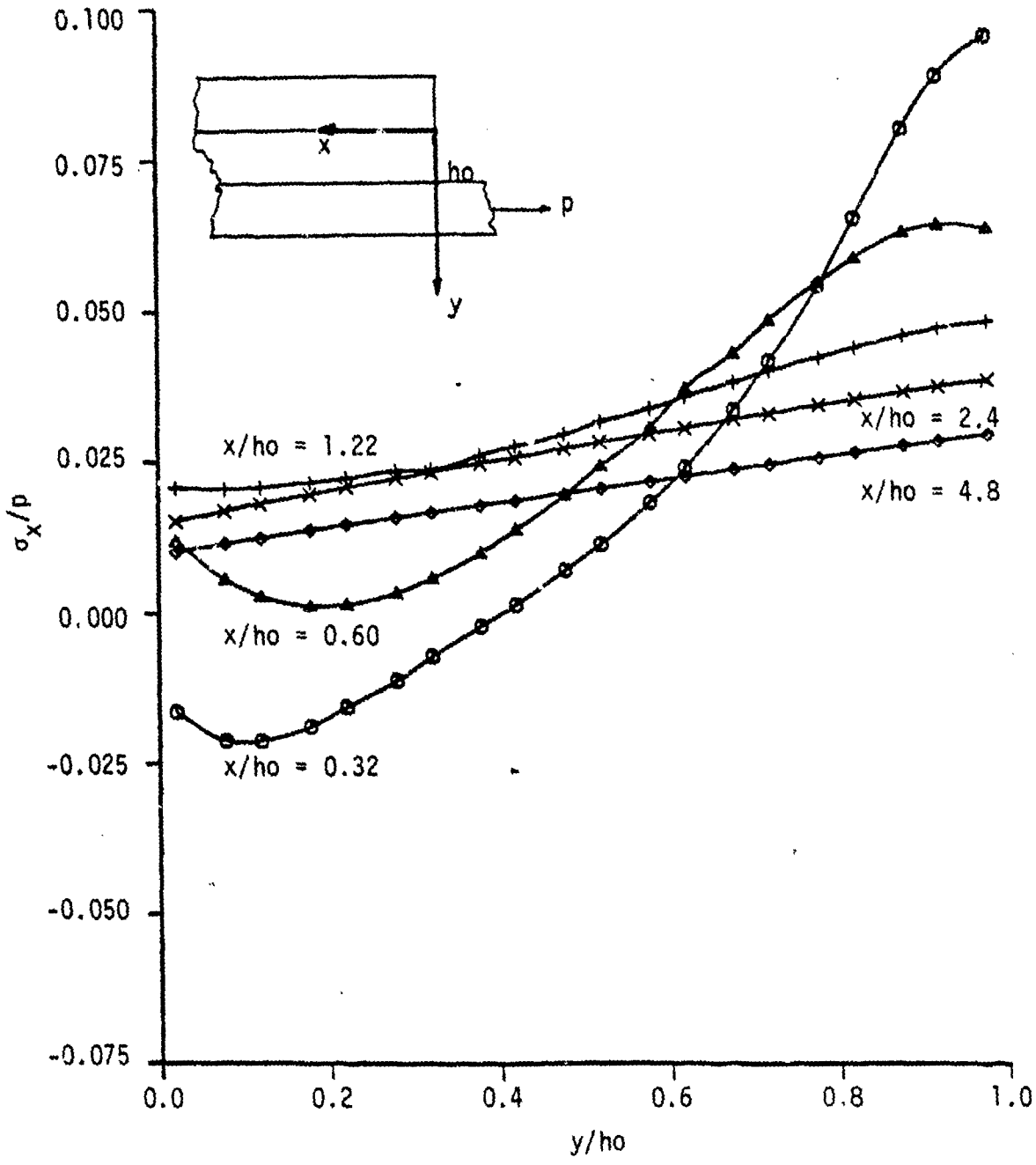

Figure 4.34: Axial Stress Gradient Across the Adhesive Layer for the First Non-Linear Case (E_1).

CHAPTER 5 SUMMARY AND RECOMMENDATIONS

5. 1. Summary

The first objective of this research was to add in the STAP [21] program an eight-noded isoparametric element, and modify it in order to analyze structures with non-linear materials. The program was then tested on problems having a closed form solution (Chapter 2).

The second objective was to analyze the single-lap joints with the program, and compare the results obtained with the Goland and Reissner's solution, and with results obtained from experimental studies (Chapter 3).

The last objective of this research was to analyze different bonded joints. The single-lap joint, thick-adherend specimen, and crack-lap joint were analyzed, and the adhesive layers were modeled with linear and non-linear material laws. The results for the two first geometries were compared with the results of Botha et al. [16], and good agreement was found. The results show that the stress distributions inside these bonded joints are strongly affected by the singularities of these geometries. It was also shown that the boundary conditions can have a

significant influence on the stress distributions in the adhesive layer.

5. 2. Recommendations

Some recommendations can be made in order to increase the effectiveness of the finite element program.

A preprocessor and postprocessor for the finite element program should be developed. The preprocessor would consist of a program generating the input data for the finite element program, and the postprocessor to consist of routines for plotting the results: stresses, strains, displacements,... Some parts of these programs have already been developed, but the interfaces between them and the main program do not exist. The creation of a preprocessor and postprocessor would help the user immensely to develop a mesh and analyze the finite element results efficiently.

The other set of recommendations is related to the finite element program, and are explained below.

1) The program should be modified in order to introduce displacement boundary conditions. With this transformation, if the structure presents symmetric or antisymmetric geometry, only half the structure could be analyzed.

2) The in-core matrix decomposition routine should be changed to an out-of-core decomposition routine. This change would permit an unlimited increase in the number of degrees of freedom irrespective of the mainframe computer system.

3) The introduction of an elastic-plastic law in the program is necessary if the stress and strain distribution near the singularities are to be investigated.

4) Near the singularity, large rotations are suspected to occur. The non-linear strain displacement relationship should be introduced in the analysis in order to evaluate the importance of this effect.

References

(1) Findley, W.N. and Lai, J.S.Y.,"A Modified Superposition Principle Applied to Creep of Nonlinear Viscoelastic Materials Under Abrupt Changes in State of Combined Stress", Trans Soc Rheology ,Vol 11, No 3, 1967, pq 361.

(2) Schapery, R.A., "An Engineering Theory of Nonlinear Viscoelasticity with Applications.", Int. J. Solids Structures ,1966,Vol.2,pp 407.

(3) Schapery, R.A., "On the Characterization of Nonlinear Viscoelastic Materials.", Polymer Engineering and Science July 1969,Vol.9,No.4.

(4) Dillard, D.A., Morris, D.H., and Brinson, H.F., "Creep and Creep to Rupture of Laminated Graphite/Epoxy Composites.",VPI&SU Report, VPI-E-81-3, March 81.

(5) Griffith, W.I., Morris, D.H., and Brinson, H.F. ,"Accelerated Characterization of Graphite-Epoxy Composites", VPI&SU Report, VPI-E-80-27, September 1980.

(6) Hiel, C., Cardon, A.H., and Brinson, H.F, "The Nonlinear Viscoelastic Response of Resin Matrix Composite Laminates", VPI&SU Report, VPI-E-83-6, March 1983.

(7) Yen, S.C., "The Creep and Creep to Rupture of SMC-R50 Under Different Thermomechanical Conditions", PhD Dissertation, Department, of Engineering Science and Mechanics, VPI&SU, Blacksburg, VA , March 1984.

(8) Tuttle, M.E. and Brinson, H.F., "Accelarated Viscoelastic Characterization of T300/5208 Graphite-Epoxy Laminates", VPI&SU Report, VPI-E-84-9, March 1984.

(9) Rochefort, M.A. and Brinson, H.F., "Nonlinear Viscoelastic Characterization of Structural Adhesives", VPI&SU Report, VPI-E-83-26, July 83.

(10) Post, D.,"Moire Interferometry at VPI&SU.", Experimental Mechanics ,Vol. 23,No. 2,pp. 203,June 1983.

(11) Krieger, R., "Stiffness Characteristic of Structural Adhesives for Stress Analysis in Hostile Environment", American Cyanamid Company, Report Bloomingdal, Havre de Grace,Maryland.

(12) Goland, M. and Reissner, E., "The Stresses in Cemented Joints.", Journal of Applied Mechanics , March 1944.

(13) Hart-Smith, L.J., "Adhesive-Bonded Single-Lap Joints.", Technical Report, January 1973, NASA CR 112236.

(14) Du Chen and Shun Cheng,"An Analysis of Adhesive-Bonded Single-Lap Joints.", Journal of Applied Mechanics ,March 1983, Vol. 50,pp 109-115.

(15) Sen, J.K. and Jones, R.M., "Stresses in Double-Lap Joints Bonded with a Viscoelastic Adhesive: Part I Theory and Experimental Corroboration.", AIAA Journal ,Vol.18, pp. 1237-1244,Oct 1980.

(16) Botha, L.R., Jones, R.M., and Brinson, H.F., "Viscoelastic Analysis Analysis of Adhesive Stresses in

Bonded Joints." VPI&SU Report, VPI-E-83-17, May 1983.

(17) Anderson, G.P., and De Vries, K.L.,"Stress State in Lap Shear Specimens.", The Adhesion Society , Newsletter, Vol. 6, No 2.

(18) Barsoum, R.S.,"The Use of Isoparametric Finite Elements in Linear Fracture Mechanics.", International Journal for Numerical methods in Engineering , Vol. 10, pp 25-37, 1976.

(19) Frederick, D. and Chang, T.S., Continuum Mechanics , Scientific Publishers, 1965.

(20) Hueberner, K.H., The Finite Element Method for Engineers , Wiley-Interscience, 1975.

(21) Bathe, K.J. and Wilson, E.L., Numerical Method in Finite Element Analysis , Prentice Hall, 1976.

(22) Ramberg, W., Osgood, W.R., "Description of Stress-Strain Curves by Three Parameters.", Naca Technical Notes No. 902,July 1943.

(23) Jones, R.M., Mechanics of Composite Materials , McGraw Hill, New York, 1975.

(24) Onaran, K. and Findley, W.N., "Combined Stress Creep Experiments on a Non-linear Viscoelastic Material to Determine the Kernel Function for a Multiple Integral Representation of Creep.", Lawrence Radiation Laboratory, University of California, EMRL-24, June 1964

(25) Zienkiewicz, O.C., The Finite Element Method , McGraw-Hill, Third Edition, 1977.

(26) Timoshenko, and Goodier, Theory of Elasticity , McGraw-Hill, Third Edition, 1970.

(27) Tuttle, M.E., Barthelemy, B.M., Brinson, H.F., "Strain Measurement Within a Single Lap Joint Using Embedded Strain Gages", Experimental Techniques. (in press), VPI&SU Report, VPI-E-84-1, January 1984.

(28) Kobayashi, A.S., "Hybrid Experimental-Numerical Stress Analysis", Experimental Mechanics , Vol. 23, no. 3, pg 338.

(29) Tuttle, M.E., Barthelemy, B.M., and Brinson, H.F., "The Experimental and Theoritical Analysis of a Single Lap Joint", to be presented at the SESA Spring Meeting, Montreal Canada, June 1984.

(30) Nagarajaw, Y.R. and Alwar, R.S., "Viscoelastic Analysis of an Adhesive-Bonded Plane Lap Joint", Computers and Strutures , V11, 6, pp. 621-627, June 1980.

(31) Dattaguru, B., Everett, R.A., Whitcomb, J.D., and Jonhson, W.S., "Geometrically Nonlinear Analysis of Adhesively Bonded Joints", NASA Technical Memorandum 84562, September 1982.

SECURITY CLASSIFICATION OF THIS PAGE *(When Data Entered)*

REPORT DOCUMENTATION PAGE		READ INSTRUCTIONS BEFORE COMPLETING FORM
1. REPORT NUMBER VPI-E-84-15	2. GOVT ACCESSION NO. AD-A140559	3. RECIPIENT'S CATALOG NUMBER
4. TITLE *(and Subtitle)* Finite Element Analysis of Bonded Joints		5. TYPE OF REPORT & PERIOD COVERED
		6. PERFORMING ORG. REPORT NUMBER
7. AUTHOR(s) Barthelemy, B. M.; Kamat, M. P.; and Brinson, H. F.		8. CONTRACT OR GRANT NUMBER(s) (ONR) N00014-82-K-0185
9. PERFORMING ORGANIZATION NAME AND ADDRESS Department of Engineering Science and Mechanics VPI&SU Blacksburg, VA 24061		10. PROGRAM ELEMENT, PROJECT, TASK AREA & WORK UNIT NUMBERS
11. CONTROLLING OFFICE NAME AND ADDRESS Office of Naval Research (ONR) Arlington, VA 22217		12. REPORT DATE April 1984
		13. NUMBER OF PAGES 139
14. MONITORING AGENCY NAME & ADDRESS*(if different from Controlling Office)*		15. SECURITY CLASS. *(of this report)* Unclassified
		15a. DECLASSIFICATION/DOWNGRADING SCHEDULE

16. DISTRIBUTION STATEMENT *(of this Report)*

Approved for public release, distribution unlimited

17. DISTRIBUTION STATEMENT *(of the abstract entered in Block 20, if different from Report)*

18. SUPPLEMENTARY NOTES

19. KEY WORDS *(Continue on reverse side if necessary and identify by block number)*

Bonded joints, finite element analysis, single-lap, thick-adherend, crack-lap

20. ABSTRACT *(Continue on reverse side if necessary and identify by block number)*

See page ii

DD FORM 1 JAN 73 1473 EDITION OF 1 NOV 65 IS OBSOLETE

SECURITY CLASSIFICATION OF THIS PAGE *(When Data Entered)*

(12)

DOT/FAA/CT-84/11

Marking and Lighting of Unpaved Runways - Inservice Testing

Victor F. Dosch
Guy S. Brown

March 1984

US Department of Transportation
Federal Aviation Administration
Technical Center
Atlantic City Airport, N.J. 08405

NOTICE

This document is disseminated under the sponsorship of the Department of Transportation in the interest of information exchange. The United States Government assumes no liability for the contents or use thereof.

The United States Government does not endorse products or manufacturers. Trade or manufacturer's names appear herein solely because they are considered essential to the object of this report.

Technical Report Documentation Page

1. Report No.	2. Government Accession No.	3. Recipient's Catalog No.
DOT/FAA/CT-84/11	AD-A140 958	

4. Title and Subtitle	5. Report Date
MARKING AND LIGHTING OF UNPAVED RUNWAYS - INSERVICE TESTING	March 1984
	6. Performing Organization Code
7. Author(s)	8. Performing Organization Report No.
Victor F. Dosch and Guy S. Brown	DOT/FAA/CT-84/11
9. Performing Organization Name and Address	10. Work Unit No. (TRAIS)
Federal Aviation Administration Technical Center Atlantic City Airport, New Jersey 08405	11. Contract or Grant No.
	13. Type of Report and Period Covered
12. Sponsoring Agency Name and Address	
U.S. Department of Transportation Federal Aviation Administration Technical Center Atlantic City Airport, New Jersey 08405	14. Sponsoring Agency Code

15. Supplementary Notes

16. Abstract

This document describes the results of inservice testing of an FAA developed unpaved runway airport marking and lighting system. Details of earlier work in connection with the development and preliminary testing of this system are contained in FAA Interim Report No. FAA-NA-76-159, "Visual Aids for Turf Runways at Utility Airports," dated June 1976, and FAA Technical Letter Report No. NA-78-34-LR, "Marking and Lighting of Unpaved Runways," dated May 1978.

Inservice testing of the prototype unpaved runway marking and lighting system was conducted at separate utility airports having essentially different evironmental conditions. User participating pilots were, in general, favorably impressed with the standardized system concept. They did, however, indicate several aspects of the system that could be improved or modified. This report details results of this inservice evaluation, and provides conclusions as to desirable changes that might enhance system effectiveness.

A complete resume of the total project effort would include this report, along with the two previously referenced reports of earlier work.

17. Key Words	18. Distribution Statement
Unpaved Runways Turf Runways Visual Guidance Low Cost Aids	Document is available to the U.S. public through the National Technical Information Service, Springfield, Virginia 22161

19. Security Classif. (of this report)	20. Security Classif. (of this page)	21. No. of Pages	22. Price
Unclassified	Unclassified	42	

Form DOT F 1700.7 (8-72) Reproduction of completed page authorized

LIST OF ILLUSTRATIONS

EXECUTIVE SUMMARY

Numerous visual guidance systems and items of equipment have evolved over the years for use in providing visual flight rules (VFR) day and night approach, landing and takeoff guidance at smaller general aviation (GA) airports utilizing unpaved taxiway and runway surfaces. While these components and systems have, for the most part, provided adequate guidance, the very nature of the decentralized development effort has resulted in a lack of standardization and consequent confusion on the part of itinerant pilots using the systems for the first time. The principal purpose of this project was to define the visual guidance requirements for unpaved runway operations and, subsequently, to develop the most economical and efficient devices and systems for providing this guidance. Finally, it was necessary to perform inservice evaluations of the resultant systems with a view toward validating the results of the developmental effort.

In order to define the visual guidance requirements for safe unpaved runway operations, the Federal Aviation Administration (FAA) contracted with Mr. Robert F. Gates, an authority in the airport lighting and marking field, to conduct a study and to make a determination of the necessary elements for such an unpaved runway lighting and marking system. The results of this contract study are detailed in the previously published FAA Interim Report No. FAA-NA-76-159, "Visual Aids for Turf Runways at Utility Airports," dated June 1976.

Using the results and recommendations outlined in the above referenced interim report, the Visual Guidance Section at the FAA Technical Center (previously NAFEC) assembled various lighting and marking components and systems for installation and preliminary testing on a typical unpaved evaluation site at the Technical Center. By a process of elimination, using pilot input from FAA Center test pilots and employee pilots, best designs for various lighting and marking components were chosen to form a marking system for unpaved runway airports. A description of the developmental effort, along with construction and installation details for the evolved system components, are contained in FAA NAFEC Technical Letter Report NA-78-34-LR, "Marking and Lighting of Unpaved Runways," dated May 1978. This report also included a strong recommendation that the developed system be installed at a number of inservice test site airports for evaluation.

Inservice tests were conducted at six airports, each located in separate states, following development work and initial testing at the Technical Center and subsequent to a preliminary inservice test. The inservice test program was conducted to validate the overall system as well as individual components used for marking and lighting unpaved runways, and to provide feedback from users that might identify any problems, possible improvements, and verify user acceptance of the system.

As a result of inservice evaluation, it is concluded that the following modifications to the tested system should be incorporated to improve system effectiveness.

1. Airport Identifier - A unique, easily recognizable, two- or three-letter abbreviation of the name of the airport should be used as an identifier on the pyramid rather than the location identifier assigned by the FAA.

2. Runway Edge Markers - White cones with black tops with a minimum diameter of 36 inches should be considered as an alternative to the flat runway edge markers.

3. Go-Around Markers - These markers should not be used as a standard component of the system but could be considered as an option by the airport management.

4. Aiming Point Markers - These markers should not be used as a standard component of the system but could be considered as an option by the airport management.

5. Runway Edge Marker Separation - A separation distance of 400 feet between edge markers will probably provide adequate runway edge delineation.

6. Night Runway Lighting - It is possible that the proposed system using only runway threshold and end lights will not adequately define the lateral limits of the landing area. Incorporation of low intensity runway edge lights, at an extended spacing of 400 feet, with a minimum of three lights per side, should provide the required runway edge definition.

7. Aiming Point Lights - These lights should not be used as a standard component of the system, but could be considered as an option by the airport operator.

8. Poor Man's Optical Aid (POMOLA) - The POMOLA, in both day and night configurations, provides reliable visual glide slope guidance under all conditions, and should be included as a required part or component of any recommended unpaved runway lighting and marking system.

A complete resume of the total project effort would include this report, along with the two previously referenced reports of earlier work.

INTRODUCTION

PURPOSE.

The work described herein was performed under Subprogram T19-03, "Airport Lighting and Visual Aids," Project T19-03E, "Marking and Lighting for Unpaved (Turf) Runways." The project, for the development and testing of improved, economical marking and lighting systems for use on unpaved runways, was initiated at the request of officials of the State of New Jersey. The Director of Aeronautics, Bureau of Aviation, Department of Transportation of the State of New Jersey, requested that the Systems Research and Development Service (SRDS) in Washington, through the National Aviation Facilities Experimental Center (NAFEC) (now the Federal Aviation Administration (FAA) Technical Center), assist in solving visual guidance problems encountered with unpaved (turf) runway operations.

BACKGROUND.

Numerous visual guidance systems and items of equipment have evolved over the years for use in providing visual flight rules (VFR) day and night approach, landing and takeoff guidance at smaller General Aviation airports utilizing unpaved taxiway and runway surfaces. While these components and systems have, for the most part, provided adequate guidance, the very nature of the decentralized development effort has resulted in a lack of standardization and consequent confusion on the part of itinerant pilots using the systems for the first time. The principal purpose of this project was to define the visual guidance requirements for unpaved runway operations and, subsequently to develop the most economical and efficient devices and systems for providing this guidance. Finally, it was necessary to perform inservice evaluations of the resultant systems with a view toward validating the results of the developmental effort.

In order to define the visual guidance requirements for safe unpaved runway operations, the FAA contracted with Mr. Robert F. Gates, an authority in the airport lighting and marking field, to conduct a study and to make a determination of the necessary elements for such an unpaved runway lighting and marking system. Mr. Gates, with the help of an advisory group that included state aviation officials from New Jersey, Pennsylvania, Maryland and Delaware, FAA experts from various General Aviation District Offices (GADO's), and other noted aviation authorities, successfully accomplished this task. The results of this contract study are detailed in the previously published FAA interim report No. FAA-NA-76-159, "Visual Aids for Turf Runways at Utility Airports," dated June 1976.

Using the results and recommendations outlined in the above referenced interim report, the Visual Guidance Section at the FAA Technical Center (previously NAFEC) assembled various lighting and marking components and systems for installation and preliminary testing on a typical unpaved evaluation site at the Technical Center. By a process of elimination, using pilot input from FAA Center test pilots and employee pilots, best designs for various lighting and marking components were chosen to form, when assembled together, an economical, standardized lighting and marking system for unpaved runway airports. A description of the developmental effort, along with construction and installation details for the evolved system components, are contained in FAA NAFEC Technical Letter Report NA-78-34-LR, "Marking and Lighting of Unpaved Runways," dated May 1978 (reference 1). This report also included a strong recommendation that the developed system be installed at a number of inservice test site airports for evaluation.

This report, then, concludes the project with a description of the inservice evaluation portion of the effort, and provides not only evaluation results, but also conclusions as to desirable changes for a system that might be detailed in an FAA Advisory Circular on unpaved runway airport lighting and marking. A complete resume of the total project effort would include this report, along with the two previously referenced reports of earlier work.

SYSTEM DESCRIPTION.

Appendix A contains a complete description of the marking and lighting system as installed for day and night use at the inservice test sites. Figure 1 pictorially depicts the system components for quick reference while reading the report. Figures 2, 3, 4, and 5 are photographs depicting principal components of the daylight marking system.

DISCUSSION

PRELIMINARY INSERVICE TEST.

Preliminary flight tests, to evaluate the system and components and refine installation techniques, were conducted at Twin Pines Airport near Trenton, New Jersey. This was the first installation completed for inservice testing, and was accomplished in cooperation with the airport owner and the State of New Jersey, Division of Aeronautics. Only the day-marking portions of the system were installed for preliminary evaluation.

Questionnaires, along with an "Informational Package" were mailed to aviation user groups throughout the state by the New Jersey Division of Aeronautics. The informational package contained a sketch of the installation, as shown in figure 1, along with an explanation of the purpose and use of the various components of the experimental system. Pilots, as well as airport operators and owners, were encouraged to participate in the evaluation.

INSERVICE TEST AT SIX AIRPORTS.

Inservice tests were conducted at six airports, each located in separate states, following development work and initial testing at the Technical Center and subsequent to the preliminary inservice test. The inservice test program was conducted to validate the overall system as well as individual components used for marking and lighting unpaved runways, and to provide feedback from users that might identify any problems, possible improvements, and verify user acceptance of the system.

The test sites were selected in diverse parts of the country to test the system under different conditions of terrain and under varying weather conditions to include snow. The systems were installed as a cooperative effort with states and/or airport owners and operators.

These inservice tests were conducted over a 2- to 3-year period, subsequent to the preliminary tests previously discussed, at the following airports:

1. Twin Pine Airport, Trenton, New Jersey
2. Pleasant Valley Airport, Brodheadsville, Pennsylvania

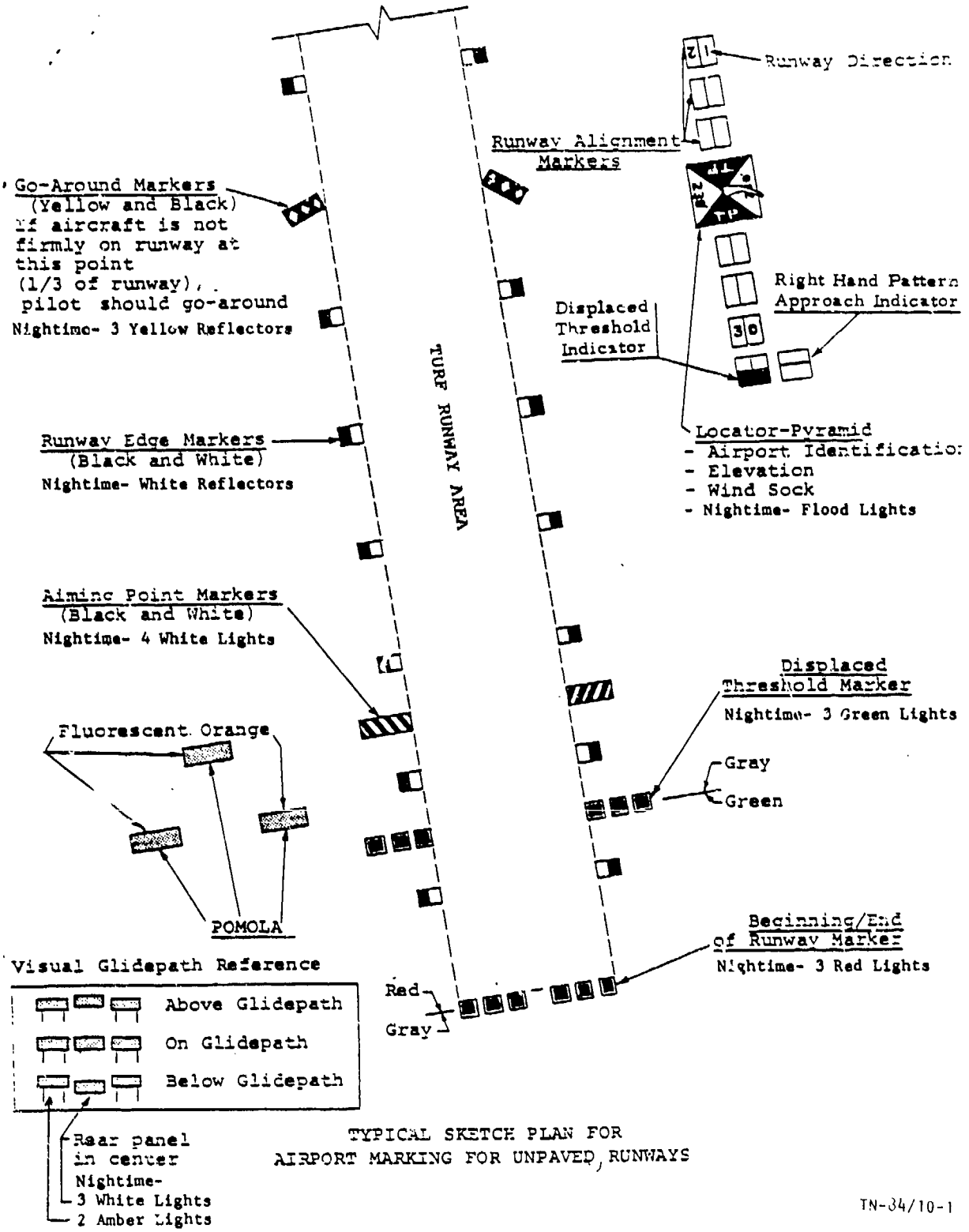

FIGURE 1. TYPICAL SKETCH PLAN FOR AIRPORT MARKING FOR UNPAVED RUNWAYS

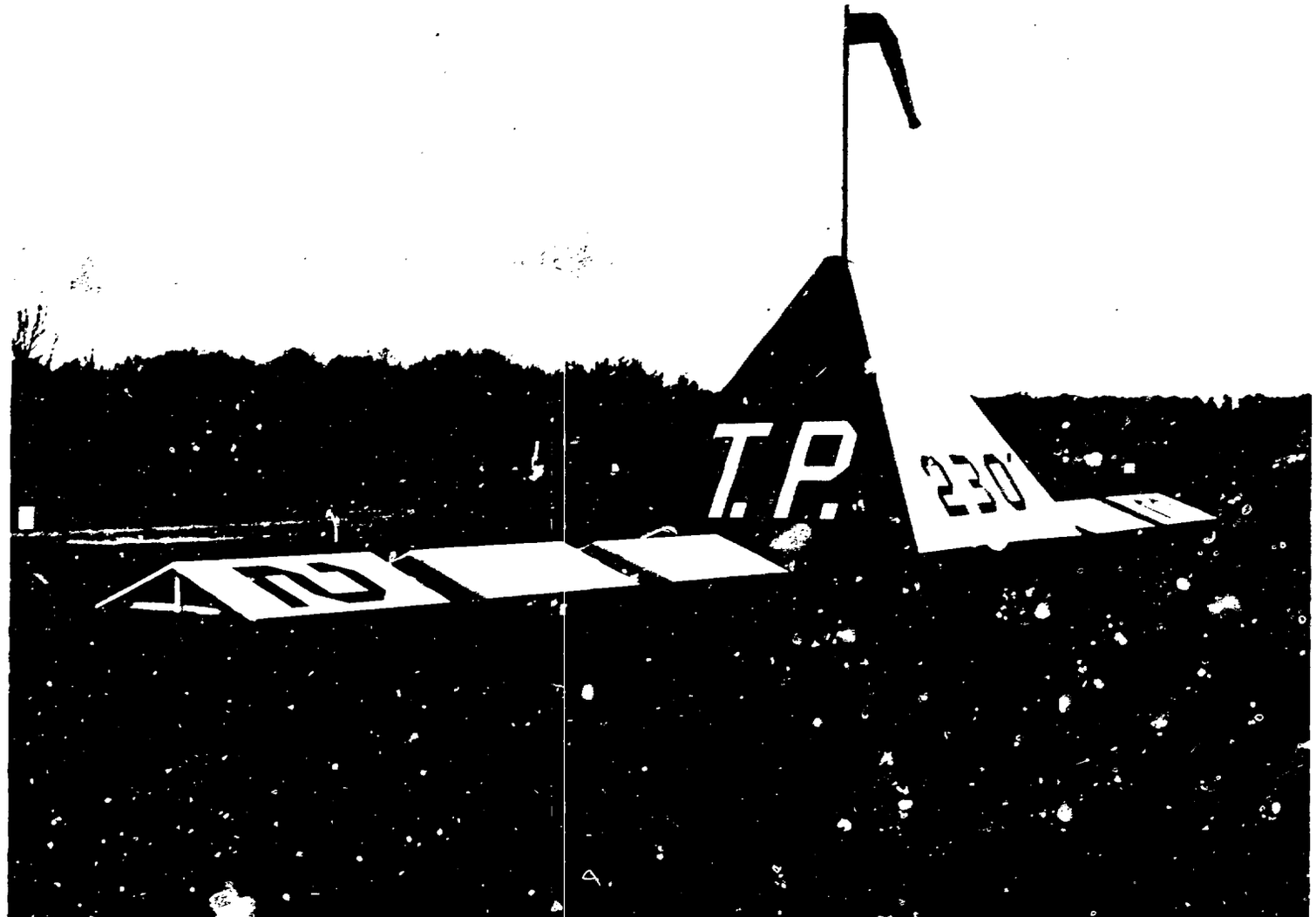

FIGURE 2. LOCATOR PYRAMID WITH R/W ALIGNMENT MARKERS

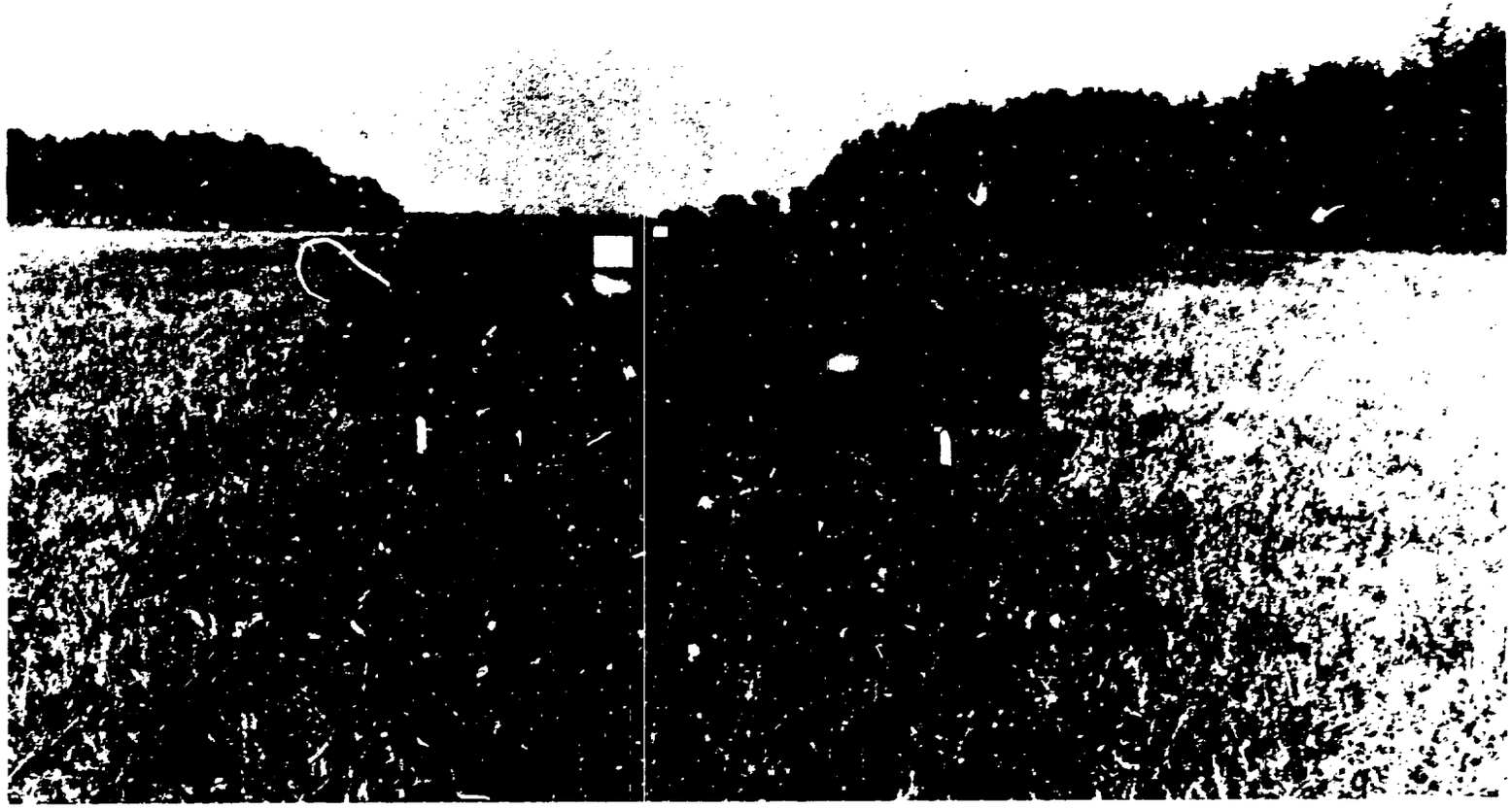

FIGURE 3. GO-AROUND MARKERS

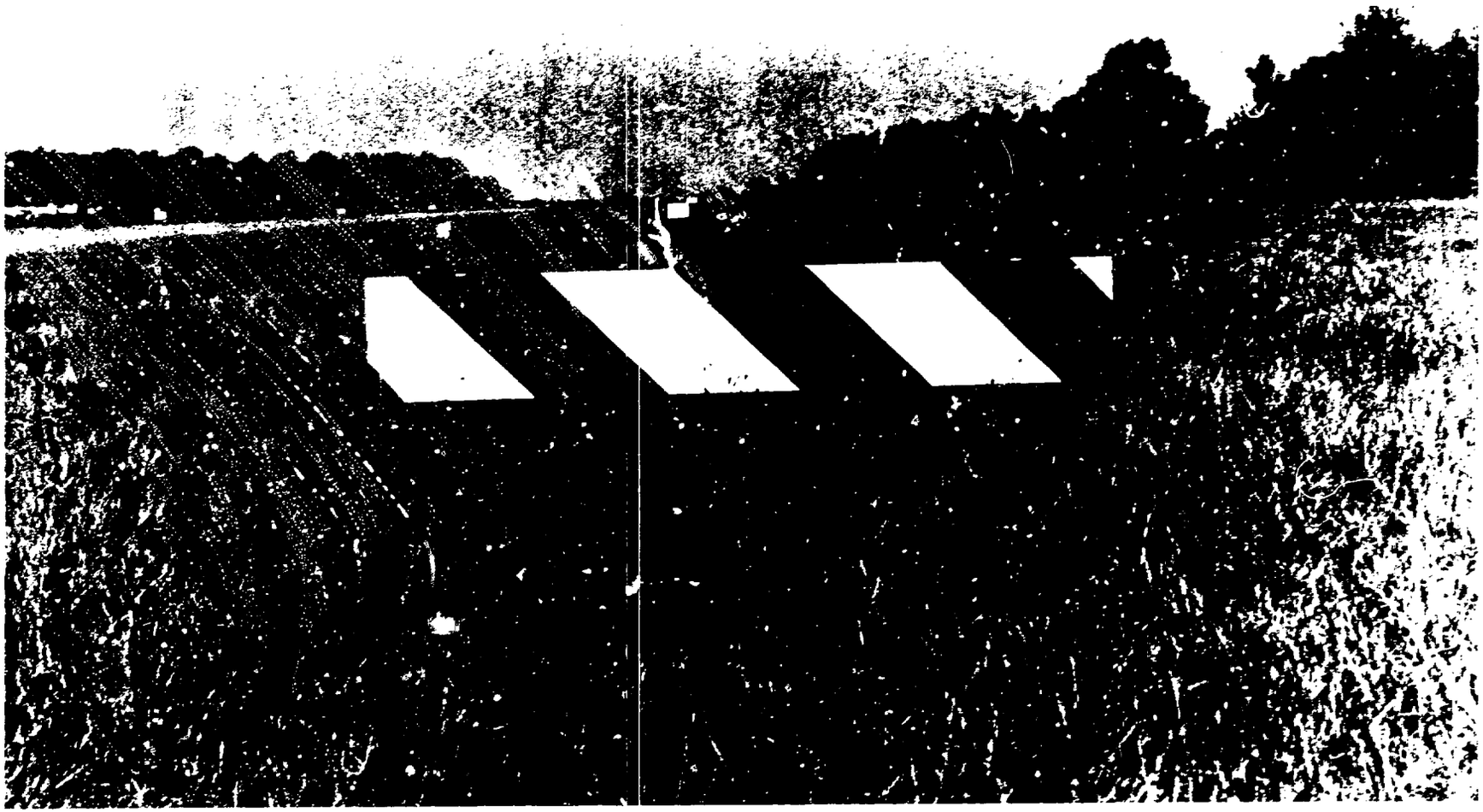

FIGURE 4. ARMIJO POINT MAP 3

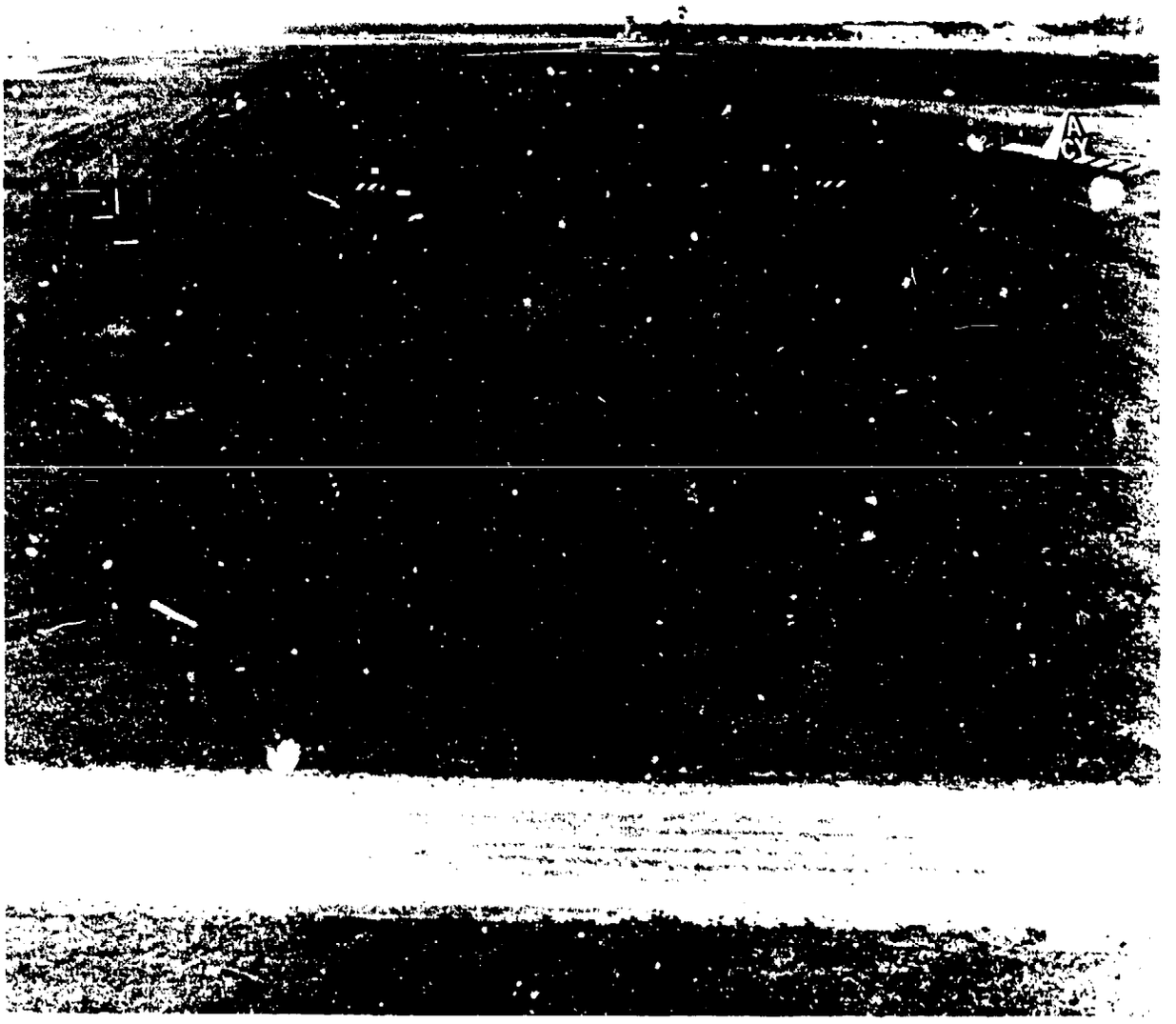

FIGURE 5. UNPAVED RUNWAY DAY MARKER SYSTEM

3. Gadabout Gaddis Airport, Bingham, Maine
4. Jennings Municipal Airport, Jennings, Louisiana (Day System Only)
5. Elliott Field, Clinton, Montana (Day System Only)
6. Columbus Municipal Airport, Columbus, North Dakota

Inservice test results were obtained through questionnaires (for sample, see appendix B) distributed to user pilots by the airport operators, and through written comments from pilots, owner/operators, and involved State aviation officials.

RESULTS

PRELIMINARY INSERVICE TEST.

The results from the preliminary inservice test, including pilot comments, are presented in this report, independent of the results obtained from the revised questionnaire which was used for the subsequent inservice evaluation at six airports. It was felt that the questions on the preliminary test questionnaire could not be directly equated to those used later on the revised questionnaire.

SUMMARY OF QUESTIONNAIRE RESPONSES. Eleven pilots responded to this initial questionnaire used for the preliminary evaluation. A summary of questionnaire responses, along with pilot comments received, follows:

Question 1. To what extent did the turf runway marking help you to identify this airport and the runway alignment?

		Responses	
A.	Significant	8	
B.	No Change	2	
C.	Confusing. How?	0	
D.	Other	1	(Only the pyramid helped)

Question 2. At what distance from the airport were you able to identify the airport through this marking system?

		Responses
A.	3 Miles or More	6
B.	Entering pattern	3
C.	Final Approach	0
D.	Other	2 miles

Question 3. Did the Poor Mans Optical Aid (POMOLA) help establish and maintain a consistent approach slope on final approach?

		Responses	
A.	Yes	7	
B.	No	4	(was not below slope)

Comments:

1. I especially like the POMOLA. In strange territory, with obstacles, it's really great to have a visual indication for a safe glide.

2. Do not feel POMOLA is necessary with small aircraft.

Question 4. Was the POMOLA approach angle:

	Responses
A. Too High	3
B. Too Low	1
C. Just Right	6
D. Other	0

Comments:

1. Approach angle much too steep, should be same as any other VASI, 3 degrees.

2. It better be! I was depending on it! (Approach Angle)

3. A great aid in approach and glidepath, helpful in identifying airport. Would like to see more of these installations.

Question 5. Please identify the components of this turf marking installation from most beneficial to least beneficial in ascending numerical order. (No. 1 most beneficial.)

Order of Merit	
1	A. Pyramid
4	B. Runway Alignment Markers
5	C. POMOLA
2 (tie)	D. Runway Edge Markers
7	E. Displaced Threshold Markers
6	F. Runway End Markers
2	G. Aiming Point Markers
0	H. Go-Around Markers

Question 6. What percentage of your overall operations are at turf fields?

	Responses
A. 0% - 25%	4
B. 25% - 50%	2
C. 50% - 75%	3
D. 75% - 100%	2

Question 7. What type/model/make of aircraft did you use?

	Responses	
Single engine, fixed gear:	Ercoupe	1
	Cessna 150	3
	Cessna 172	2
	Piper PA28	2
	Homebuilt	2
Twin engine, fixed gear:	Islander	1

Question 8. Is your aircraft based at this field?

	Responses
A. Yes	1
B. No	10

Question 9. Operational Data

	Responses
A. Landing Direction:	East 5, West 7
B. Time of Day:	Various to include 5 p.m. and dusk
C. Visibility:	Clear 9, Hazy 3

SUMMARY OF COMMENTS.

1. Very functional system.

2. It was like landing in a hostile pasture surrounded by sheep. Markers are too high.

3. Very large improvement over normal markings or lack thereof at other turf fields.

4. Too many signs.

5. Spotted fluorescent orange POMOLA long before the pyramid, which should be painted orange. Runway markers were an extreme hazard. If you have them, at the very least, have them laying flat so you can run over them. I am really enthusiastic about this system and hope these improvements will be considered. I especially like the POMOLA.

6. Runway markers too close - will damage low wing or biplanes if struck. Hard to see from behind radial engine; move them back!

7. The myriad of markers was confusing. Although a few were quite nice, the majority were found to be unnecessary.

8. Bigger wind sock is needed.

9. Two letters were received by the Director of Aeronautics, State of New Jersey, from pilots who probably did not complete a questionnaire. Both pilots fly "taildraggers," one having a large radial engine with poor visibility. Both pilots felt strongly that the 100-foot width of the runway markers is so narrow as to constitute a safety hazard. As one pilot expressed, "inviting accidents by particular types of aircraft."

SUMMARY OF PRELIMINARY INSERVICE TEST RESULTS.

Responses to the 11 preliminary questionnaires and comments from these pilots, plus comments from two pilots who wrote letters, are summarized as follows:

Eight of the pilots said that the turf runway markings helped to identify the airport and runway alignment (question 1) to a significant degree.

The most beneficial component (question 5) was judged to be the pyramid. The runway edge markers and the aiming point markers were tied in score as the second most beneficial. As noted under pilot comments, four pilots said that the edge markers were either; too high, too close together (limiting runway width), or confusing with the majority of markers being unnecessary. Two of these pilots, plus two who commented by letter, said or inferred that the edge markers were hazardous. Of these pilots, three flew "taildraggers" which, for the most part, have poor forward visibility when the tail wheel is on or near the ground.

The go-around markers were judged to be the least beneficial, while the other markers were ranked as shown in question 5.

Seven pilots said that the POMOLA helped establish and maintain a consistent glidepath while four responded in the negative. Six pilots said the approach angle (5°) was about right while three said it was too high and one said too low. The pilots comments were positive except for one pilot's comment that it was much too steep and should be the same as other VASI's, at 3°.

The results of this preliminary evaluation confirmed, in general, those results obtained during the developmental stage of the project at the Technical Center. This will be discussed further in the results section of this report for the inservice testing effort.

INSERVICE TEST AT SIX AIRPORTS.

The results of pilot responses to the questionnaire for daytime operations, with the totals combined for the six participating airports, are presented, along with pilot comments concerning the particular question or system component. Comments by airport owner/operators and by state organizations are included and referred to as "Other Comments." Comments of a general nature or those which cannot be directly related to a specific question are also presented and discussed.

Results of testing of the nighttime systems, conducted at only four of the six airports as previously mentioned, are presented following the results section devoted to daytime operations. As with the daytime inservice test, results data for the nighttime tests were obtained through questionnaires distributed to the user pilots by airport operators and from written comments from pilots, owner/operators, and from state aviation officials.

INSERVICE TEST RESULTS - DAY SYSTEM.

During the inservice test, 124 pilots completed questionnaires and provided comments concerning the effectiveness of the daytime marker system. A summary of questionnaire responses, along with user comments received, follows:

Question 1. Does the pyramid with runway alignment markers help you locate the airport in VFR conditions?

Yes	No
114	10

Comments:

1. The function of the pyramid was unclear - confusing.

Other Comments:

One state commented that a fluorescent windsock, in combination with a properly maintained segmented circle, is much more visible and recognizable than the pyramid. Another state commented that the pyramid is a good airport locator and windsock placement.

An owner/operator commented that the pyramid has been the most commented on aspect of the system and has made the identification of a turf runway much easier for pilots. Several pilots landed successfully in bad weather conditions after they spotted his airport and, he felt, that two pilots were saved from possible accidents because they could wait out the weather on the ground. Also, two Medevac flights located the airport easily when forced to sit out bad weather. He recommended that the pyramid be installed at all unpaved runway airports and that information describing the system should be presented to all pilots as a safety factor.

SUMMARY OF RESPONSES AND COMMENTS. A significant majority of the pilots said "Yes" to the question "Does the pyramid with runway alignment markers help locate the airport in VFR conditions?" Also, the majority of comments, considering those on the system in general, are quite favorable.

Question 2. Does the airport identifier and airport altitude painted on the pyramid (airport locator) provide any useful information to you?

Yes	No
116	7

Comments:

1. Must overfly the airport to see the runway direction and airport identifier - suggest larger numbers.

2. Identifier and elevation numbers were confusing.

3. Altitude (field elevation) was particularly helpful.

Other Comments:

One state commented that the three-character identifier painted on the pyramid is useless and confusing to nearly all pilots.

Three other state officials said that the identifier and altitude (field elevation) provided useful information.

An owner/operator commented that, with the elevation painted on the pyramid, pilots have immediate information without checking charts.

SUMMARY OF RESPONSES AND COMMENTS. Again a significant majority of the pilots responded "Yes" to the question, "Does the airport identifier and airport altitude painted on the pyramid provide any useful information?"

The majority of the comments were also quite favorable.

Question 3. Do you find the combination of pyramid with windsock on top, runway alignment markers, and runway direction numbers to provide adequate information for selection of proper runway for landing and circling guidance?

Yes	No
115	9

Comments:

1. Three pilots commented that the windsock was hard to see (one said "with white background").

2. Windsock should be larger.

3. The windsock (mounted) on the pyramid is very useful and ends hunting for it.

4. Runway alignment markers are not essential, especially with more than one runway.

5. The right traffic indicator did not provide enough info, maybe one more block (section) would help identification.

Other Comments:

No specific comments were received from states or owner/operators. However, the windsock was raised in height in some installations to alleviate interference from the pyramid. An owner/operator increased the spacing between the runway alignment markers to accomodate the width of his mowing machine. Others have raised the markers (cinder blocks) to alleviate moisture accumulation problems, and some have used roofing material or tar paper around the markers to keep grass/weed growth down and to accomodate mowing.

SUMMARY OF RESPONSES AND COMMENTS. Again, a significant number of the pilots responded "Yes" to the question concerning the windsock, runway alignment markers, and runway direction numbers.

There were no specific comments from state or owner/operators, but, in general, the overall system was favorable to the majority.

Question 4. Do the runway edge markers provide adequate lateral guidance on final approach?

Yes	No
119	4

Comments:

1. Probably don't need as many black and white runway markers.

2. Edge markers are obstructions.

3. Airport is overmarked and may be considered confusing.

4. Runway markers too tall.

5. Runway markings are a big improvement over most unpaved strips - especially for first timers.

6. Edge markers provide good approach guidance.

7. Markings are the best I have ever seen at a grass strip; easier to pick out airport and runways than with grass runways.

8. Very good system.

9. Highly recommend it.

10. Marking system is quite useful and width is more than adequate.

11. Great runway.

12. Edge markers provide positive identification on the limits of the landing turf and are superior to tires, cones, or lights.

13. A letter from a pilot said the marking system is good but could be improved by adding fluorescent paint to the black and white edge markers. Five specific suggestions were made, with drawings, to provide more contrast, particularly in snow conditions.

Other Comments:

One state commented that the edge markers, while quite visible on approach, are not visible from above or either side of the runway. Also, the state questioned whether the edge markers would withstand snowplowing (heavy and frequent snow fall). Fiberglass cone markers have been used for nearly 20 years and they conclude that the 36-inch cone is a superior marking system, from both the cost standpoint and for installation and ongoing maintenance. (Additional details were given which will be discussed later.)

Another state said that runway markers made from wood or metal are rather hazardous and would rather see all markers made of plastic.

Two other states commented that black and white panels are always distinguishable or conspicious regardless of the ambient light or color of the background.

One owner/operator commented that the unpaved marking system, tested for over 3 years, has been more than adequate for its purpose, to aid pilots in locating and landing on turf runways.

Another owner/operator commented that the edge markers provided adequate guidance for final approach; however, when on downwind leg, they are almost impossible to see. Also, pilots have expressed concern about damage if the edge markers were hit.

SUMMARY OF RESPONSES AND COMMENTS. In response to the question "Do the runway edge markers provide adequate lateral guidance on final approach?" a significant majority of the pilots said "Yes."

Even though the response to this specific question was in the affirmative, the question elicited numerous comments from pilots as well as from state aviation officials and from owner/operators. Six out of 14 comments from the pilots were negative, as were several comments during the preliminary inservice test. Also, some of the states and owner/operators had negative comments.

The concern about too many markers and clutter of the runway will be discussed in connection with the last two questions. As to the use of plywood, it is noted under "Recommendations" in reference 1, that other materials such as plastic, vinyl, or fiberglass could be used which may prove to be more frangible and cause less damage if accidently struck.

Also, an alternative to panels would be the use of 36-inch diameter white plastic/vinyl cones with a black top for runway edge markers. Tests were conducted with one type of cone and it was found that the colors (except black and white) faded after exposure to ultraviolet rays from the sun. Black and white plastic flat panels were also tested; however, some of them warped badly. One state advised they are looking at plastic panels from another manufacturer. It is felt that, in time, manufacturers will have materials available to overcome these problems.

Question 5. Does the POMOLA provide adequate vertical guidance, glidepath guidance, and obstruction clearance on final approach?

Yes	No
110	8

Comments:

1. POMOLA hard to see until close final. (Trees have been reported as obscuring POMOLA at some locations until aligned on final approach.)

2. POMOLA is perfect for teaching soft field landings.

3. POMOLA worked excellent.

4. POMOLA is particularly useful, especially on runway 33 approach. Suggest handout sheets mailed to pilots to explain meaning of markers.

5. POMOLA markers provide good approach guidance.

Other Comments:

One state commented that one of the major benefits of the system is the value of POMOLA as a landing aid to assist in determining final approach angle and stressed the need for POMOLA or other visual aid, particularly for the transient pilot.

Another state commented that the POMOLA has the most promise of any part of the system, in as much as it is relatively simple and does provide adequate vertical guidance on approach. The state feels, however, that international orange may not be the best color, and they also suggest that a substantial amount of publicity and educating of the flying public would be necessary for its eventual acceptance.

Another state commented that the POMOLA gives good accuracy for landing in the touchdown zone and the 15:1 approach criteria should be clarified with FAA airspace people who still use 20:1 as standard.

SUMMARY OF RESPONSES AND COMMENTS. Again a significant majority of the pilots answered "yes" to the question "Does the POMOLA provide adequate vertical glidepath guidance and obstruction clearance on final approach." In response to a similar question during the preliminary inservice test, a majority of the pilots responded in the affirmative and said that the glidepath angle of 5 degrees was "just right."

Comments from the pilots, state officials, and owner/operators were all positive with the exception of two comments made during the preliminary test. One pilot commented that the POMOLA was not necessary with small aircraft and another said the approach angle was too steep.

These results show that the low-cost POMOLA (references 4 and 5), used where the cost of a standard red/white VASI cannot be justified, will provide adequate daytime vertical guidance for obstruction clearance and confirms previous tests results (reference 2). The inservice tests also confirm that a 5-degree approach angle is optimum for small general aviation aircraft using turf runways less than 3000 feet in length. Previous tests at the Technical Center (references 2 and 6) and tests by NASA, (reference 7) also concluded that a 5-degree approach angle is most commonly used by such aircraft on shorter runways.

Question 6. Do the aiming point markers and threshold or displaced threshold markers provide proper indication for touchdown guidance?

Yes	No
117	7

Comments:

1. The displaced threshold and runway end markers are confusing on the first landing.

2. Threshold markers provide guidance; aiming point does not.

Other Comments:

One state commented that the displaced threshold must be an integral component of the system as it is one of the key elements (when considering obstacle clearance and approach slope protection). Another state commented on the location of displaced thresholds and this subject will be discussed later.

A third state said that the marking for a displaced threshold is very useful and is a good design.

An owner/operator commented that threshold markers provide an adequate indication for touchdown guidance and that aiming point markers were not needed.

SUMMARY OF RESPONSES AND COMMENTS. In response to the question, "Do aiming point markers and threshold or displaced threshold markers provide proper indication for touchdown guidance?" again, a significant majority of the pilots said "Yes."

Some pilots commented that the markers are confusing, which shows again that they must be educated as to the meaning and use of the many parts of the system. Three states and an owner/operator commented on the need for, and the usefulness of, the displaced threshold markers, as noted above, while others commented that the aiming point markers were not needed.

Based on total responses and comments, including those from the preliminary inservice test, both the threshold and displaced threshold markers were judged to provide adequate and useful guidance.

Question 7. Do you consider the aiming point markers useful?

Yes	No
107	11

Comments:

1. Aiming point markers are very useful.

2. Aiming point markers provide good approach guidance.

3. Touchdown markers are very useful.

4. My aiming point is runway end and I believe your end markers may serve this purpose.

5. Aiming point markers are of limited usefulness.

Other Comments:

One state commented that the aiming point and go-around markers are too confusing and may not be needed.

Another state commented that the purpose of aiming point markers is not well understood and that they are, in their opinion, unnecessary.

As noted under the previous question, an owner/operator said that threshold markers provide adequate indication for touchdown guidance and that aiming point markers were not needed. Another owner/operator commented that aiming point and decision markers are used by pilots once they are familiar with the system.

SUMMARY OF RESPONSES AND COMMENTS. Even though a majority of the pilots responding were in favor of the aiming point markers, consideration should be given to the adverse comments, including those concerning clutter on the runway with too many markers as previously noted. An argument was made by some pilots that the back panel of the POMOLA serves as an aiming point. Others feel that the glidepath signal will be disregarded at some point after clearance of obstructions. The pilot will then aim for a point near the threshold and will probably "duck-under" the glidepath in an attempt to touch down near the threshold and prior to the glidepath intercept point. Others contend that the final aiming point should be left to the individual, taking into consideration his particular aircraft, wind, and other conditions, and that threshold and edge markers provide adequate guidance.

Question 8. Do the "go-around" markers perform a useful function?

Yes	No
96	17

Comments:

1. Go-around markers are too close to touchdown and leave too much usable runway. Markers must be a "positive go-around," otherwise, no one will respond to them.

2. Go-around markers are too close to threshold but otherwise are very useful.

3. They do not serve a useful function.

Other Comments:

One state questioned the real value of go-around markers and said they, (and aiming point markers) are too confusing and may not be needed.

An official from another state said he did not see any value in the go-around markers; thinks they could be eliminated. Some of the comments he addressed were regarding the number of panels that mark the runway. Some have no apparent meaning, and the system seems very cluttered.

Another state commented that the go-around markers are not understood and it is questionable whether any education effort would change this substantially.

One owner/operator said that we should not dictate to the pilot when he should or should not go-around on an approach. Weather and wind conditions, aircraft type and configuration, runway length, and pilot proficiency are all factors that must be taken into consideration. He said that, in his opinion, these markers merely clutter the side of the runway. Another owner/operator said the decision and aiming point markers are used by pilots once they are familiar with the system.

SUMMARY OF RESPONSES AND COMMENTS. Again, a majority of the pilots responded "Yes" to the question, "Do the go-around markers perform a useful function?" Of the

total responses, fewer pilots responded to this question than to any other question and a greater precentage of pilots responded negatively. The go-around markers were also judged to be the least beneficial of the markers in the system during the preliminary inservice test.

INSERVICE TEST RESULTS - NIGHT SYSTEM.

The nighttime system, consisting of lights and retroreflective runway edge markers, were installed for inservice testing at four locations:

1. Twin Pine Airport, near Trenton, New Jersey,

2. Pleasant Valley Airport, Brodheadsville, Pennsylvania,

3. Gadabout Gaddis Airport, Bingham, Maine, and

4. Columbus Municipal Airport, Columbus, North Dakota.

As with the daytime inservice tests, data for nighttime operations were obtained through questionnaires distributed to pilots by the airport operators and by written comments from user pilots, airport owner/operators and from state aviation officials.

The total number of questionnaires received for nighttime test of the system was limited, with only 27 pilots responding. As we have learned, pilots are reluctant to complete questionnaires unless there is a personal contact to encourage response. This need for personal contact has been a problem throughout the inservice testing since some of the airports are unattended or attended part-time. Accordingly, there were relatively few questionnaire responses from pilots concerning the nighttime system, and few comments were received from state aviation officials and owners/operators.

A summary of questionnaire responses, along with pilot comments received, follows:

Question 1. Is the beacon, in combination with lighted pyramid with runway alignment markers, adequate for locating the airport at night?

Yes	No
27	0

Comments:

1. Beacon extremely bright and somewhat distracting (located too close to r/w).

2. Without rotating beacon, could not find airport or adjust pattern.

3. Beacon was overpowering - move airport beacon.

4. Beacon too close to runway - high brightness interferes with alignment on flare and touchdown.

5. Lights do not provide enough illumination on runway alignment markers.

6. Need more light on runway alignment markers.

Other Comments:

One owner/operator said that the Medivac (helicopter) pilots can see our beacon when they lift off from the hospital; a distance of 25 miles. Another said that their beacon could not be seen more than a few miles at lower altitudes. It was suggested that aiming of the lights should be checked against the manufacturer's specifications. Another owner/operator said they planned to add additional lights on the pyramid to better light the alignment markers.

SUMMARY OF RESPONSES AND COMMENTS. All pilots said yes to the question, "Is the beacon in combination with the lighted pyramid with runway alignment markers adequate for locating the airport at night?" Based on these and comments of a general nature, these components of the system appear to be adequate for nighttime operations. There was common agreement that one particular beacon, adjacent to the pyramid, was located much too close to the edge of the runway.

Question 2. Is nighttime lighting adequate to identify airport and obtain wind information (from windsock on top of pyramid) and runway landing direction?

Yes	No
22	4

Comments:

None.

Other Comments:

See comment to previous question regarding plans to better illuminate the runway alignment markers.

SUMMARY OF RESPONSES AND COMMENTS. A great majority of the pilots responded in the affirmative to the above question. The general comments concerning the overall system were favorable and these lighting components of the system appear adequate for night operations.

Question 3. Do the runway end lights provide adequate circling guidance and lateral alignment on final approach?

Yes	No
21	6

Comments:

1. Must learn system for runway alignment.

2. Increase intensity of red lights at far end of runway to aid in lining-up.

3. If lights are installed on runway, they should include the full length of runway.

Other Comments:

No specific comments were made by states or owner/operators about this part of the system. It is known, however, that one owner/operator explains the system to pilots operating at night from his airport.

SUMMARY OF RESPONSES AND COMMENTS. A majority of the pilots said "Yes" to the above question; however, a greater percentage of pilots responded "No" to this question than to the other questions. When considering the design of the system and the comments that were made, the need for pilots to learn and understand the system is further amplified.

Question 4. Does the nighttime POMOLA provide adequate vertical glidepath guidance and obstruction clearance on final approach?

Yes	No
23	2

Comments:

1. POMOLA gives good guidance for obstacle clearance, especially for night fog conditions.

2. Must learn system for use of POMOLA.

3. Makes night landings much easier.

Other Comments:

One state commented that one of the major benefits from the project is the value of the POMOLA as a landing aid to assist in determining final approach glide angle, particularly for the transient pilot. If the POMOLA, or other visual aid, is utilized at night, it must be lighted. Other states commented on the approach slope and obstruction clearance criteria which will be discussed under Vertical Approach Guidance and Obstruction Clearance. One owner/operator would prefer a low cost VASI, due to limited space for the POMOLA. Another said pilots had learned to align POMOLA lights.

SUMMARY OF RESPONSES AND COMMENTS. A majority of the pilots said "Yes" to the above question and there were no adverse comments from the states and owner/operators. Based on the test results and comments, the lighted POMOLA provides adequate guidance, but pilots must learn to use the system, since it is not a commonly used standard such as the red/white VASI.

Question 5. Do the retroreflective runway edge markers provide sufficient delineation of the runway during the latter portion of the final approach, flare, landing, and taxiing?

Yes	No
25	2

Comments:

1. Retroreflective markers are surprisingly bright.

2. Reflectors are really bright.

Other Comments:

One state said that the use of reflectors on panels for runway edge and taxiway guidance was a major benefit for night operations and that the 200-foot spacing and 100-foot width is perfectly acceptable.

Other than overall comments about the system, other state officials made no specific comments concerning the retroreflective markers. One owner/ operator said that most pilots are amazed by the effectiveness of the retroreflectors. Another said they provided good guidance and other pilots reported they were adequate when picked up with the landing light.

SUMMARY OF RESPONSES AND COMMENTS. A large majority of the pilots said "Yes" that the retroreflective runway edge markers provide sufficient delineation of the runway. All comments were favorable. Based on the results of the inservice and previous tests, the retroreflective runway edge markers will provide adequate guidance for those pilots who understand the system and are operating aircraft with landing lights located on or near the nose of the aircraft. Wing-mounted lights will not be as effective due to the large angle between the light source, the retroreflectors, and the pilot's eyes.

Question 6. Do the white aiming point lights and threshold or displaced threshold lights provide proper indication for touchdown guidance?

Yes	No
22	4

Comments:

1. Suggest three aiming point lights, as two are not enough and four are overpowering.

Other Comments:

The states and owner/operators made no specific comments about the aiming point, threshold, or displaced threshold lights. One state commented, however, that the displaced threshold indication must be an integral component of the system as it is one of the key elements.

SUMMARY OF RESPONSES AND COMMENTS. A majority of the pilots said "Yes" to the question "Do the white aiming point lights and threshold or displaced threshold lights provide proper indication for touchdown guidance?" The lack of comments does not help in identifying dissatisfaction with any of the system components. As noted in the test results of the daytime system, the threshold and displaced threshold markers were well received, while the usefulness of the aiming point markers was questioned. It was suggested that the rear panel of the POMOLA, located adjacent to the runway, could serve as an aiming point, and the same logic

could be applied to POMOLA lights located on the back panel. The threshold and displaced threshold lights are considered satisfactory and they conform to FAA standards.

Question 7. Do the yellow "go-around" retroreflective markers perform a useful function?

Yes	No
19	6

Comments:

None specific to the question.

Other Comments:

None specific to the question.

SUMMARY OF RESPONSES AND COMMENTS. A majority of the pilots said "Yes" to the above question, while six, or 24 percent said "No." No comments were received that related specifically to the retroreflective go-around markers. Individual pilots are able to determine an appropriate go-around point, if they wish, dependent on the field length, the type of aircraft, and other factors previously discussed.

COMMENTS ON VERTICAL APPROACH ANGLE

In addition to the results of the questionnaire and comments on the POMOLA 5° approach slope (question 5), the following comments were received that pertained to the approach slope and the ratio used for obstruction clearance.

One state said the POMOLA has the most promise of any part of the system in as much as it is relatively simple and does provide adequate vertical guidance on approach. Also, they suggested that a substantial amount of publicity and education of the flying public would be necessary for its eventual acceptance.

Another state official said he liked the (POMOLA) system, but that the 15:1 approach criteria should be clarified with FAA airspace people who still use 20:1 as standard. An owner/operator said they were using a 5° glide slope with clear zones of 15:1 (and) for large twin engine aircraft using a grass runway, and that this might have to be altered to better meet their needs. Another owner/operator was satisfied with a 5° approach and a 6° approach in the opposite direction. The 6° slope was necessary to provide sufficient runway landing length after clearing a ridge near the end of the runway.

A third state said one of the major benefits of the program is the value of the POMOLA as a landing aid to assist in determining final approach glidepath angle, particularly for the transient pilot. Also, it was established factually and operationally that the 15 to 1 approach slope protection is not only feasible, but practical and effective for the lower performance general aviation aircraft that would normally operate from unpaved runways. This 15 to 1 slope protection ratio permits the unrestricted, safe use of runways by such aircraft. It was further

stated that final approach angles of 5° to 6° are, in fact, those commonly flown by smaller aircraft; even though 3° to 4° approach slope angles are currently believed to be the norm.

A fourth state said that approach clearance ratios such as used on this project (15:1) were adequate for the type of aircraft that use unpaved airports. The 15:1 approach clearance ratio, they said, is acceptable and appropriate for the 5° to 6° approach angles used by small, general aviation aircraft. Therefore, this could be accepted as a standard approach clearance ratio for small general aviation airports. The state further said that it recommends adopting this same criterion for displaced thresholds, that is, to locate the displaced threshold at the point on the runway where a clear 15:1 approach ratio can be achieved.

SUMMARY OF COMMENTS ON VERTICAL APPROACH GUIDANCE AND OBSTRUCTION CLEARANCE.

Four state aviation officials and two owner/operators commented favorably on the vertical approach guidance of the 5° POMOLA and the approach slope obstruction clearance ratio of 15 to 1 for small, single engine, general aviation aircraft that would use short unpaved runways. One state said the ratio could be a standard adopted by the FAA for small, general aviation airports. As previously noted, such recommendations were made following tests at the Technical Center (references 1 and 2.)

GENERAL COMMENTS ON SYSTEM CONCEPT.

General comments are those received which could not be directly related to the system components referred to in the questionnaire.

One state commented favorably on the system and said that it is extremely important to translate the project results into an Advisory Circular to achieve standardization and reduce aircraft accident potential from this source.

An official from a second state commented that, in reviewing the system, he feels personally that a standard turf runway marking system is needed. This system is financially cheaper than systems used in the past, and is equally efficient and, in addition, provides night capability. The system requires a lot of time to install but creates summer jobs for youths in the community. Another official from this state said he would like to see all markers made of plastic rather than wood, as it would entail less maintenance. He feels this is a good system and would like to see more installed. He foresees that his state agency will promote its use on unmarked turf strips.

A fourth state commented that they found the fabrication of the marking system components and the installation work to be extremely labor intensive, and expensive by comparison with other marking systems in use. Because of soil conditions, installation of the pipe receptacles required driving them into the ground using a special driving tool together with a tractor mounted postdriver. Eighteen employee-days were spent installing the system, cone markers can be installed to mark an entire runway in one day by two workers. This airport was built on glacial stone making it difficult to insert pipes for markers. The cones used are 36-inch diameter cones and were affixed to the ground by driving four 12-inch spikes at four points along the edge. The state said, in summarizing, that they feel the experimental system has met with very little acceptance by the flying public. They have used white fiberglass cone markers for nearly 20 years and conclude that they

are a superior marking system from both the installed cost standpoint and the ongoing maintenance requirements, not to mention better visibility overall. They also said that, although the foregoing lends very little support to the experimental marking system, they feel it is important that it was given a fair test in the field, rather than being dismissed out-of-hand without evaluation.

An owner/operator commented that the system tested for the last three years has been more than adequate for its purpose, to aid pilots in locating and landing on turf runways. The maintenance has been minimal and marking unpaved runways will make flying safer.

Another owner/operator commented, as stated under question 4, that the plywood markers provide adequate guidance on final approach. However, when on downwind leg, they are almost impossible to see. Also, pilots expressed concern about damage if the edge markers were hit. He has used, and suggests, five gallon plastic buckets where snow is not a factor. A third owner/operator expressed satisfaction with the system and said it was well received by visiting pilots.

SUMMARY OF GENERAL COMMENTS.

There were three comments concerning the need to achieve standardization. The substitution of cones, plastic buckets, or other materials for runway markers, with a size approximating that provided by the panels, should provide a degree of flexibility which results in a standardized pattern that pilots will recognize. One state said they foresee that their agency will promote use of the system, while another said that it was extremely important to translate the results of these tests into an Advisory Circular to achieve standardization and reduce aircraft accident potential.

CONCLUSIONS

Questionnaire data from the daytime system tests, including comments from user pilots, airport owner/operators, and from state aviation officials, appear to be adequate to make reasonable conclusions relative to the value of various components of the system. However, the data for the nighttime system represented a relatively small sample (27) with relatively few comments. This required some interpolation, from the daytime system and previous test experience, resulting in conclusions which are considered reasonable for marking and lighting unpaved runways for nighttime use.

For the most part, the marking and lighting system developed at the Technical Center was found acceptable during the 2- to 3-year inservice test period. The few changes resulting from the inservice tests should improve the system and provide a basis for an Advisory Circular governing marking and lighting of unpaved runways. This Advisory Circular could be used by local governments as a criteria for their certification of unpaved runway airports. Also, it would encourage standardization among states.

While we recognize that many of the negative comments resulted from the lack of education relative to details of this new system, we must realize that this, in itself, is a significant problem. Educating the pilot population to a new system,

or to components of a system, is a slow process, particularly when deviating considerably from previous standards. However, we should not let this deter us from making changes where safety can be significantly improved.

Based upon the results of the inservice test program, it is concluded that the following changes should be made to the system which is described in Appendix A and Letter Report NA-78-34-LR:

1. Airport Identifier - A unique, easily recognizable, two- or three-letter abbreviation of the name of the airport should be used as an identifier on the pyramid rather than the location identifier assigned by the FAA.

The concept of using the standard FAA assigned location identifier would be a good approach if all airports were so labeled on the sectional charts and were commonly known as such. However, pilots (particularly VFR only pilots) are often confused by these official identifiers which are frequently meaningless to them. Participating pilots were much more receptive to common abreviations, such as P.V. for Pleasant Valley Airport and T.P. for Twin Pine Airport, which were used by two airports in the program instead of their FAA assigned location identifiers.

2. Runway Edge Markers - White cones with black tops and a minimum diameter of 36 inches should be considered as an alternative to flat runway edge markers.

One of the complaints about the flat edge markers was that they could not be seen from the side. However, the runway alignment markers were incorporated to provide circling guidance to compensate for this deficiency. The runway edge markers are primarily to provide lateral guidance on final approach and departure, for which they are well suited. The use of cones of adequate size will, of course, assist in circling guidance since they can be seen from the side and top as well. The commonly used 24-inch or less in diameter cone does not present enough surface viewing area to accomplish the above purpose. The minimum size cone that will adequately perform this function is the white/black cone of 36-inch diameter or larger, which has slightly less frontal area than the recommended flat edge marker. The 36-inch diameter cone may be more expensive, however, maintenance could be less with improved materials.

3. Go-Around Markers - These markers should not be used as a standard component of the system but could be considered as an option by the airport management.

According to the questionnaire results, this component was considered the least important and received the most negative comments. While most pilots who were familiar with its meaning considered it useful, many pilots were opposed to use of the go-around markers, indicating that there were too many variables to the proper location of the marker and that it only contributed to the "clutter" of many panels.

4. Aiming Point Markers - These markers should not be used as a standard component of the system but could be considered as an option by the airport management.

This component of the system received the second most negative comments. While the majority of the pilots considered the aiming-point-markers useful, they felt that they did contribute to the "clutter" of too many markers and were considered superfluous by many pilots who considered the threshold (or displaced threshold markers) adequate. In addition, the rear panel of the daylight POMOLA system, while some

distance from the runway edge, can also be condsidered as an aming point marker. Indeed, if the six panel POMOLA is used, two of the rear panels of this unit do replace the aiming-point-markers.

5. Runway Edge Marker Separation - A separation distance of 400 feet between edge markers should provide adequate runway edge delineation.

Considerable comment concerning the number of edge panels and their possible hazard to aircraft exiting the runway area was received. The 200 foot spacing between edge markers specified for the evaluation was proposed and derived from the distance usually chosen for placement of conventional runway edge lights. Considering the larger physical size of the daylight markers, it is probable that a greater spacing, as concluded above, will reduce the physical hazard and still provide adequate definition of the runway edge location. A spacing of 400 feet between markers was not evaluated during the inservice test, but could be accomplished with a minumum of effort should it become necessary.

6. Night Runway Lighting - The proposed system of runway threshold and end lights only will probably not adequately define the lateral limits of the landing area. Incorporation of low intensity runway edge lights, at an extended spacing of 400 feet should provide the required runway edge definition.

While the participating pilots judged the nighttime system marginally adequate, the low number of questionnaire responses was not sufficient to insure a firm determination of system effectiveness. In particular, concern was expressed over the reduced effectiveness of the edge panel mounted retroreflectors under crosswind landing conditions. With a strong crosswind, many pilots will use the "crab" technique for maintaining runway alignment during the approach. In this situation, the landing lights on the aircraft will be aligned to one side or the other of the runway, rendering the reflectors totally ineffective. Hence the need for supplemental runway edge lights to provide additional guidance under all conditions.

7. Aiming Point Lights - These lights should not be used as a standard component of the system, but could be considered as an option by the airport operator.

The aiming point lights, when serving as the rear component of the nighttime POMOLA system, must be used, but only since they form a portion of that system in providing visual glide slope guidance.

8. POMOLA - The POMOLA, in both day and night configurations, provides reliable visual glide slope guidance under all conditions, and should be included as a required part or component of any recommended unpaved runway lighting and marking system.

The POMOLA system proved to be very effective and was extremely well received by the user pilot group participating in this inservice test. Questionnaire responses indicated almost universal acceptance of the system, with the pilots judging it to be one of the most desirable components of the proposed lighting and marking system.

REFERENCES

1. Dosch, Victor F., Marking and Lighting of Unpaved Runways, FAA NAFEC Technical Letter Report No. NA-78-34-LR, May 1978.

2. Dosch, Victor F., Low-Cost Visual Approach Slope Indicator (VASI), FAA NAFEC Technical Letter Report No. NA-78-52-LR, February 1979.

3. Gates, R.F., Visual Aids for Truf Runways at Utility Airports, Report No. FAA-NA-76-159, DOT/FAA, NAFECC, June 1976.

4. Brown, G.S., State of the Art Survey of Low-Cost Visual Glideslope Guidance Aids, Letter Report NA-77-9-LR, FAA/DOT, NAFEC, March 1977.

5. Baxter, J.R., Gay, R.H., and Lane, J.C., The Sensitivity of the Precision Visual Glidepath (PVG) at Long Range, Human Engineering Note No. 5, Department of Supply, Australian Defense Scientific Service, Aeronautical Research Laboratories, February 1960.

6. Brown, G.S. and Sulzer, R.L., Test of Glideslope With and Without Simplified Abbreviated Visual Approach Slope Indicator, Interim Report No. FAA-RD-74-139, October 1974.

7. Par , L.C. and Goode, M.W., General Aviation Approach and Landing Practices, NASA Aircraft Safety and Operating Problem Conference, NASA SP-416, Langley Research Center, Hampton, Virginia, October 18-20, 1976.

8. Carpent , R., POMOLA: Poor Man's Optical Landing Aid, Pilots Safety Exchange Bulletin, 58 1093, Flight Safety Foundation Inc., New York, New York, April 25, 1958.

9. Gates, R.F., and Paprocki, T., Visual Approach Indicator (VAPI) Evaluation, FAA-ARD-72-49.

APPENDIX A

MARKING AND LIGHTING OF UNPAVED RUNWAYS
OPERATIONAL DESCRIPTION OF SYSTEM
AS INSTALLED FOR INSERVICE TESTING

PURPOSE.

The marking and lighting system for unpaved runways was developed to provide a low cost, economical system that will provide improved safety of operations at small, unpaved general aviation airports utilized by single engine and light twin aircraft. The marking and lighting system was developed to satisfy the following functional requirements:

1. Airport Location
2. Airport Identification
3. Runway Selection for Landing
4. Circling Guidance
5. Final Approach Guidance
6. Touchdown and Rollout Guidance
7. Exit Identification
8. Taxiing Guidance

Items 7 and 8 are of lesser importance and may or may not be included in the system.

It should be understood that this system is designed for short unpaved runways where the runway length is usually in the order of 1,600 to 3,000 feet long, with the majority in the neighborhood of 2,000 to 2,600 feet in length. Most of the aircraft being flown into these airports are light single engine aircraft with slow approach speeds from 50 mile per hour (mi/h) to 90 mi/h, with the majority in the upper 60 mi/h to low 70 mi/h range. The aircraft circling approach is generally in the range from 1/4 mi to 1 1/4 mi, with the median at 3/4 mi from the runway. These light aircraft normally execute relatively steep approaches ranging from 4° to 6° with a median of 5°. In general, the shorter the runway, the steeper the approach angle to insure maximizing runway length for landing and slow approaches (full flaps) to minimize landing distance.

DAYTIME MARKER SYSTEM.

Locating an airport with unpaved runways (figure 1) can be difficult unless there are many parked aircraft, since otherwise the airport usually blends into the surrounding terrain. In order to enhance the ability to visually locate the airport, a black and white pyramid locator with adjacent runway alignment markers is placed in a central location of the airport to provide a unique structure such that it can be readily differentiated from the surrounding structures and terrain. The pyramid locator can generally be seen within 3 miles or the minimum VFR visibility. It is expected that aircraft will utilize normal navigation such as pilotage, dead reckoning, VOR, or other techniques, to come within the 3-mile visual acquisition area.

After visual acquisition of the pyramid locator, the pilot can verify that he is approaching the correct airport by reading the airport identifier white letters on the black side of the pyramid.

While overflying the pyramid, other required information becomes available i.e., the windsock on top of the pyramid provides guidance for landing (runway direction) and the runway magnetic bearing (first two digits — i.e., 12 for 120°) is visible

on top of the third runway alignment marker located on each side of the pyramid. The runway alignment markers are always parallel to the runway. Therefore, this provides the necessary information to determine runway selection for landing.

The combination of pyramid and runway alignment markers, parallel to the runway, provide a visual reference for circling guidance to the appropriate runway. If the runway requires right-hand patterns, an additional runway alignment marker is placed 90° from the normal alignment markers to provide that indication. Additionally, on the white sides of the pyramid parallel to the runway, the runway elevation is imprinted in black lettering to provide information for proper circling approach altitude and altimeter setting when on the ground. In addition, if a displaced threshold is required on one or both ends of the runway, a fourth runway alignment marker is placed on the displaced threshold end with the outer half painted red to indicate the potential danger of a displaced threshold. While flying the downwind portion of the approach, the pilot will generally not be able to see most of the edge markers and must depend upon the runway alignment markers adjacent to the pyramid for guidance (these markers are always parallel to the runway).

When on base leg of an approach, the pilot will begin to see the edge markers and the panels of the POMOLA. As the pilot approaches the final approach area. he will see the edge markers for providing lateral guidance, and the POMOLA panels for vertical guidance, as shown in figure A-1. The edge markers are black and white in order to provide maximum visibility contrast with the background and within the two components of the marker. When approaching "down sun" (sun on your back) reflection of light from the white portion of the panel can be seen at a considerable distance with the black portion also generally visible but not nearly as prominent. When approaching "up sun" (facing the direction of the sun), the white portion of the edge markers will generally not be visible; however, the black portion of the marker will be in evidence. The distance that these markers are visible will vary as a function of the sun location, brightness, cloudiness, background colors, and other environmental conditions. However, they will generally be visible for 1 to 1 1/4 miles under minimum VFR visibility conditions (3-mile visibility) such as to provide appropriate lateral final approach guidance. (Note: circling guidance and final approach for most small general aviation airports is 1/4 to 1 1/4 miles with the median of about 3/4 mile.)

The POMOLA panels will also be visible on final approach to provide vertical guidance and obstruction clearance. These panels are painted fluorescent orange and are generally very visible. (Note: Under many conditions, fluorescent orange is more visible than black and white; however, the paint is expensive and needs to be repainted about every 6 months; therefore, this color was limited to the POMOLA.) The POMOLA can be seen adequately for vertical guidance out to a distance of about 1 1/4 miles under good conditions and less under poor visibility conditions. However, under most conditions, it can be used from 3/4 mile down to near threshold, which is adequate for unpaved runway operations. The approach slope is generally set at 5° with a buffer of about 1.2° from an obstruction slope of 15:1 (3.81°), to provide a safe approach over obstructions in the approach zone.

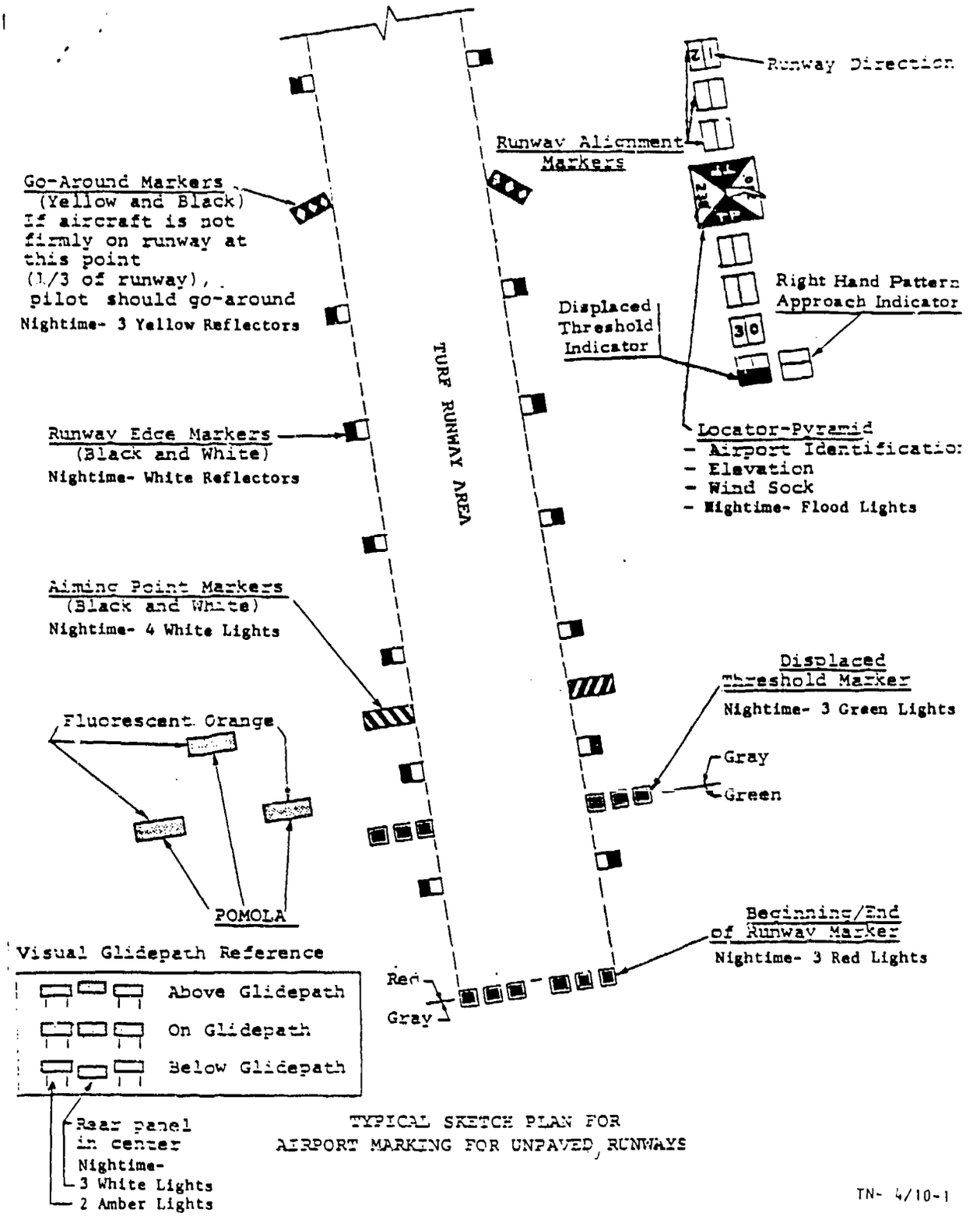

FIGURE A-1. TYPICAL SKETCH PLAN FOR AIRPORT MARKING FOR UNPAVED RUNWAYS

As final approach is being accomplished, a black and white diagonal stripped aiming point marker on each side should be used as an intercept point to which the landing will be attempted. This tends to provide a fixation point to which the pilot can aim the aircraft approach for landing with safety and yet maximizing utilization of the runway.

The threshold or displaced threshold markers, because of their reduced size and color configuration (green for threshold and red for runway end with a 3-inch white edge for greater conspicuity), are not as visible as the larger black/white edge markers and may not be seen until the approach is near the threshold (1/4 to 1/2 mile). However, their importance is greater near the threshold where they should be utilized in the final phase of the approach and flare, and they supplement the aiming point marker for delineating the area available for the final phase of the approach.

The black and white edge markers continue to be valuable as an aid in the flare, touchdown, and rollout phase for lateral guidance. In addition, a "go-around" marker of three yellow diamonds on a black background is provided on both sides of the 100 foot wide runway at a point approximately one-third the length of the runway. While this feature is optional and may be considered unnecessary by some pilots, it has been found to be a valuable guide for short runway operations. It provides a decision point for the pilot to determine if he can stop the aircraft, knowing that he has two-thirds of the runway left or if he should "go-around."

As an option, where taxiways are to be delineated, an exit identification marker (yellow arrow on black background) may be used on the edge of the runway to indicate an exit onto a taxiway area. Taxiway guidance can be accomplished with almost any type of a marker colored either blue or yellow. The use of blue plastic posts with bands of yellow retroreflective material or yellow plastic posts with bands of blue retroreflective material work satisfactorily.

NIGHTTIME SYSTEM.

Nighttime location of unpaved runways should be accomplished with an airport beacon. This may be a standard airport beacon of 250 watts, 500 watts, or 1,000 watts. However, instead of white/green for the standard lighted airport, the green filter is removed to provide a white/white signal which represents an unlighted or an unpaved, partially lighted, airport. The beacon is located at some convenient location on the airport, but should not be immediately adjacent to the runway.

After locating the airport with the beacon, the pilot should fly over the pyramid which is floodlighted to obtain the same information as in the daytime (see daytime system for explanation) for proper identification of the airport and runway selection for landing. This information should be reasonably visible from an altitude of 1,500 feet or lower.

Circling guidance is achieved by a combination of the pyramid/runway alignment markers and the green and red lights which outline the runway at the threshold and end of the runway, along with white aiming point lights. The red and green lights are about 30 watts each, in consideration of the filtering of the colored lenses to balance light intensity with the 15-watt clear lamps of the aiming point lights. Circling approaches at night should remain close in (approximately 1 mile or less) because the range of the low wattage lamps is limited. (Note: Range is adequate for low ambient lighted conditions; however, higher wattage lamps may be required under high ambient light conditions where many other lights are within the vicinity.)

Where high trees or other foliage restricts visibility, the pyramid and/or beacon may be required to provide assistance for the downwind portion of the approach. The two ends of the runway, as delineated by the runway threshold (6 green lights) and runway end (6 red lights) should provide circling guidance for the downwind and base leg portions of the approach as well as lateral guidance for the final approach phase.

After achieving lateral alignment with the runway utilizing the green/red threshold/runway end lights as well as the white aiming point lights (4 or 8, depending on the configuration), vertical approach guidance is achieved by use of the nighttime POMOLA or the Cumming Lane System, depending on which is installed. The nighttime POMOLA consists of placing three clear 15-watt incandescent bulbs on top of the single front panel and two 30- or 40-watt incandescent bulbs with a yellow or amber lens on top of each of the two rear panels. The system is then flown by aligning the three white front lights with the two sets of two yellow lights on the rear panels, as indicated, for the daytime system. It should be noted that the white lights on the front panel are in line with the white aiming point lights. When used with the nighttime POMOLA, the aiming point lights consist of four lights, two on each side of the runway. The Cumming Lane System, consists of eight aiming point lights (four on each side) aligned with one or two yellow lights on each side of the runway when on the correct glidepath angle. The white aiming point lights should be utilized as a fixation point at which the pilot wants the aircraft to land on the runway in a similar manner to the daytime aiming point marker.

Retroreflectors (these are differentiated from reflectors in that they reflect light back to the source of that light) are placed on all the daytime markers. Therefore, the edge markers will suddenly blossom as if edge lights were turned on. The location and distance from the runway at which this happens depends upon several variables, such as the distance from the light source and the angle the light makes with the approach path. The closer the landing light is to the pilot's eyes, the earlier the retroreflectors are seen and the more intense they will be (i.e., lights on the aircraft nose are better than on the wing). The retroreflectors can be seen as far out as 1 1/2 miles under good conditions; however, they are generally useful from about 1/2 to 3/4 miles out.

If a crosswind approach is necessary, it is recommended that the wing low and/or cross control technique be utilized in lieu of the crabbing method to keep the longitudinal axis of the aircraft, and hence the landing lights, in line with the runway. With a properly adjusted landing light, the retroreflectors will provide adequate intensity for proper guidance during the latter part of the final approach, flare, touchdown, and rollout. The go-around marker is also appropriately outlined by retroreflective material such that the three yellow diamonds can

readily be distinguished for go-around guidance, as discussed for the daytime systems.

If exit identification is provided, the yellow arrow will be of retroreflective material so that it can be seen during night operations. Likewise the taxiway guidance, if provided, will incorporate either blue or yellow retroreflective material which, will provide ample taxiway guidance.

During takeoff operations, the retroreflectors on the edge markers will provide adequate guidance for the takeoff roll and lift-off.

APPENDIX B

STATISTICAL SUMMARY OF QUESTIONNAIRE RESPONSES

QUESTIONNAIRE

DAYTIME OPERATIONS — MARKING AND LIGHTING OF UNPAVED RUNWAYS

	Total Responses	
	Yes	No
1. Does the pyramid with runway alignment markers help you locate the airport in VFR conditions?	114 (92%)	10 (62%)
2. Does the airport identifier (TP) and airport altitude painted on the pyramid (airport locator) provide any useful information to you?	116 (95%)	7 (6%)
3. Do you find the combination of pyramid with windsock on top, runway alignment markers, and runway direction numbers to provide adequate information for selection of proper runway for landing and circling guidance?	115 (93%)	9 (7%)
4. Do the runway edge markers provide adequate lateral guidance on final approach?	119 (97%)	4 (3%)
5. Does the POMOLA provide adequate vertical glidepath guidance and obstruction clearance on final approach?	110 (93%)	8 (7%)
6. Do the aiming point markers and threshold or displaced threshold markers provide proper indication for touchdown guidance?	117 (97%)	4 (3%)
7. Do you consider the aiming point markers useful?	107 (91%)	11 (9%)
8. Do the "go-around" markers perform a useful function?	96 (85%)	17 (15%)

REMARKS: (additional comments)

SUGGESTIONS FOR IMPROVEMENT: